THERMODYNAMIC AND TRANSPORT ANALYSIS OF A BERNOULLI FLOW METER SYSTEM FOR ANY REAL FLUID

FOR

NASA MARSHALL SPACE FLIGHT CENTER

7561 FM 1960 East, Suite 288, Humble, Texas 77346 Phone 832.257.3818
Consultant@QMC.net www.QMC.net

THERMODYNAMIC AND TRANSPORT ANALYSIS OF A BERNOULLI FLOW METER SYSTEM FOR ANY REAL FLUID

For
NASA
Marshall Space Flight Center

by
Paul D. Van Buskirk, MSChE
Director of Technology
Quality Monitoring & Control

Reviewed and approved
by
William A. Heenan, Ph.D. PE
Dean of Engineering
Texas A & M University-Kingsville
Vice President, Technology
Quality Monitoring & Control

April 2006
PTK-8, Revision 3

Table of Contents

List of Tables

List of Figures

A+ FLOWTEK, a NASA Spin-off Company

In a collaboration between NASA's MSFC and Quality Monitoring and Control (QMC) of Humble, Texas, state-of-the-art balanced flow meter technology has been developed. Based upon its work with NASA, QMC founded A+ FlowTek, also of Humble, Texas, to commercialize the balanced flow meter technology.

This Balanced Flow Meter invention has been nominated for NASA's 2006 Space Technology's Hall of Fame.

The Balanced Flow Meter determines the flow rate in piping, channel, and conduit systems. It provides highly accurate flow metering, flow limiting, or flow conditioning in any fluid flow system. As a flow meter, the technology provides flow measurement with minimal intrusion into the flow path and requires no moving parts. When compared to a standard orifice plate, it provides a 100% increase in pressure recovery, a 10-fold increase in accuracy, and a 15-to-1 reduction in acoustic noise generation. As a flow-limiting device, the technology can simulate fluid flow loads for facility certification and provide accurate flow limiting for safety and process control systems. The technology's sizing is more accurate than the currently used orifice plate technology, and it requires less space and cost when compared to venturi flow technology while maintaining similar performance. As a flow-conditioning device, the technology may improve process and equipment performance by conditioning fluid flow and fluid energy profiles around elbows, combustion chambers, pump inlets, etc.

Fluid flow measurements are used extensively in the processing industries for refineries and chemical, power, and pharmaceutical plants. The Balanced Flow Meter's applications to NASA's liquid propulsion systems and test facilities are numerous.

Disclaimer

This document contains information confidential and highly sensitive to QMC. The methods and procedure used are the sole property of QMC. These methods and procedures are used within the fluid processing industries for high accuracy flow measurement, and are the approaches taken by the US industry leaders in the field, such as Dresser-Rand, ABB, DuPont, Rosemont, etc. The development of these methods and procedures are used by QMC clients, such as DuPont, Dresser-Rand, and ABB. Rosemount and others in the field are considered QMC (and A+ FLOWTEK) competitors. The method and procedures provided herein enables QMC (A+ FLOWTEK) and associated clients, competitive leadership in the field and are not to be disclosed to any individual or entity without the written consent of QMC.

This document is provided to NASA/MSFC for understanding of the "head" meter/Bernoulli equation technical background and application for accurate flow measurement for any fluid system. These methods and procedures may be patented by NASA/MSFC and QMC, and are applicable to all components of the SSME and other new rocket designs. These components include conduits, valves, turbines, expanders, mixers, combustion chambers, and nozzles. The general applicability is for any mass, momentum, energy, power, and thermodynamic balance, as applied to any fluid, mixture, and reaction process of any phase.

Additionally, the Modified Iterative Measurement Test (MIMT©) algorithm developed for flow meter error detection is owned exclusively by Heenan and Serth, Ltd. It is copyrighted by the American Institute of Chemical Engineering (AIChE). The algorithm is under exclusive contract with QMC. The methods and procedures for utilization of the MIMT© algorithm cannot be used by NASA/MSFC or any other entity, without the expressed written consent of QMC.

Questions concerning the technical basis or use of the information contained within are to be directed to: Jane Van Buskirk, CEO, Quality Monitoring & Control.

Balanced Flow Meter Technical Basis: Units, and Fundamental Definitions ©

Foreword

The analysis and design of the Balance Flow Meter is based on the units, fundamental definitions, and nomenclature as used in the U.S. chemical process industries, such as refineries and chemical plants. The chemical industry engineer deals primarily with internal boundary layer flow (e.g., pipe flows) with mass, momentum, energy and entropy balances. This is different from the force and momentum basis as used for open-channel, external, inviscid-streamline, or potential flow analysis for other engineering applications.

Bernoulli's Theorem

Bernoulli's theorem is used in the solution of hydraulics problems. This theorem is a special case of the first (conservation of energy) and second laws of thermodynamics in which changes in the energy content of a fluid system are balanced against one another. Although friction losses are evident as heat, the theorem is concerned only with the pressure and energy changes, and heat is considered lost energy.

$$\left.\begin{array}{l} Z_a(\text{static head}) \\ +\dfrac{u_a^2}{2g}(\text{velocity head}) \\ +P_aV_a(\text{pressure head}) \\ +W(\text{mechanical work}) \end{array}\right\} = \left\{\begin{array}{l} Z_b \\ +\dfrac{u_b^2}{2g} \\ +P_bV_b \\ +F\ (\text{friction}) \end{array}\right. \qquad \textbf{Equation 1}$$

Each item in the above equation must be expressed in the same units, i.e., feet of head or pounds per square inch, etc.

The Engineering Bernoulli Equation

The main application of the Balanced Flow Meter is for internal boundary-layer flow of single stream systems, such as the orifice, venturi or other *Bernoulli energy-head* meters. The design basis is the compressible-fluid steady-flow balance for total mass, energy and entropy. The equation uses *Bernoulli's theorem* for conservation of the various mass-specific energy-head forms and associated groupings. The *engineering Bernoulli equation* combines the energy and entropy balance into a single equation and is applicable to any incompressible, compressible or two-phase fluid. The steady state *engineering Bernoulli equation* for flow systems of any thermodynamic path is given by,

$$\Delta\left(\frac{\alpha v^2}{2g_c}\right)+\Delta\frac{gZ}{g_c}+\int\frac{dP}{\rho}+W_{shaft}+LW_{friction}=0. \qquad \textbf{Equation 2}$$

It is based on steady state energy, entropy balance and Gibbs relation as given below.

$$\left(H+\frac{\alpha v^2}{2g_c}+\frac{gZ}{g_c}\right)_a \delta m_a-\left(H+\frac{\alpha v^2}{2g_c}+\frac{gZ}{g_c}\right)_b \delta m_b+\delta Q-\delta W_{shaft}=0$$ **Equation 3**

$$-TdS+\delta LW+\delta Q=0 \; and, \; dH=TdS+dP/\rho$$ **Equation 4**

Bernoulli's equation is used extensively and is the chemical industry basis for head-type flow meter analysis and design, and from which the *orifice equation* is developed. The primary references and authority used for these fundamental definitions and basis are,

1. Perry's Chemical Engineers' Handbook(s), and
2. Transport Phenomena, by Bird, Stewart and Lightfoot.

Mechanical Units

The units and dimensions of three mechanical properties, force, mass and weight, are commonly used. Mass is the quantity conserved in all non-nuclear flows. Material balances are in terms of mass, not weight. The amount of mass is not affected by body forces, such as gravitational. Weight λ is defined from the mass M as, $\lambda=M(g/g_c)$.

Several systems of units and dimensions are defined and used for the quantities in engineering equations. One such system is the SI (Systeme International d'Unites) system. Another is the foot-pound-second (fps) system. The kinetic and potential energies in the various dimensional systems are given below:

Table 1 - Potential and Kinetic Energy Units

Potential and Kinetic Energies		
Energy	cgs/mks/SI units	fps units
Potential	MgZ	MgZ/g_c
Kinetic	$Mu^2/2$	$Mu^2/2g_c$

The fps units are commonly used in the U.S. and used as the dimensional basis for the Balanced Flow Meter. This approach preserves and provides continuity with the many technical papers and results developed over the last century as associated with the Bernoulli flow meter. A Units Conversion Program is available from A+ FLOWTEK at www.AplusFlowTek.com.

Fluid Physical and Thermodynamic Properties

For *any* fluid (gas, vapor, liquid, or two-phase) the density ρ is calculated with an equation-of-state (EoS$=f(T,P)$ at constant composition) by,

$$\rho(T,P)=\frac{P}{z(T,P)\Re T}=\left(\frac{\partial P}{\partial H}\right)_S=\left(\frac{\partial P}{\partial G}\right)_T,$$ **Equation 5**

where z is the compressibility factor. The thermodynamic properties are calculated by,

$$U(T,P)_b - U(T,P)_a = -(U^\circ - U)_b + \int_{T_a}^{T_b} C_V^\circ dT + (U^\circ - U)_a \; Internal\ Energy \qquad \textbf{Equation 6}$$

$$S(T,P)_b - S(T,P)_a = -(S^\circ - S)_b + \int_{T_a}^{T_b} \frac{C_P^\circ dT}{T} - R\ln\left(\frac{P_b}{P_a}\right) + (S^\circ - S)_a \; Entropy \qquad \textbf{Equation 7}$$

$$H(T,P)_b - H(T,P)_a = -(H^\circ - H)_b + \int_{T_a}^{T_b} C_P^\circ dT + (H^\circ - H)_a \; Enthalpy\,\textbf{.} \qquad \textbf{Equation 8}$$

$(B^\circ - B)$ is the departure function from the ideal gas B° reference state. For two-phase fluid flow systems, a flow-regime analysis is required to determine the homogeneous enthalpy H, density ρ, and associated kinetic energy correction factor α, which are typically based on a no-slip interface and transport-phenomena.

Flow Meter Radial Corrections

For extremely accurate flow measurements $<< 0.25\%$, corrections may be applied for pipe radial variations in temperature, pressure, density, enthalpy, etc. In developed flow, radial equivalent pressure is considered uniform and temperature variation by viscous heating is typically minimal for Mach numbers less than 0.3. Turbulent mixing reduces any radial temperature and density variations. Radial pressure variations must time average to zero since there is no net radial flow. Calculation methods are listed in the above references or other publications for non-isothermal macroscopic system analysis of pipe flows. Pipe radial variations are considered secondary, small effects and these methods are typically not required with proper design and placement of pressure and temperature taps. There are numerous publications on design and placement of taps, with calculation methods to apply correction factors. See for example: the “Flow Measurement Engineering Handbook”. Piezometer chambers or correction factor algorithms are available with the A+ FLOWTEK flow meters.

Flow Meter Gravitational Correction

The orifice equation correction for out-of-plane gravitational fields or variable-directional accelerations is made by re-positioning the pressure tap locations or by use of the following equation(s),

$$m = \rho_a A_a \sqrt{\frac{\left(2g_c J\Delta H_S + 2g\Delta Z\cos(\phi)\right)\eta_{eff}}{\left(\left(\frac{1}{C_c\beta^2}\frac{\rho_a}{\rho_b}\right)^2 - \alpha_a\eta_{eff}\right)}} = \frac{C_D\gamma A_b}{\sqrt{1-\beta^4}}\sqrt{\rho_a\left(2g_c\Delta P + 2g\rho_a\Delta Z\cos(\phi)\right)}\,\textbf{.} \qquad \textbf{Equation 9}$$

The local gravitational factor g is dependent on elevation and location on the surface of the earth. The gravitational constant of g_c is 32.17405 lb/lb$_f$-sec^2. For a one-mile elevation rise, g is approximately 0.9995 times g_c, e.g. within 0.05 percent. Therefore, g is taken as g_c for applications within the elevations of Death Valley to Denver.

The weight force in Newton's of a 1-kg mass is

$$W = \frac{g}{g_c} m = 9.80665\, F_L m \qquad \textbf{Equation 10}$$

where F_L is the g/g_c correlation factor and 9.80665 m/sec² = 32.17405 ft/sec².

The kilogram mass is, by international agreement, the mass of a certain bar of platinum-iridium located in Sevres, France. The pound-mass in the English engineering system is exactly 0.45359237 kg, (0.45359237 kg = 1 lb). With long vertical pipelines, the local gravity field *may* affect calculated pressure distributions. Equation-of-state calculations will compensate accordingly as based on total pressure measurements.

The equator is farther from the center of the earth than at the poles. There is a steady increase in the measured value of g as one goes from the equator (latitude 0°) to either pole (latitude 90°). This is shown in the following table.

Table 2 - Variation of g with Latitude at Sea Level

Latitude	g, feet/sec^2	Latitude	g, feet/sec^2
0°	32.08789	50°	32.18737
10°	32.09301	60°	32.21516
20°	32.10765	70°	32.23780
30°	32.13022	80°	32.25259
40°	32.15784	90°	32.25778

The ratio of local gravity g to the dimensional constant g_c (= 32.17405 lb/lb$_f$-sec^2) can be approximated to within 0.005 percent with an expression given by Benedict,

$$F_L = \frac{g}{g_c} = 1 - 2.637\,x\,10^{-3} \cos 2\phi - 9.6\,x\,10^{-8} Z - 5\,x\,10^{-5} lb_f / lb_m \qquad \textbf{Equation 11}$$

where ϕ is the latitude in degrees, and Z the altitude in feet above sea level. However, these effects can be neglected with correct differential-producer lead-line design as shown below.

Elevation Correction for Inclined or Vertical Head Meter Installations

The measured differential includes the potential energy term for inclined installations. Shown in the figure (a) below, is a differential producer inclined with respect to the horizontal. Bernoulli's equation along a stream tube is written as

$$\frac{P_{f1}}{\rho_f}+\frac{\overline{V}_{f1}^2}{2g_c}+\frac{g}{g_c}H_{EL,1}=\frac{P_{f2}}{\rho_f}+\frac{\overline{V}_{f2}^2}{2g_c}+\frac{g}{g_c}H_{EL,2} \quad \textbf{Equation 12}$$

Figure 1- Bernoulli's Equation Applied to an Inclined Differential Producer (a) Stream Tube (b) Lead-Lines at Same Elevation

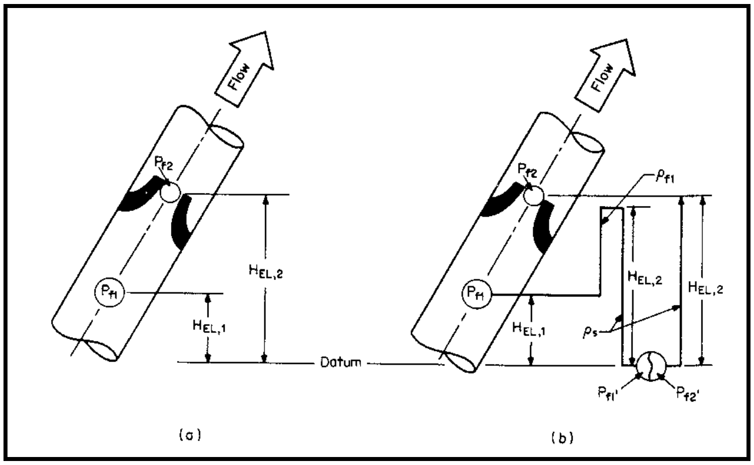

Rearranging gives

$$\frac{P_{f1}-P_{f2}}{\rho_f}+\frac{g}{g_c}(H_{EL,1}-H_{EL,2})=\frac{\overline{V}_{f2}^2-\overline{V}_{f1}^2}{2g_c}. \quad \textbf{Equation 13}$$

Mass flow continuity requires that

$$m=\rho_{f1}A_1\overline{V}_{f1}=\rho_{f2}A_2\overline{V}_{f2}. \quad \textbf{Equation 14}$$

Using the beta factor results in

$$\overline{V}_{f1}^2=\left(\frac{\rho_f A_2}{\rho_f A_1}\right)^2\overline{V}_{f2}^2=\beta^4\overline{V}_{f2}^2. \quad \textbf{Equation 15}$$

Substitution of the above equations yields

$$\frac{P_{f1}-P_{f2}}{\rho_f}+\frac{g}{g_c}\left(H_{EL,1}-H_{EL,2}\right)=\frac{1-\beta^4}{2g_c}\overline{V}_{f2}^2 \quad \textbf{Equation 16}$$

which, when rewritten for mass flow rate gives

$$\frac{P_{f1}-P_{f2}}{\rho_f}+\frac{g}{g_c}\left(H_{EL,1}-H_{EL,2}\right)=\frac{1-\beta^4}{2g_c}\frac{m^2}{\rho_f^2A_2^2}. \quad \textbf{Equation 17}$$

The mass flow equation for an inclined installation of any orientation is

$$m=\frac{\pi}{4}\sqrt{2g_c}\frac{d_F^2}{\sqrt{1-\beta^4}}\sqrt{\left[P_{f1}-P_{f2}+\frac{g}{g_c}\left(H_{EL,1}-H_{EL,2}\right)\right]\rho_f}. \quad \textbf{Equation 18}$$

For a horizontal installation $\left(H_{EL,1}=H_{EL,2}\right)$, this reduces to the fundamental mass flow equation:

$$m=\frac{\pi}{4}\sqrt{2g_c}\frac{d_F^2}{\sqrt{1-\beta^4}}\sqrt{\left(P_{f1}-P_{f2}\right)\rho_f}. \quad \textbf{Equation 19}$$

The difference between the equations for a horizontal and an inclined installation is the potential-energy term

$$\frac{g}{g_c}\left(H_{EL,1}-H_{EL,2}\right)\rho_f \quad \textbf{Equation 20}$$

within the radical.

Shown in the figure (b) above, is a differential pressure-measuring device located at a common elevation datum. Upstream lead lines have been brought to the same elevation as the downstream lead lines, so that $H_1=H_2$. The upstream pressure measured at the datum can be expressed as

$$P_{f1'}=P_{f1}-\frac{g}{g_c}\left(H_{EL,2}-H_{EL,1}\right)\rho_{f1}+\frac{g}{g_c}H_{EL,2}\rho_s \quad \textbf{Equation 21}$$

and the downstream pressure at the datum is

$$P_{f2'} = P_{f2} + \frac{g}{g_c} H_{EL,2} \rho_s \qquad \textbf{Equation 22}$$

where ρ_s is the density of the seal fluid in the lines.

The differential pressure transmitted to the differential pressure measuring device, for the same seal fluid density and provided the lines are at the same elevation, is

$$P_{f1'} - P_{f2'} = P_{f1} - P_{f2} + \frac{g}{g_c}\left(H_{EL,1} - H_{EL,2}\right)\rho_{f1}. \qquad \textbf{Equation 23}$$

The equation above is the measured differential pressure; when it is substituted into the flow equation, it results in,

$$m = \frac{\pi}{4}\sqrt{2g_c}\,\frac{d_F^2}{\sqrt{1-\beta^4}}\sqrt{\left(P_{f1'} - P_{f2'}\right)\rho_f}\,. \qquad \textbf{Equation 24}$$

This equation relates the measured differential to the flow rate, and the measured differential automatically adjusts for the potential-energy term for any orientation and gravitation field.

Fanning Friction Factor

Friction factors are used to determine viscous shear stress, pressure loss, radial velocity profiles, and momentum and kinetic energy correction factors in developed steady flow for pipes and conduits. The Fanning friction factor is used with Balanced Flow Meter (BFM) applications. Another friction factor in use is the Darcy-Weisbach. The relation between these friction factors is shown by use of the shear-stress τ representations,

$$f_{Fanning} = \frac{\tau}{\left(\rho v^2/2\right)} : f_{Darcy-Weisbach} = \frac{4\tau}{\left(\rho v^2/2\right)} \Rightarrow f_{Fanning} = \frac{f_{Darcy-Weisbach}}{4}. \qquad \textbf{Equation 25}$$

PTK-800 Nomenclature ©

The nomenclature as listed below is used for A+ FLOWTEK technical articles and publications. Please contact A+ FLOWTEK for consultation and proper usage of any A+ FLOWTEK Technical Papers concerning your project application.

Table 3 - Nomenclature for Balanced Flow Meter Technical Publications

a	Acceleration	R	Ideal gas constant; pipe radius
A	Helmholtz free energy	$\Re$	Particular fluid constant, R/M_W
A_b	Area of the head-meter constriction	r	Positional radius
B°	Ideal gas state for any property B	r_h	Hydraulic radius
B	Property of real fluid	s	S subscript, constant entropy path
BFM	Balanced Flow Meter	S	Entropy
C_{BFM}	Balanced Flow Meter discharge coefficient	SI	Systeme International d'Unites
C_c	Coefficient of vena-contracta area contraction	T	Temperature
C_D	Discharge coefficient	u	Kinetic velocity
cgs	Centimeter-Gram-Second System	U	Internal energy
C_o	Orifice plate discharge coefficient	v	Average velocity
C_P	Specific heat at constant pressure	$v_{x,r}$	x direction velocity profile at radius r
C_V	Specific heat at constant volume	V , $\overline{V}$	Specific volume of fluid, Average velocity
Const	Constant	Vol	Volume
d	Derivative; small/hole diameter	v_r	Local average velocity at radius r
D	Diameter for fluid flow	W_s, W_{shaft}	Shaft work
D_a	Pipe diameter	X	Amount vaporized; miscellaneous variable
D_b	Equivalent diameter of the hole or holes	X	Thermodynamic departure function
D_h	Hole-diameters	$\vec{x}$	Axial velocity flow
ELK EoS	Extended Lee-Kesler Equation-of-State	z	Compressibility factor
E_K	Kinetic energy per pound of fluid	Z	Distance above a datum plane
f	Fugacity, friction factor or function	ω	Acentric factor
F	Force	∂	Partial derivative
fps	Foot-pound-second units system	σ	Collision diameter
g	Local acceleration of gravity	ρ	Density $=(\partial P/\partial H)_S = (\partial P/\partial G)_T$
G	Gibbs free energy	ρ_a	Upstream density
G^*	Total Gibbs free enthalpy	μ	Dipole moment
g_c	Newton's Law conversion factor, 32.174 ft-lb/lb$_f$-sec^2	β	Diameter ratio

$\vec{G}$	Mass velocity	β	Elliptic eccentricity
h	Planck's constant	β_{BFM}	Balanced Flow Meter beta ratio
H , H_{EL}	Enthalpy, Elevation head	β_D	Head-meter diameter ratio
H^*	Total enthalpy head	β_o	Orifice beta ratio
$h_{L,f}$, h_f	Frictional velocity head-loss	α	Kinetic energy correction factor; polarizability
IG EoS	Ideal Gas Equation-of-State	Δ	Difference
J	Mechanical equivalent of heat, 778.26 ft-lb_f/Btu	ΔP	Pressure difference
k	Velocity head loss; Boltzmann's constant	ΔH	Enthalpy change
k_{ff}	Friction factor velocity head	ΔU	Internal energy change
k_f	Form-drag frictional velocity head	$\Delta P / \Delta L$	Pressure drop per foot of wall surface
lb	Lb-mass	$\in_0$	Minimum potential energy
lb_f	Lb-force or mass weight	Θ	Q factor, ELK-EoS correlating parameter
LW	Lost work	σ	Radius-of-gyration; BFM hole sizing relation velocity exponent
$LW_{friction}$	Lost work from friction	η	Viscosity
m	Mass or moles	δ	Differential amount
m_{tot}	Control volume of mass	τ	Shear stress
M	Body mass	τ_w	Wall shear stress
MBWR	Modified Benedict-Webb-Ruben Equation-of-State	λ	Weight of mass, lb-force; ratio of specific heats
mks	Meter-kilogram-second units system	γ	Density correction factor
M_W	Molecular weight	Φ	Potential
η_{eff}	Thermodynamic efficiency	θ	Angle within the pipe
P	Pressure	$^\circ$	Degree symbol; ideal gas reference state

PTK-801 Beta Ratio Conversion of any Head-Meter to the Balanced Flow Meter ©

Forward

A method to convert the beta ratio of a head-meter, venturi or orifice plate to the Balanced Flow Meter (BFM) beta ratio β is required when improving an application to the BFM flow metering standard. The following provides this conversion procedure and technical basis.

Technical Summary

The following two figures provide a conversion method for the beta ratios of the BFM β_{BFM} to the orifice β_o, and vice versa. The graphs are based on an orifice discharge coefficient C_o of 0.61, and a discharge coefficient C_{BFM} of 0.89 for the Balanced Flow Meter.

Technical Development

For head-type flow metering or flow-restriction applications the Bernoulli equation applies, and may be put in the following form,

$$\left(\frac{1}{A_b^2}-\frac{1}{A_a^2}\right)=C_D\left(2g_c\gamma\left(\frac{\rho}{m}\right)^2\frac{\Delta P}{\rho}\right). \qquad \textbf{Equation 26}$$

For the same tap differential pressure ΔP, density correction factor γ, density ρ, and mass flow-rate m, the ratio of the discharge coefficient C_D for any head meter to the discharge coefficient C_{BFM} for the Balanced Flow Meter is,

$$\frac{C_D}{C_{BFM}}=\frac{\left(\frac{1}{A_b^2}-\frac{1}{A_a^2}\right)_D}{\left(\frac{1}{A_b^2}-\frac{1}{A_a^2}\right)_{BFM}} \text{ or } \frac{C_D}{C_{BFM}}=\frac{\left(\frac{1}{\beta_D^4}-1\right)}{\left(\frac{1}{\beta_{BFM}^4}-1\right)}=\frac{\left(\beta_{BFM}^4/\beta_D^4-\beta_{BFM}^4\right)}{\left(1-\beta_{BFM}^4\right)}. \qquad \textbf{Equation 27}$$

Where the beta ratio is defined as $\beta=D_b/D_a$, $\beta^2=A_b/A_a$, $(A_a)_D=(A_a)_{BFM}$, D_a is the pipe diameter and D_b is the equivalent diameter of the hole or holes. With a known head-meter beta β_D, the Balanced Flow Meter beta ratio β_{BFM} is,

$$\beta_{BFM}=\frac{\beta_D}{\left(C_{BFM}/C_D\left(1-\beta_D^4\right)+\beta_D^4\right)^{1/4}}. \qquad \textbf{Equation 28}$$

With a known Balanced Flow Meter beta ratio β_{BFM}, the head-meter beta ratio β_D is,

$$\beta_D=\frac{\beta_{BFM}}{\left(C_D/C_{BFM}\left(1-\beta_{BFM}^4\right)+\beta_{BFM}^4\right)^{1/4}}. \qquad \textbf{Equation 29}$$

Figure 2 - Orifice to Balanced Flow Meter Beta Ratio Conversion

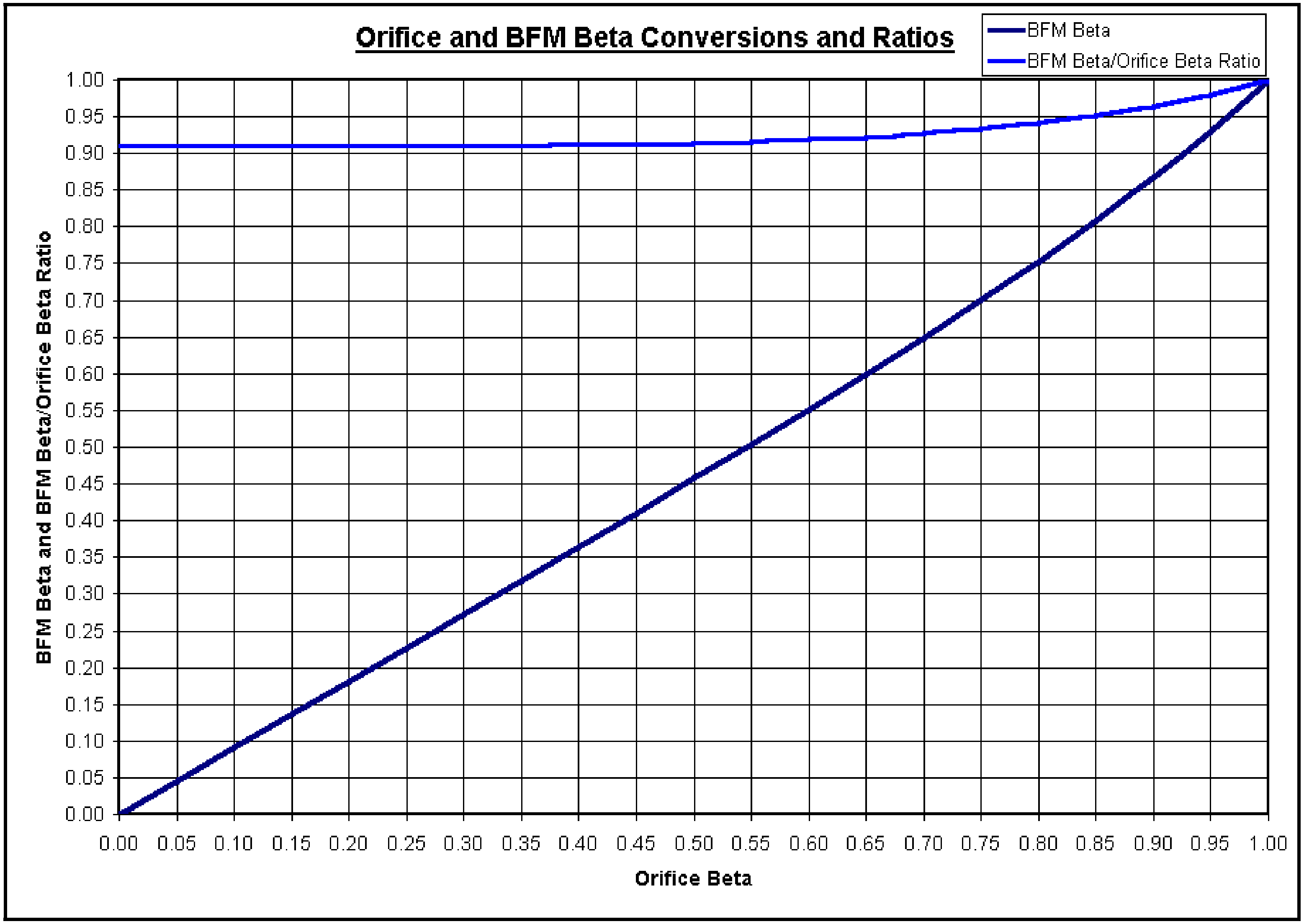

Figure 3 - Balanced Flow Meter to Orifice Beta Ratio Conversion

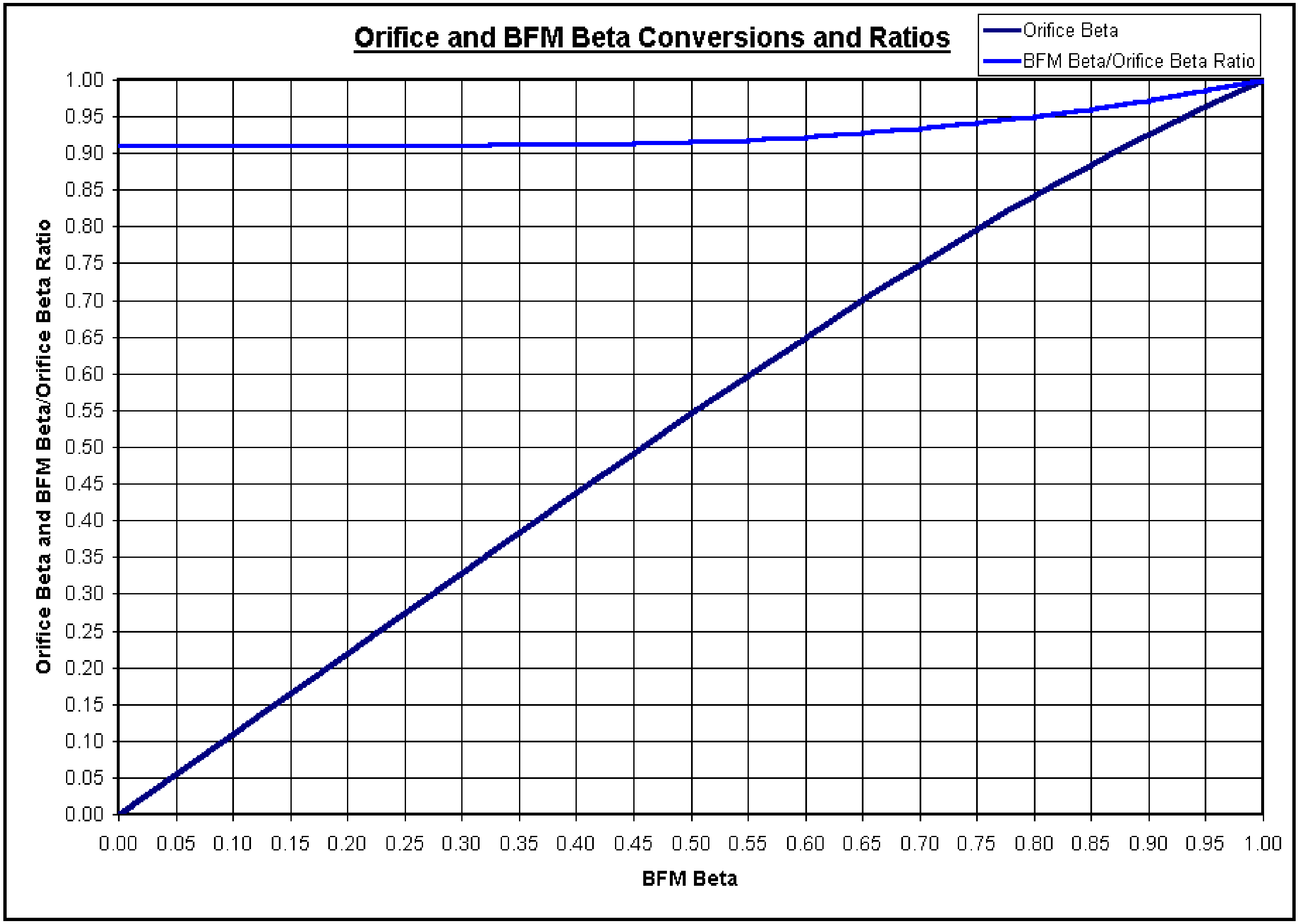

PTK-802 Balanced Flow Meter Shear Stresses ©

Forward

The shear stress and potential for hole-surface erosion in a Balanced Flow Meter (BFM) is significantly reduced when compared to an orifice plate. High wall/surface shear leads to an increase in hole-erosion. The following provides the ratio of the hole-shears of the single-holed orifice plate to the multi-holed Balanced Flow Meter. This ratio provides an estimate of the reduction in erosion potential with the Balanced Flow Meter design when compared to an orifice plate with the same beta ratio. For a sharp-edged orifice, the erosion of the edge is highly increased. The Balanced Flow Meter holes for the standard plate design are square-cut to further reduce the potential for erosion.

Technical Summary

The figure on the next page shows the orifice to Balanced Flow Meter (BFM) shear stress ratio $\tau_{w,o} / \tau_{w,BFM}$. The ratio depends on the number of holes used with the particular Balanced Flow Meter design. The ratio is always greater than one (1) with the BFM plate, which shows that the erosion potential is significantly reduced with the Balanced Flow Meter. This figure demonstrates that the shear stresses are much higher with the single-holed orifice plate when compared to the BFM:

1. For the same flow,
2. Operating at the same process conditions, and
3. With the same beta β factor.

A concern with orifice plate is hole erosion that induces dimensional changes. The multi-holed Balanced Flow Meter provides a significant reduction in the shear stress and, accordingly, reduces the potential for hole-wall surface erosion. Additionally, the standard BFM holes are square, beveled, or bell-mouthed cut, *not* knife-edged. The following figure shows that the knife-edged orifice has considerable *higher* levels of shear stress.

The standard BFM design, with a 1-8 hole-layout, has 9 holes. This BFM design provides a 3 to 1 decrease in shear stress and erosion potential compared to the orifice plate. The decrease is 7 to 1 when compared to the knife-edged orifice plate.

Designs for saturated liquids and vapors use the 33-hole configuration, with a 1-16-16 hole-layout. This design provides a 5 to 1 decrease is surface shear stress. With this reduced shear stress, the potential for cavitation effects are reduced. Additionally, the multi-holed BFM essentially eliminates any vapor or liquid buildup upstream of the plate.

Further shear stress reduction is provided by using a 1-n-2n configuration as used in cavitating flows. An example is the 1-16-32 configuration, which has 49 holes. This layout configuration provides added holes for the same β specification.

Figure 4 - Shear Stress Ratio Increase of the Orifice Plate to the BFM

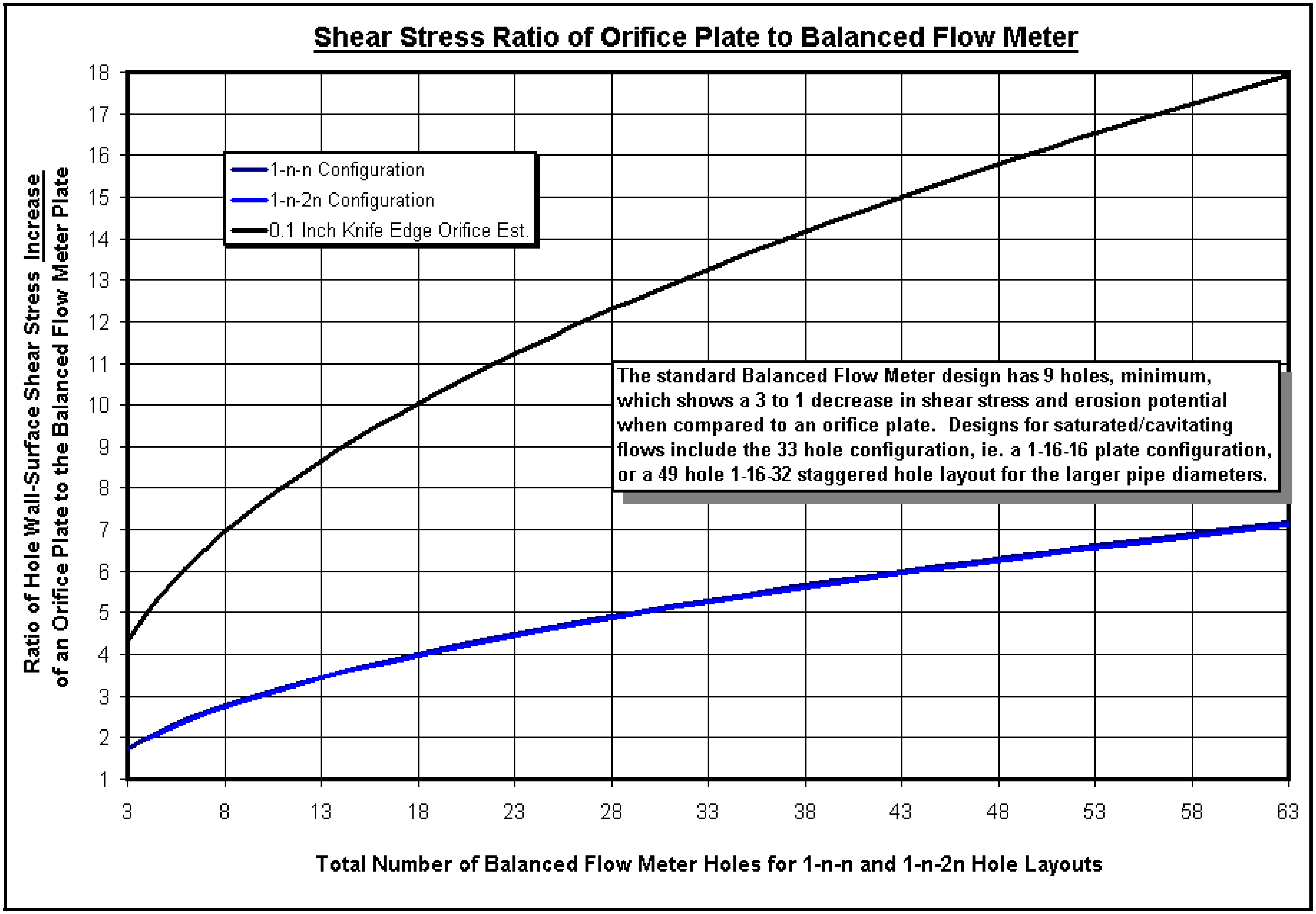

Orifice to Balanced Flow Meter Equation Development

For any Reynolds number and flow regime, laminar, transition or turbulent,

$$\tau_w = \frac{f \rho v^2}{2 g_c}. \quad \textbf{Equation 30}$$

Where τ_w is the wall shear stress, ρ is the fluid density, v is the average velocity, and g_c is the Newton conversion factor. The friction factor f is defined as,

$$f \equiv \frac{1}{2}\frac{\Delta P}{\Delta L}\frac{D g_c}{\rho v^2}. \quad \textbf{Equation 31}$$

$\Delta P / \Delta L$ is the pressure drop per foot of wall surface and D is the diameter for fluid flow. The wall shear stress τ_w is calculated by,

$$\tau_w = \frac{F_w}{\pi D \Delta L} = \frac{F_w}{A_w} = \frac{\Delta P\left(\pi D^2/4\right)}{\Delta L(\pi D)} = \frac{D}{4}\frac{\Delta P}{\Delta L}. \quad \textbf{Equation 32}$$

The hydraulic radius, r_h, is defined as,

$$r_h \equiv A_{flow} / L_{perimeter}. \quad \textbf{Equation 33}$$

For a single orifice hole,

$$r_{h,o} = \frac{A_o}{\pi D_o} = \frac{D_o}{4}. \quad \textbf{Equation 34}$$

For the multi-hole Balanced Flow Meter, the hydraulic radius is,

$$r_{h,BFM} = \frac{A_{BFM}}{\pi \sum D_i}. \quad \textbf{Equation 35}$$

The single hole to multi-hole ratio of hydraulic radii is,

$$\frac{r_{h,o}}{r_{h,BFM}} = \frac{A_o \sum D_i}{A_{BFM} D_o}. \quad \textbf{Equation 36}$$

For the same pipe diameter and beta factor,

$$\frac{A_o}{A_{BFM}} = 1. \quad \textbf{Equation 37}$$

With this specification, the hydraulic radius ratio is,

$$\frac{r_{h,o}}{r_{h,BFM}} = \frac{\sum D_i}{D_o}. \quad \textbf{Equation 38}$$

Using the same pressure drop through the holes of the Balanced Flow Meter and the single-hole orifice gives,

$$\frac{\tau_{w,o}}{\tau_{w,BFM}} = \frac{r_{h,o}(\Delta P/\Delta L)_o}{r_{h,BFM}(\Delta P/\Delta L)_{BFM}} = \frac{\sum D_i}{D_o} \,. \qquad \textbf{Equation 39}$$

The tap pressure drop is less for the same flow with the Balanced Flow Meter at the same beta factor as an orifice plate. This analysis will be conservative (by approximately 10 % or less) with respect to the Balanced Flow Meter, since A_o / A_{BFM} ranges from 1.0 to 1.1.

The single-hole orifice diameter is,

$$D_o = \left(\frac{4}{\pi} A_o\right)^{1/2} . \qquad \textbf{Equation 40}$$

The Balanced Flow Meter diameters with a single center hole and two rings of outer holes are,

$$D_1 = \left(\frac{4}{\pi}\frac{A_1}{1}\right)^{1/2}, D_{i,2} = \left(\frac{4}{\pi}\frac{A_2}{n}\right)^{1/2}, D_{i,3} = \left(\frac{4}{\pi}\frac{A_3}{n}\right)^{1/2}, \qquad \textbf{Equation 41}$$

where n is the number of holes in each ring.

The shear stress ratio is,

$$\frac{\tau_{w,o}}{\tau_{w,BFM}} = \frac{\left(\frac{4}{\pi}A_1\right)^{1/2} + \sum_{i=1}^{n}\left(\frac{4}{\pi}\frac{A_2}{n}\right)^{1/2} + \sum_{i=1}^{n}\left(\frac{4}{\pi}\frac{A_3}{n}\right)^{1/2}}{\left(\frac{4}{\pi}A_o\right)^{1/2}} = \frac{(A_1)^{1/2} + (nA_2)^{1/2} + (nA_3)^{1/2}}{(A_o)^{1/2}} . \qquad \textbf{Equation 42}$$

The Balanced Flow Meter relationship of hole-areas to the single-hole orifice plate is,

$$A_o = (A_1 + A_2 + A_3)_{BFM} . \qquad \textbf{Equation 43}$$

The Balanced Flow Meter relationship of areas is,

$$X_1 A_1 = A_2 \textbf{, } X_2 A_1 = A_3 \textbf{ and } X_1 / X_2 = A_2 / A_3 \textbf{,} \qquad \textbf{Equation 44}$$

where X_1 and X_2 are multipliers greater than one and X_1 is typically less than X_2.

The area relationship is then,

$$A_o = (A_1 + X_1 A_1 + X_2 A_1)_{BFM} . \qquad \textbf{Equation 45}$$

The area ratios are,

$$\frac{A_1}{A_o} = \frac{1}{1+X_1+X_2}, \quad \frac{A_2}{A_o} = \frac{X_1}{(1+X_1+X_2)}, \text{ and } \frac{A_3}{A_o} = \frac{X_2}{(1+X_1+X_2)}. \qquad \textbf{Equation 46}$$

The corresponding shear stress ratios are,

$$\frac{\tau_{w,o}}{\tau_{w,BFM}} = \left(\frac{1}{1+X_1+X_2}\right)^{1/2} + \left(\frac{nX_1}{1+X_1+X_2}\right)^{1/2} + \left(\frac{nX_2}{1+X_1+X_2}\right)^{1/2} = \frac{1+(nX_1)^{1/2}+(nX_2)^{1/2}}{(1+X_1+X_2)^{1/2}}.$$

Equation 47

The equation above is the basis for the shear stress ratios as shown on the figure above. n is the number of holes in each ring of holes.

PTK-803 Total Head Loss Through Balanced Flow Meter Holes ©

Forward

The relations for the frictional and form-drag losses of a fluid flowing through the Balanced Flow Meter holes provides the effect of plate thickness on total head loss. The losses reported for permanent pressure loss of orifices are for thin plates, typically 1/4 inch or less. This technical document provides a basis to determine frictional and form-drag velocity head-losses with thick plates.

The friction k_{ff} and form-drag k_f head-loss factors are used to determine the hole-pressure loss from,

$$\int \frac{\partial P}{\rho} = (k_f + k_{ff}) \frac{v^2_{BFM\ hole}}{2g_c}. \qquad \textbf{Equation 48}$$

These pressure losses are in addition to the permanent pressure loss for the standard 1/4" plate thickness design.

Technical Summary

The first and second figures below show the variation of the mean-value velocity head factors for the wall-friction k_{ff} and form-friction k_f, and the sum of these factors. Experimental values are also provided for the $(k_f + k_{ff})$ sum. The second and third figures provide the point values of these same k factors. Also shown are the *vena-contracta*, free-jet effects at low x/D ratios.

Two ranges are used to provide plots for x/D_h ratios: 1) less than the crossover and 2) less than one hundred (100). The Fanning friction factor used for all plots is 0.0025 in turbulent flow. A ratio of friction factors may be used for estimation to other Reynolds numbers by,

$$k_{\mathrm{Re}>2{,}300} = \left(\frac{k}{2.5x10^4} \right) f_{Fanning} \qquad \textbf{Equation 49}$$

These plots apply to all orifice-holes, ducts or pipes of constant diameter in turbulent flow. Corrections may be obtained for the laminar and transition regimes. Flow analysis may be applied to extend these methods to two-phase flow regimes, such as annular, wave, dispersed, etc.

NASA testing with thick Balanced Flow Meter plates and data from other sources show a reduced permanent pressure loss with increasing plate thickness. As the following four figures show, values of about 1 is at a maximum. As the thickness increases, the form drag decreases rapidly, due to velocity-profile development. Frictional losses start to dominate for X/D values > ~15. For the range of $\sim 1 < X/D < \sim 15$, the k factor decreases.

Figure 5 - Balanced Flow Meter Integrated Velocity Head Loss for Plate Thickness, Large Scale

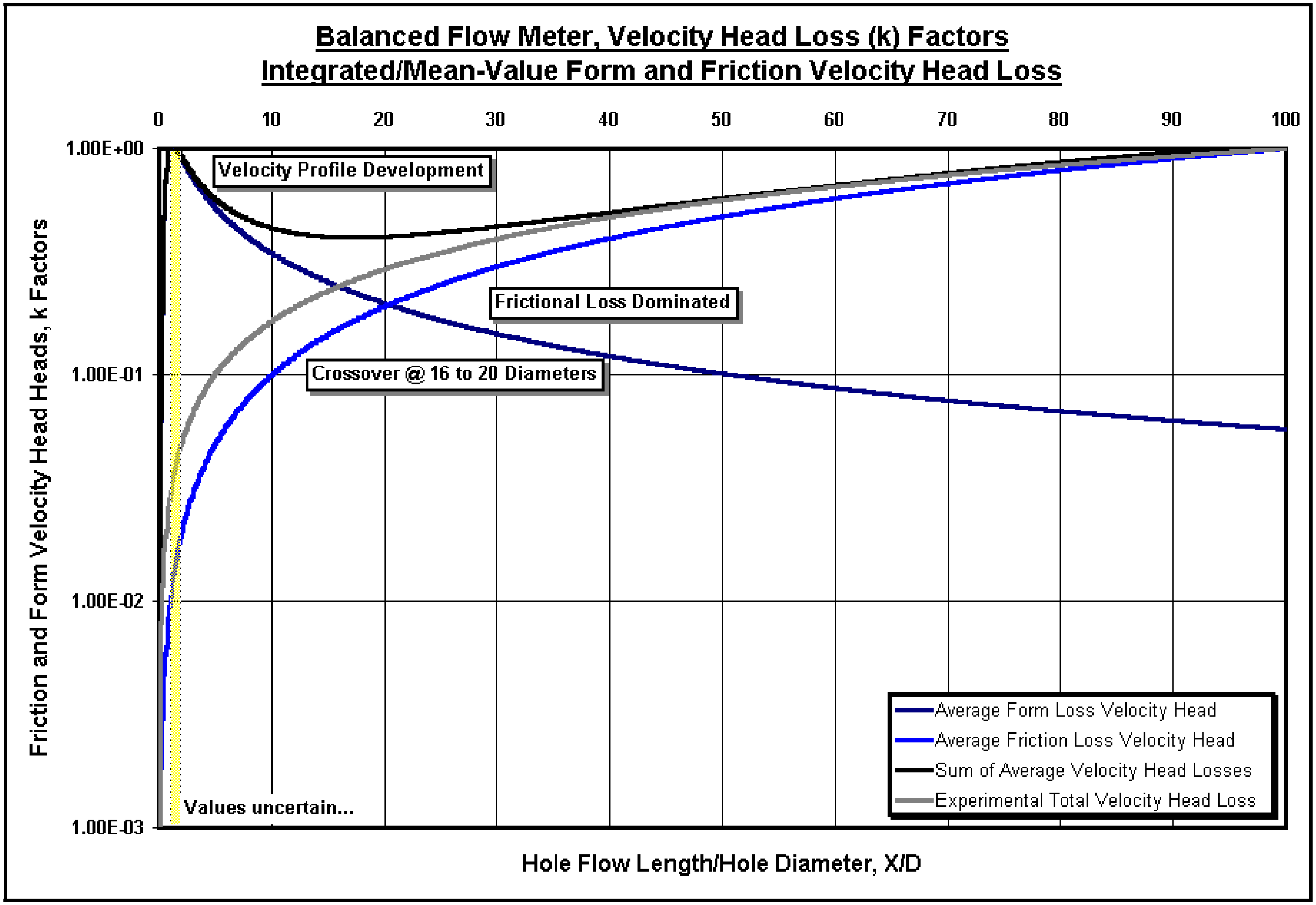

Figure 6 - Balanced Flow Meter Integrated Velocity Head Loss for Plate Thickness, Reduced Scale

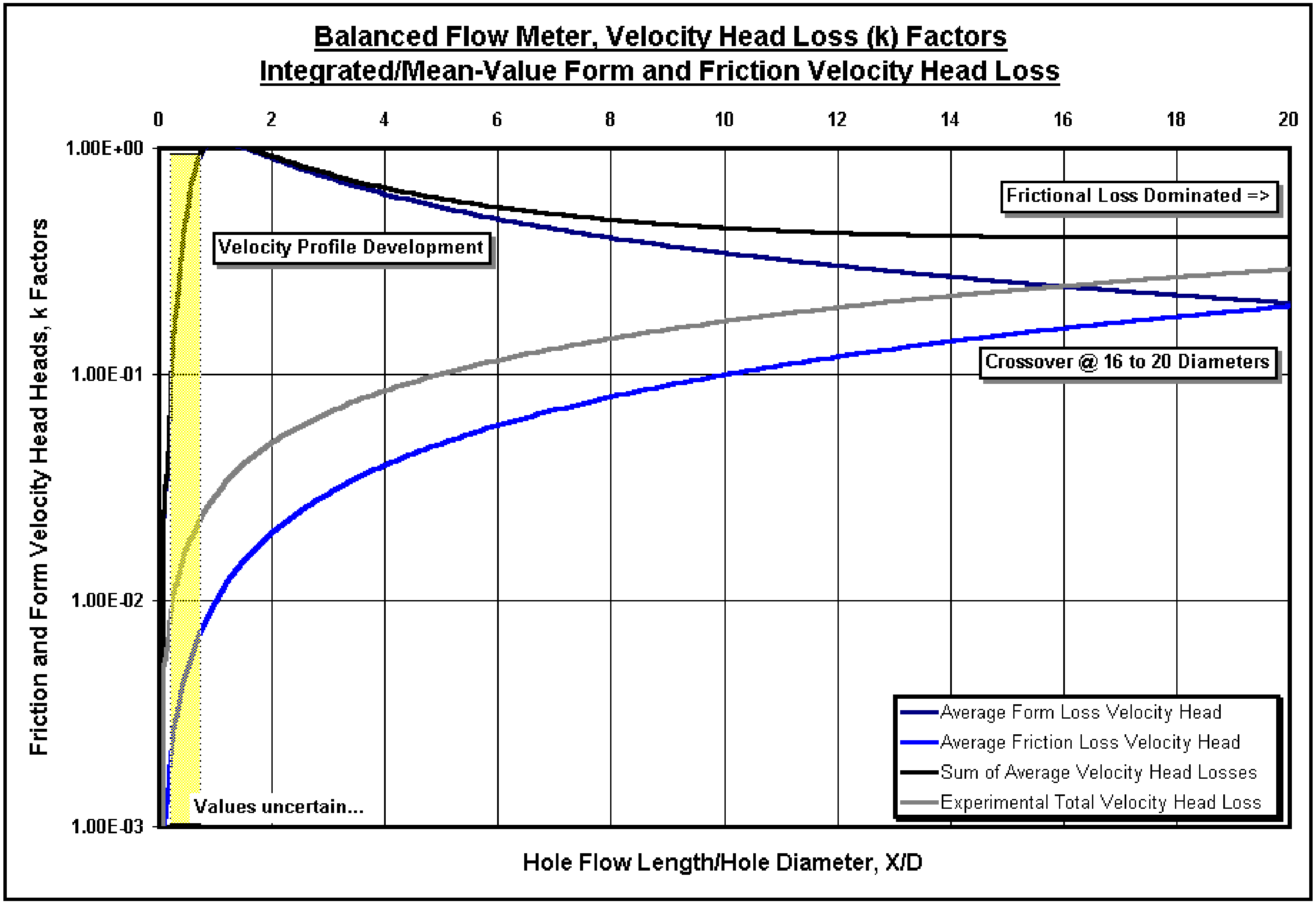

Figure 7 - Balanced Flow Meter Point Values Velocity Head Loss for Plate Thickness, Large Scale

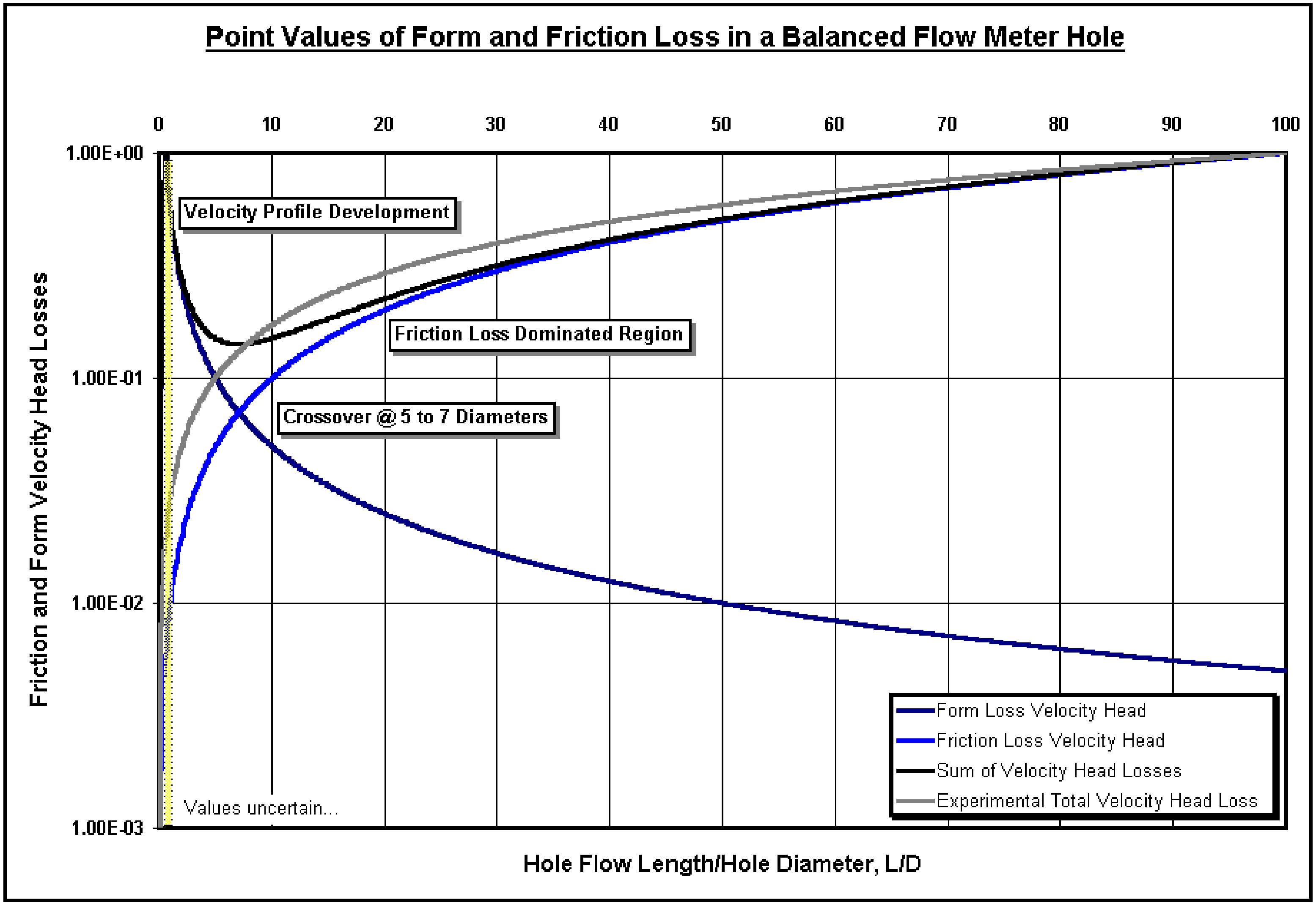

Figure 8 - Balanced Flow Meter Point Values Velocity Head Loss for Plate Thickness, Reduced Scale

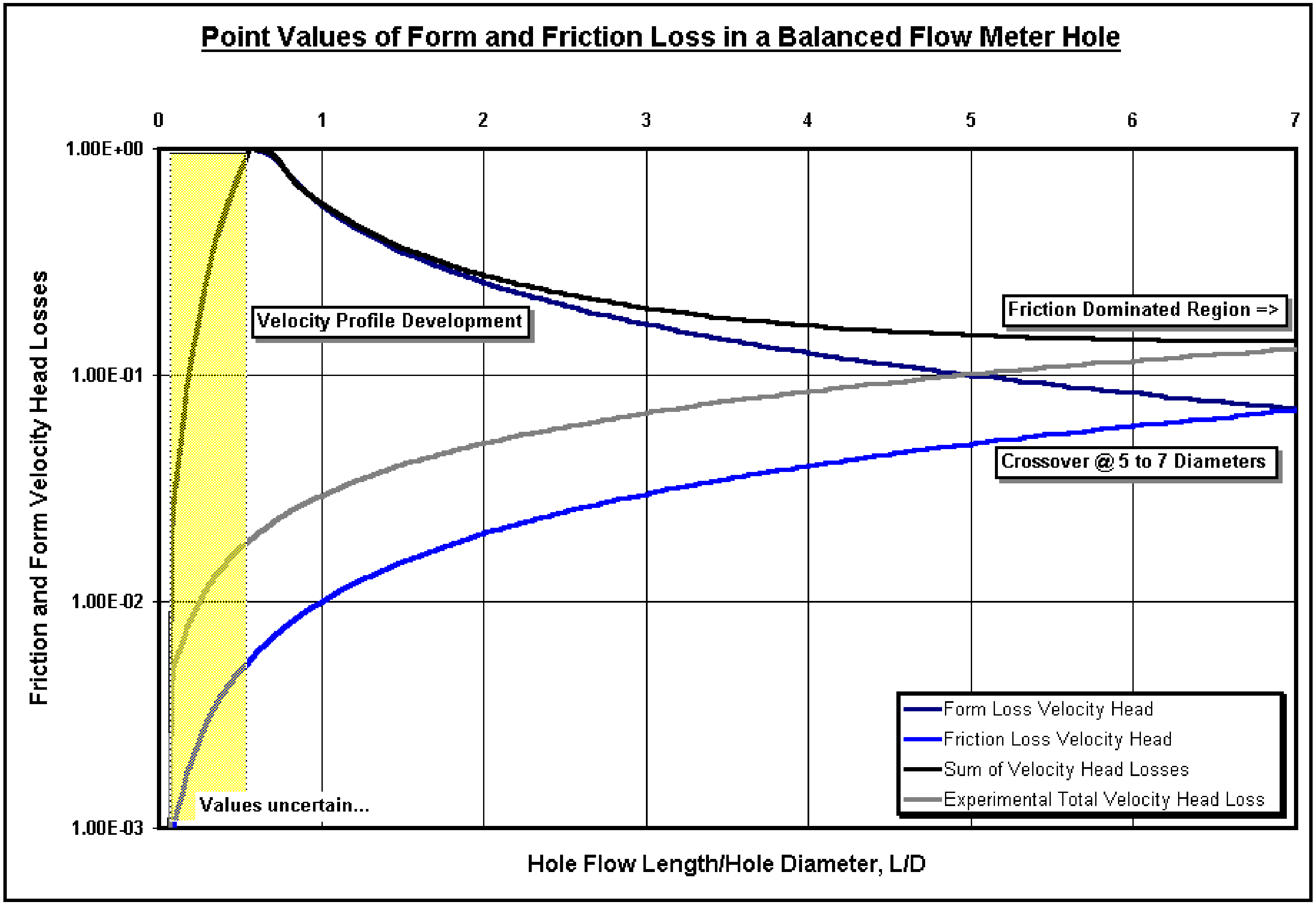

Technical Basis

The frictional velocity head-loss in turbulent flow is based on,

$$h_{L,f} = k_f \frac{v^2}{2g_c}. \qquad \textbf{Equation 50}$$

The frictional velocity head k_f is given by,

$$k_f = \frac{4fL}{D}. \qquad \textbf{Equation 51}$$

An estimate for the form-drag velocity head k_{ff} may be made from the following velocity profile changes, as dependent on hole length and position within the hole:

1) A uniform constant radial velocity where $v_{average} = v_{\max}$, at the hole-inlet.
2) A changing velocity profile that passes though a semi-parabolic flow.
3) Fully developed flow of plug-flow profile as associated with turbulent flow.

The velocity profile development for laminar and turbulent flow regimes are shown in the figures of the following table.

Table 4 - Velocity Profile Development in Laminar and Turbulent Flow Regimes

Velocity Development in Laminar Flow	Velocity Development in Turbulent Flow
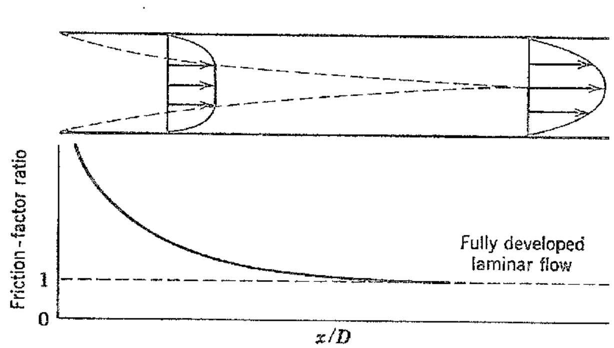	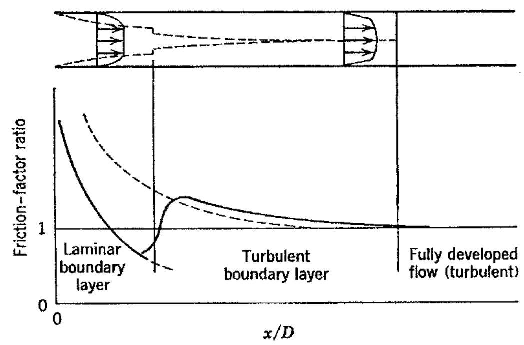

Typical velocity profiles for the parabolic-laminar and plug-flow turbulent flow regimes are shown on the following figure. The change in velocity profile causes a head-loss, or pressure drop, of the fluid as it flows through the hole due to form-drag. Form-drag dominates as the boundary layer develops, then frictional effects dominate. The effect of form-drag provides a higher-pressure loss per unit length than frictional loss

Figure 9 - Radial Velocity Distribution

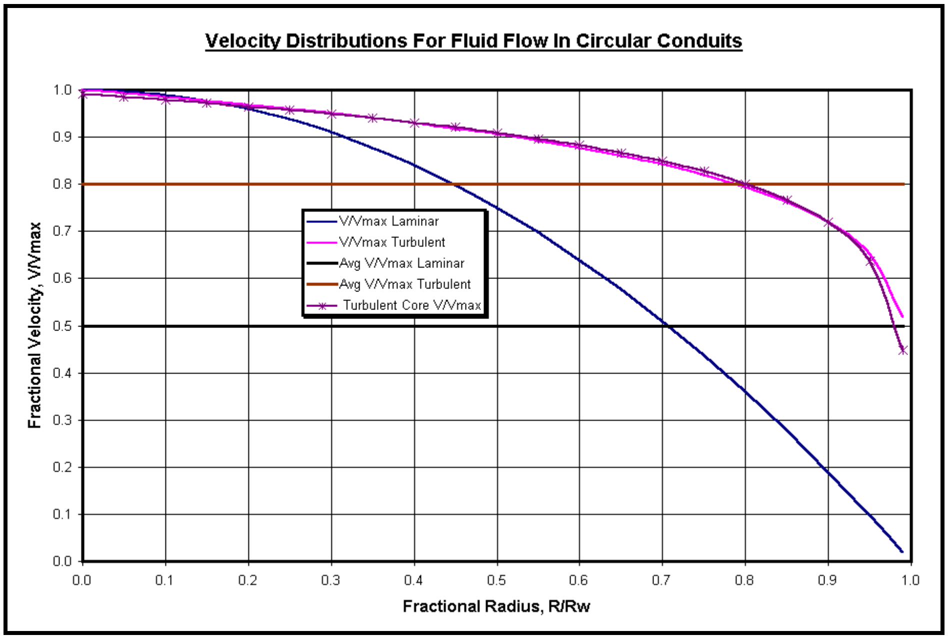

The entrance velocity head losses, which result in pressure loss, are reduced with properly designed tapers and/or using nozzle or bell-mouth designs at the inlet. As an example for a tapered inlet, the following figure shows the initial velocity profile and final profile in laminar flow.

The figure below shows the velocity profiles with a tapered inlet. With this tapered inlet design, for either laminar or turbulent flows, a reduction in pressure loss due to inlet effects are reduced.

Figure 10 - Flow Entrance Effects

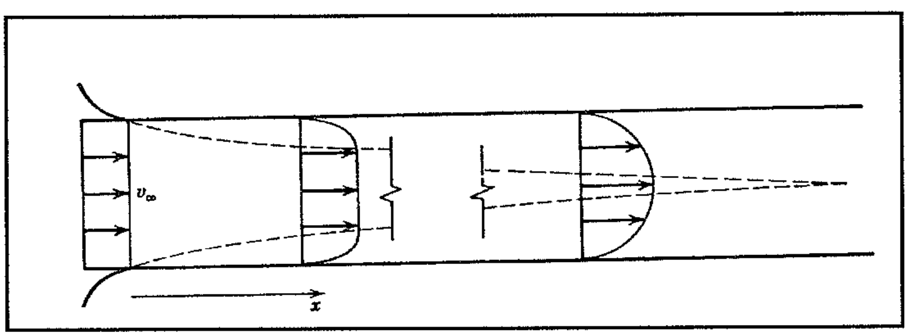

As the velocity profile shifts, from a uniform-constant velocity at the plate hole entrance to the final turbulent velocity distribution at some distance down the hole, a pressure loss occurs. These entrance effects typically last for 5 to 50 diameters dependent on Reynolds number and hole design. Frictional affects then dominate the pressure loss.

The velocity head-loss is estimated from several methods, such as change in momentum or kinetic-energy correction factors, velocity profile difference-integration, or experimental. The following figure provides experimental values for the velocity head loss, $k_{ff}\,x/D_h$, as a function of position in dimensionless units as number of hole-diameters x/D_h. This figure is based on a constant diameter entrance.

Figure 11 - Entrance Velocity Head Loss

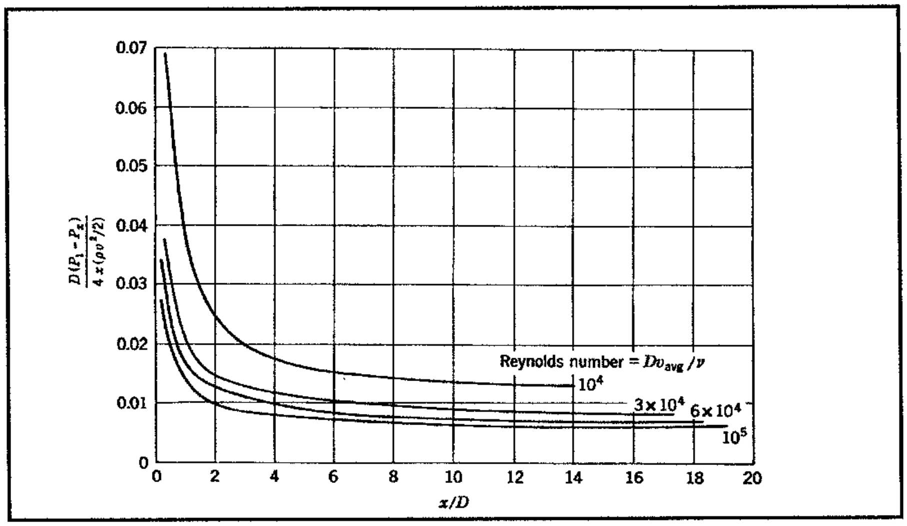

Another approach uses a turbulent-core exponential model. One such model provides the velocity profile $v_{x,r}$ in the x direction, at any r as the fluid flows through the hole,

$$\frac{v_{x,r}}{v_{avg}} = \frac{2r/x}{\exp((r/x)^2)}. \qquad \textbf{Equation 52}$$

With velocity profile changes, the velocity head-loss may be determined. Integrating across the radial flow area with a fixed diameter D_h for any hole-distance x from the entrance gives the velocity profile change or differential head-loss to position x,

$$\Phi_x = \frac{2x}{D_h}\left[\exp\left(-\left(\frac{D_h}{2x}\right)^2\right) - 1\right]. \qquad \textbf{Equation 53}$$

Evaluation with increasing values of x provides an estimation of the velocity head factors for form-friction k_{ff} as a function of position. The boundary conditions are:

1. Uniform velocity profile at $x = 0$.
2. Fully developed velocity-profile at $x/D_h \sim 7$, i.e. seven (7) diameters.
3. Maximum velocity profile change at $x/D_h < 1 : x/D_h = \pi/(\pi+2) \sim 0.61$ is used.

PTK-804 The Balanced Flow Meter Density Correction Factor ©

The general Bernoulli head-meter equation for mass flow-rate m measurement is,

$$m = \frac{C_D \gamma A_b}{\sqrt{1-\beta^4}} \sqrt{2 g_c \rho_a \Delta P} \equiv Orifice\ Equation\,, \qquad \textbf{Equation 54}$$

where ΔP is the differential pressure, ρ_a is the upstream density, g_c is the Newton's-law conversion factor, C_D is discharge coefficient, β is the diameter ratio, A_b is the area of the head-meter constriction, and γ is the density-correction factor used for <u>any</u> compressible fluid. The Orifice Equation applies to the Balanced, Orifice, Venturi, Wedge, or any "Bernoulli-Type" flow meter. This form is for flow in a horizontal pipe with an area change. It is the defining equation for mass flow in the process industries with millions of successful applications, from ideal to severe, over numerous decades.

For an ideal incompressible fluid, γ =1. For an ideal gas, γ is dependent on the head-meter design. As an example, for the standard knife-edged orifice plate, γ is given by,

$$\gamma = 1 - \frac{0.41 + 0.35\beta^4}{\lambda}\left(1 - \frac{P_b}{P_a}\right). \qquad \textbf{Equation 55}$$

The venturi and BFM density-correction factor (expansion coefficient) for an ideal gas is,

$$\gamma = \left(\frac{P_b}{P_a}\right)^{1/\lambda} \left\{ \frac{\lambda\left(1-\beta^4\right)\left[1-\left(P_b/P_a\right)^{1-1/\lambda}\right]}{(\lambda-1)\left(1-P_b/P_a\right)\left[1-\beta^4\left(P_b/P_a\right)^{2/\lambda}\right]} \right\}^{\frac{1}{2}}. \qquad \textbf{Equation 56}$$

In these equations λ is the ratio of specific heats, $\lambda = C_P / C_V$, and $P_b = P_a - \Delta P$. Values of γ for atmospheric air at various β ratios for both head-meter designs are given in the following figure for air expansion coefficients. The orifice density correction factor γ

Figure 12 - Air Expansion Coefficients and Eddy Turbulence

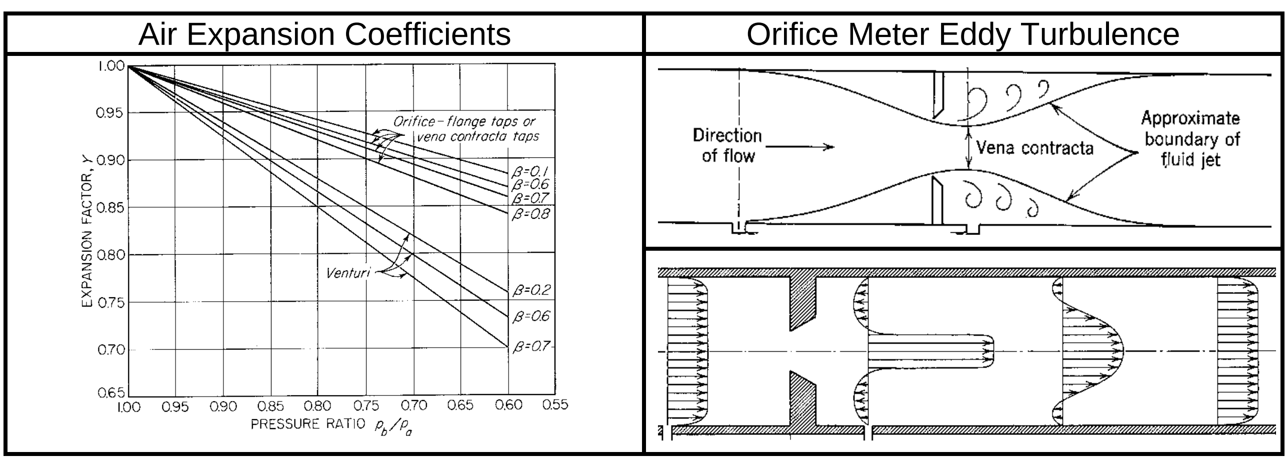

corrects for both axial and radial gas-expansion due to eddies and associated radial-velocity effects. These concentric orifice-plate flow effects are shown in the above figure for orifice meter eddy-turbulence.

The venturi meter is well known for improved accuracy, repeatability and pressure recovery when compared to the single-holed orifice plate. The venturi γ equation is based on an adiabatic-isentropic expansion of the ideal gas since the gas expands only in the axial direction. In a venturi flow tube, there are no significant radial or axial eddies, and the gas expansion is in the axial direction only, with a well-defined and uniform velocity profile in the throat as shown below.

Figure 13 - Standard Venturi Profile

Standard Venturi Tube w/Piezometer Taps	Venturi Throat & Exit Velocity Profiles
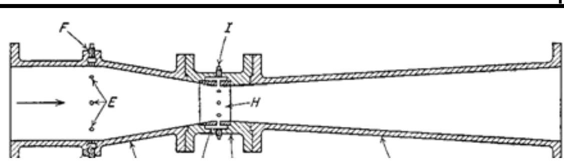	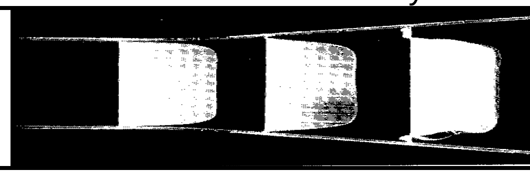

The design of the multi-holed Balanced Flow Meter (BFM) is based on the relation $\kappa\rho A v^{\sigma} =$ constant for each hole. This relation is optimized to provide the performance of a venturi flow tube in a single plate design. The following pictures provide various views for the configurations and wide applications of the Balanced Flow Meter plate.

Figure 14 - Balanced Flow Meter Plate Configurations and Applications

		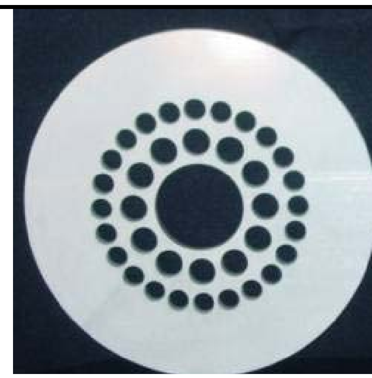
Standard Design	Mass Flow and Density Meter	2-Phase Flow

The performance of the Balanced Flow Meter follows that of the venturi meter, based on testing by NASA/Marshall Space Flight Center, and as verified by Texas A&M University, at Kingsville. The radial velocity and density variations are significantly reduced when compared to an orifice plate, as depicted on the following figure. As with the venturi tube, only axial variations of density and velocity are significant for a compressible fluid with the Balanced Flow Meter.

Figure 15 - Plate Pressure and Velocity Profiles

Orifice Plate Pressure & Velocity Profiles	BFM Plate Pressure & Velocity Profiles
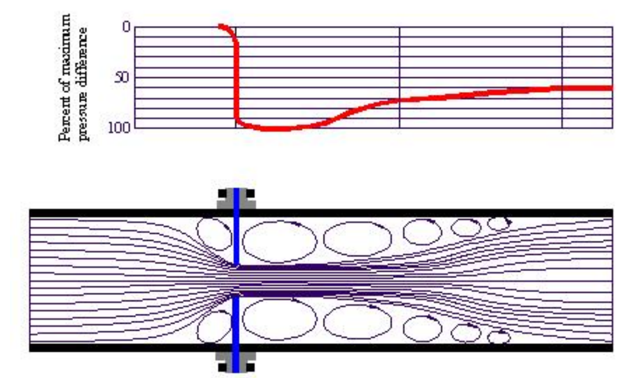	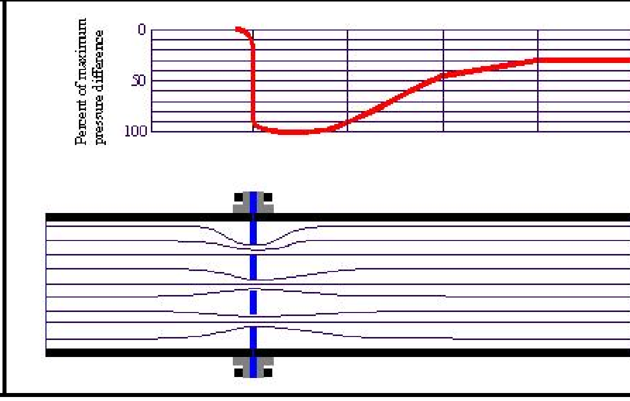

For these reasons, the venturi density-correction factor γ applies to the Balanced Flow Meter. For <u>any</u> fluid the BFM density-correction factor is determined by,

$$\gamma = \left(\frac{ \left(\frac{\Delta H}{\Delta P}\right)\left(\left(\frac{\rho}{\alpha}\right)_a (1-\beta^4)\right) }{ \left(\frac{(\alpha_b + k_f)}{\alpha_a}\left(\frac{\rho_a}{\rho_b}\right)^2 - \beta^4 \right) } \right)^{\frac{1}{2}} = \left(\frac{ \left(\frac{\Delta U + ((P/\rho)_a - (P/\rho)_b)}{\Delta P}\right)\left(\left(\frac{\rho}{\alpha}\right)_a (1-\beta^4)\right) }{ \left(\frac{(\alpha_b + k_f)}{\alpha_a}\left(\frac{\rho_a}{\rho_b}\right)^2 - \beta^4 \right) } \right)^{\frac{1}{2}}$$ **. Equation 57**

Frictional effects k_f and the kinetic energy correction factors $\alpha's$ are combined into the coefficient of discharge C_D. This approach reduces the above equation to,

$$\gamma = \left(\frac{ \left(\frac{\Delta H}{\Delta P}\right)_S (\rho_a(1-\beta^4)) }{ \left(\left(\frac{\rho_a}{\rho_{b,S}}\right)^2 - \beta^4 \right) } \right)^{\frac{1}{2}} = \left(\frac{ \left(\frac{\Delta U + ((P/\rho)_a - (P/\rho)_b)}{\Delta P}\right)_S (\rho_a(1-\beta^4)) }{ \left(\left(\frac{\rho_a}{\rho_{b,S}}\right)^2 - \beta^4 \right) } \right)^{\frac{1}{2}}$$ **, Equation 58**

where ΔH is the enthalpy change, ΔU is the internal energy change, and the S subscript is for a constant entropy path. With an equation-of-state for the fluid,

$$\gamma^2 = \left(\frac{\Delta H}{\Delta P}\left(\frac{\partial P}{\partial H}\right)_a\right)_S \frac{(1-\beta^4)}{\left(\left(\frac{\partial P}{\partial H}\right)_a^2 \left(\frac{\partial H}{\partial P}\right)_b^2 - \beta^4\right)_S}.$$ **Equation 59**

Fluid enthalpy derivatives are uniquely related for an isentropic-pressure change. This equation-of-state method provides an exact and uniform basis for fluid γ calculations.

PTK-805 The Balanced Flow Meter Mass, Momentum, Energy Balances, with "Real-Fluid" Equations-of-State and Multi-Sensors ©

Foreword

The design and sizing equations for the Balanced Flow Meter (BFM) are based on:

1. The Laws of Conservation of Mass and Energy,
2. Newton's Laws of Force, Momentum and Acceleration,
3. The Laws of Thermodynamics,
4. The Law of Corresponding States, for an Equation-of-State (EoS) with real-fluid physical, thermodynamic, and transport properties,
5. Boundary Layer Theory, with
6. The Balanced Flow Meter multi-holed sizing and layout relation, $\kappa\rho A v^{\sigma} =$ constant for each hole, that substantially reduce eddies and radial velocity and density effects.

Coupled with powerful non-linear model constrained statistical methods, such as Modified Iterative Measurement Test (MIMT©), with multiple pressure-temperature sensors, flow measurement errors may be reduced to negligible values. Also, pressure, temperature and flow sensor accuracy, repeatability and performance are monitored and verified. Continuous on-line calibration is provided with the MIMT© method.

Technical Basis

A steady flow process in which a single stream of any fluid material is flowing through any fixed-volume device is shown below.

Figure 16 - Diagram for a Steady Flow Process

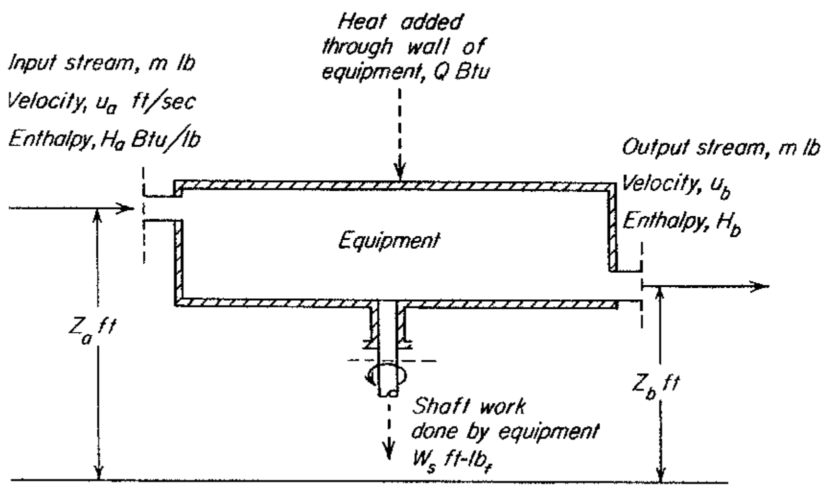

For this process, the following equation derived from technical thermodynamics applies,

$$m\left[\frac{u_b^2-u_a^2}{2g_cJ}+\frac{g(Z_b-Z_a)}{g_cJ}+H_b-H_a\right]=\dot{Q}-\frac{\dot{W}_s}{J}.$$ **Equation 60**

This is the basis used to calculate the mass flow rate by use of the Bernoulli Theorem with mass balance. With no heat or work interaction $(\dot{W}_s=\dot{Q}=0)$ and with the inlet and outlet pressure taps at the same reference elevation $(\Delta Z=0)$, the mass flow rate is,

$$m=\sqrt{\frac{2g_c\ J\Delta H}{\Delta\left(\frac{\alpha}{(\rho A)^2}\right)}}=\sqrt{\frac{2g_c\ J\Delta H_S}{\Delta\left(\frac{\alpha+k}{(\rho A)_S^2}\right)}}=\left(\frac{C_D\gamma A_b}{\sqrt{1-\beta^4}}\sqrt{2g_c\rho_a\Delta P}\equiv m\right),$$ **Equation 61**

where ΔP is the tap differential pressure, ρ_a is the upstream density, C_D is the discharge coefficient, β is the diameter ratio, A_b is the area of the head-meter constriction, and γ is the density-correction factor as used for <u>any</u> compressible fluid. The constant J is the mechanical equivalent of thermal energy and g_c is the Newton's-law conversion factor.

ΔH is the enthalpy change, ρ is the density, and the S subscript is for a constant entropy path. The enthalpies and densities are calculated from an equation-of-state for the fluid (and thermodynamic path if P,T sensor measurements are not provided).

k_f is the velocity head-loss, as developed from the momentum balance, and accounts for frictional head-losses. The kinetic energy correction factors $\alpha's$ are calculated from radial velocity distributions and range from 1 to 1.1 at Reynolds numbers above 60,000.

This equation is for horizontal flow in a pipe or conduit with area change. The mass balance for compressible flow is used, with the flow area mass-velocity defined by $\vec{G}_{a,vel}^m A_a=\vec{G}_{b,vel}^m A_b=$constant. The pipe and throat areas are measured and corrected to operating conditions for thermal and pressure dimensional changes.

The first relation of the above Bernoulli mass flow rate equation is used when multiple pressure and temperature sensors are placed up and down the flow tube and/or at the Balanced Flow Meter plate throat-holes. The second and third relations are used when estimates or measured values of upstream pressure and temperature are available along with a single measured plate ΔP. The third relation defines the Orifice Equation.

Corrections for vertical Balanced Flow Meter installations, out-of-plane gravitational fields or variable and/or directional accelerations are made by re-positioning the pressure tap locations, as applicable, or by use of the following dimensional equation,

$$m = \rho_a \, A_a \sqrt{\frac{2g_c \, J\left(H_a - H_b\right) + 2g(Z_a - Z_b)\cos(\phi)}{\alpha_a\left(\dfrac{\alpha_b}{\alpha_a}\left(\dfrac{\rho_a \, A_a}{\rho_b \, A_b}\right)^2 - 1\right)}}\,. \qquad \textbf{Equation 62}$$

With a two-phase fluid, flow-regime analysis is required to determine the homogeneous enthalpy H, density ρ, and associated kinetic energy correction factor α.

The Bernoulli equation is subject to the constraints of the mass, momentum, energy, and power balances for steady flow systems. It is also subject to the constraints of the equation of state and thermodynamics. Closure is provided when $m_a = m_b = m_c = etc.$, see the figures, on the next page for examples of these mass flow constraints.

Another flow constraint example is based on the energy rate and an equation of state,

$$\left(\frac{(PA)(\alpha v^3)}{(z\Re T)(2g_c J)} + PQ\left(\frac{c_V}{zR} + 1\right)\right)_a - \left(\frac{(PA)(\alpha v^3)}{(z\Re T)(2g_c J)} + PQ\left(\frac{c_V}{zR} + 1\right)\right)_b = 0\,. \qquad \textbf{Equation 63}$$

Q is the volume flow, c_V is the specific heat, $\Re = R / M_W$, M_W is the fluid's molecular weight, and R is the ideal gas constant. The compressibility factor for the fluid is defined from, $z = P / \rho \Re T$ as calculated by an equation-of-state of various forms.

From the Bernoulli Theorem, the total-head constraint for an adiabatic system is,

$$H_S^* = (H_S + \alpha v^2 / 2g_c)_a = (H_S + (\alpha + k + 4f / LD)v^2 / 2g_c + gZ / g_c)_{b,c,\ldots} = Const \,. \qquad \textbf{Equation 64}$$

Plots for adiabatic and isothermal systems are provided on the next page. Plots for other systems, such as 2-phase flow, variable heating/cooling, gravitational, etc, can be generated using the information of the following two tables.

The following two figures are based on the two following tables. These tables provide a summary listing of additional Bernoulli/Orifice Equation constraints for various process conditions, fluid types and thermodynamic systems as related to the Balanced Flow Meter.

Figure 17 - Head-Meter Enthalpy-Entropy Plot

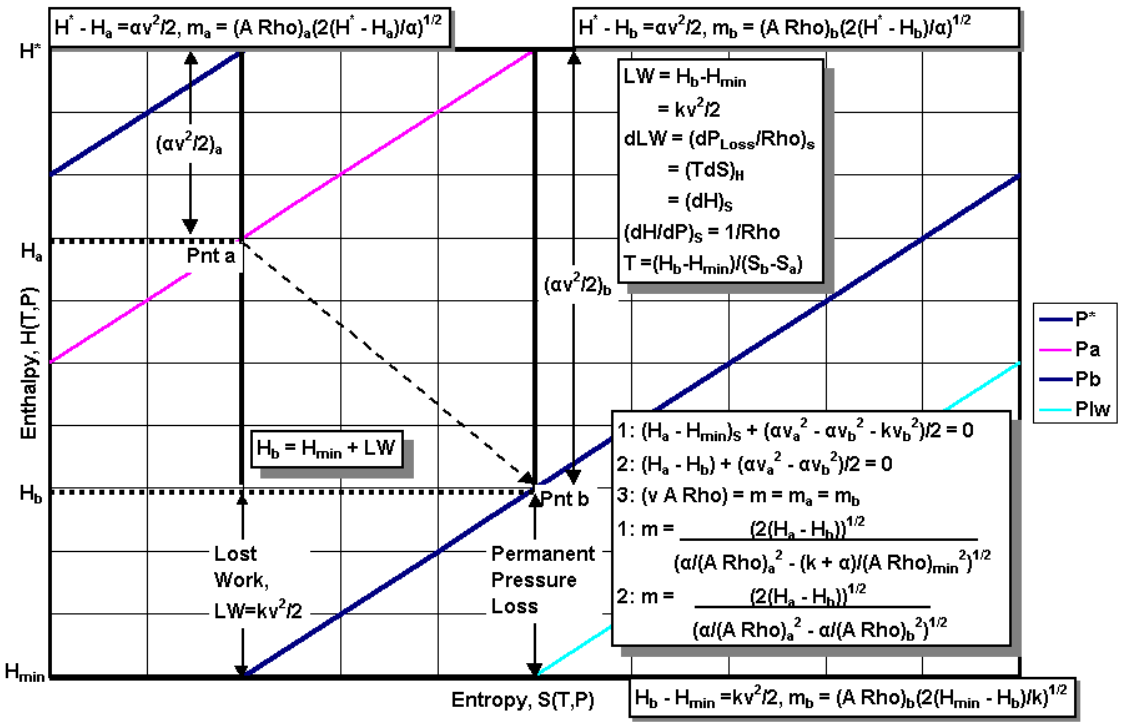

Figure 18 - Head-Meter Gibbs Free Enthalpy-Temperature Plot

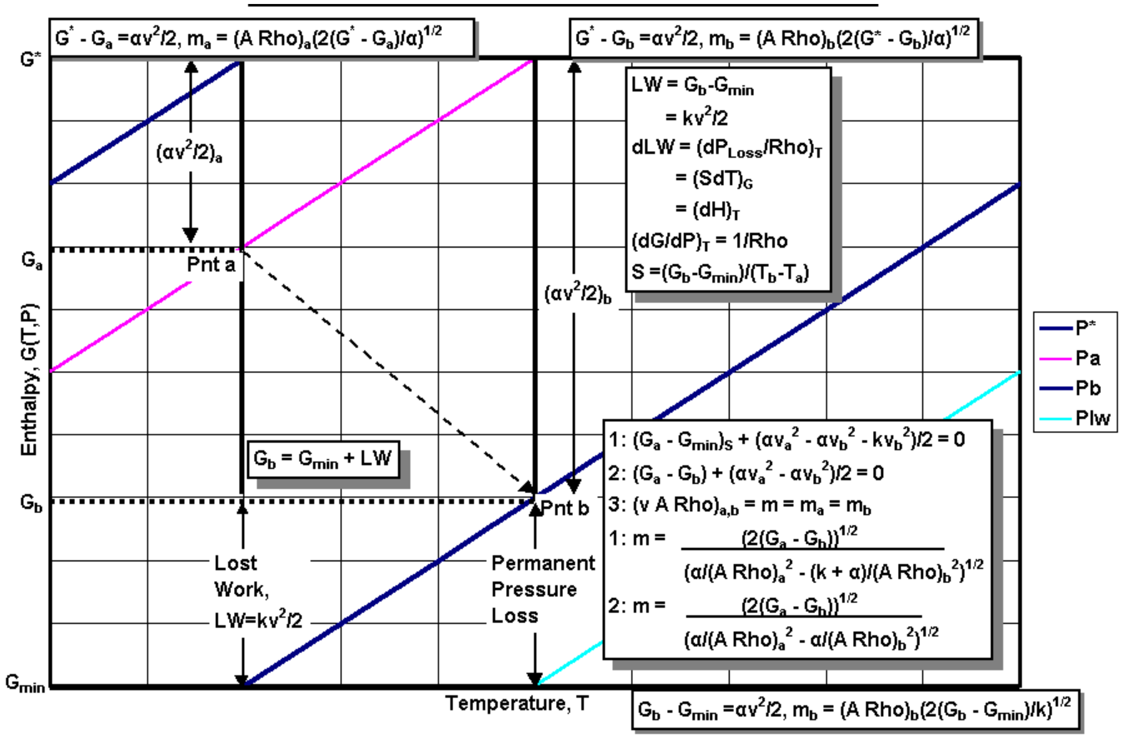

Note: Use absolute values with $\sqrt{\|\Delta' s\|}$ **.**

Table 5 - Summary Balanced Flow Meter Mass, Momentum and Energy Equations

FLUID FLOW MASS, MOMENTUM, ENERGY AND ENERGY RATE EQUATIONS		
Balance	Special Form	Steady State
Mass	Single Stream	$\Delta\, m = 0, \quad m_a = m_b = Const.$ $(\rho A v)_a = (\rho A v)_a = Const.$ $v = \dfrac{\vec{G}z(P,T)\Re T}{P}$ $at\ any\ a\ or\ b,\ \&\ \vec{G} \equiv m / A$
Momentum	Control Volume of mass m_{tot}	$F = -\Delta\left(\dfrac{1}{g_c}\dfrac{\langle v^2\rangle}{\langle v\rangle} m + PA\right) + m_{tot}\dfrac{g}{g_c}$
Entropy	$E_f = \int_a^b \dfrac{dP_f}{\rho} \equiv \dfrac{kv^2}{2g_c}$	$\int_a^b TdS = Q + E_f : \Delta S = \dfrac{Q}{T_{ref}} + \dfrac{E_f}{T_{ref}}$
Total Energy-Bernoulli Theorem Head-Form	Any Path	$\Delta\left(U + P/\rho + \dfrac{1}{2g_c J}\dfrac{\langle v^3\rangle}{\langle v\rangle} + \Phi_{PE}\right) = Q - W_{Shaft}$
Mechanical Energy-Bernoulli Theorem Head-Form	Isothermal	$\Delta\left(\dfrac{1}{2g_c J}\dfrac{\langle v^3\rangle}{\langle v\rangle} + \Phi_{PE} + G_T\right) + W_{Shaft} + E_f = 0$
	Isentropic	$\Delta\left(\dfrac{1}{2g_c J}\dfrac{\langle v^3\rangle}{\langle v\rangle} + \Phi_{PE} + H_S\right) + W_{Shaft} + E_f = 0$
Bernoulli Equation Combined Entropy & Enthalpy Form	Path Dependent	$\Delta\left(\dfrac{1}{2g_c J}\dfrac{\langle v^3\rangle}{\langle v\rangle}\right) + \Delta\Phi_{PE} + \int_a^b \dfrac{dP}{\rho} + W_{Shaft} + E_f = 0$
Entropy Rate	Any Path	$\Delta(S(\rho A v)) = \dfrac{\dot{Q}}{T_\sigma} + \dfrac{mE_f}{T_\sigma}$
Total Energy Rate	Any Path	$\Delta\left[\left(U + P/\rho + \dfrac{1}{2g_c J}\dfrac{\langle v^3\rangle}{\langle v\rangle} + \Phi_{PE}\right)(\rho A v)\right] =$ $\dot{Q} - \dot{W}_{Shaft}$
Mechanical Energy Rate	Isothermal	$\Delta\left[\left(\dfrac{1}{2g_c J}\dfrac{\langle v^3\rangle}{\langle v\rangle} + \Phi_{PE} + G_T\right)(\rho A v)\right]$ $+ \dot{W}_{Shaft} + mE_f = 0$

Mechanical Energy Rate	Isentropic	$\Delta\left[\left(\frac{1}{2g_cJ}\frac{\langle v^3\rangle}{\langle v\rangle}+\Phi_{PE}+H_S\right)(\rho Av)\right]$ $+\dot{W}_{Shaft}+mE_f=0$
Bernoulli Equation Combined Entropy & Enthalpy Rate	Path Dependent	$\Delta\left(\frac{(\rho Av)}{2g_cJ}\frac{\langle v^3\rangle}{\langle v\rangle}\right)+\Delta m\Phi_{PE}+\int_a^b\frac{(\rho Av)dP}{\rho}$ $+\dot{W}_{Shaft}+mE_f=0$

Table 6 - Summary BFM Equations-of-State & Thermodynamic Paths

FLUID-FLOW EQUATIONS-OF-STATE AND THERMODYNAMIC PATHS		
Fluid Type	Basic Form	Thermodynamic Path
Ideal Gas $\rho=\frac{\Re T}{P}$ $\lambda=\Theta\delta=\frac{C_P}{C_V}$ $\left(\frac{dU}{dP}\right)_T=0$	Isothermal $P/\rho=Const.$	$\Delta G_T=\int_a^b\frac{dP}{\rho}=\Re TLn\left(\frac{P_b}{P_a}\right)$
	Isentropic $P/\rho^{\lambda}=Const.$ $T/\rho^{\lambda-1}=Const.$	$\Delta H_S=\int_a^b\frac{dP}{\rho}=\int_a^b C_P dT=\frac{\lambda}{\lambda-1}\left[\left(\frac{P_b}{P_a}\right)^{\frac{\lambda-1}{\lambda}}-1\right]\frac{P_a}{\rho_a}$
	Bernoulli $P/\rho^{\delta}=Const.$ $T/\rho^{\delta-1}=Const.$	$\int_a^b\frac{dP}{\rho}=\frac{\delta}{\delta-1}\left[\left(\frac{P_b}{P_a}\right)^{\frac{\delta-1}{\delta}}-1\right]\frac{P_a}{\rho_a}$
	Any Path	$\Delta H=\int_a^b dU+\int_a^b d\left(\frac{P}{\rho}\right)=\int_a^b TdS+\int_a^b\frac{dP}{\rho}=\hat{C}_{P,lm}(T_b-T_a)$
Incompressible Liquid $\rho_a=\rho_b$ $C_P=C_V=\hat{C}$	Isothermal	$\Delta G_T=\int_a^b\frac{dP}{\rho}=\frac{P_b-P_a}{\hat{\rho}}$
	Isentropic	$\Delta H_S=\int_a^b\frac{dP}{\rho}=\frac{P_b-P_a}{\hat{\rho}}$
	Bernoulli	$\int_a^b\frac{dP}{\rho}=\frac{P_b-P_a}{\hat{\rho}}$
	Any Path	$\Delta H=\int_a^b dU+\int_a^b d\left(\frac{P}{\rho}\right)=\hat{C}(T_b-T_a)+\frac{P_b-P_a}{\hat{\rho}}$
Single Phase $Ln\left(\frac{\rho_b}{\rho_a}\right)=\kappa(P_b-P_a)-\varepsilon(T_b-T_a)$ $\Delta T,\Delta P\le\delta X\Rightarrow$ $\kappa=Const.$ $\varepsilon=Const.$ $\left(\frac{\partial\rho}{\rho}\right)_S=\kappa_s dP$	Isothermal	$\Delta G_T=\int_a^b\frac{dP}{\rho}=\frac{1}{\kappa}\left(\frac{1}{\rho_b-\rho_a}\right)$
	Isentropic	$\Delta H_S=\int_a^b\frac{dP}{\rho}=\frac{1}{\kappa}\left(\frac{1}{\rho_b-\rho_a}-\varepsilon(T_b-T_a)\right)$
	Bernoulli	$\int_a^b\frac{dP}{\rho}=\frac{1}{\kappa}\left(\frac{1}{\rho_b-\rho_a}-\varepsilon(T_b-T_a)\right)=\frac{\kappa_S}{\rho_a}\left(e^{\kappa_S\Delta P}-1\right)$
	Any Path	$\Delta H=\int_a^b dU+\int_a^b d\left(\frac{P}{\rho}\right)=C_{V,lm}(T_b-T_a)+\frac{P_b}{\rho_b}-\frac{P_a}{\rho_a}$

Single Phase $\rho=\frac{z(T,P)\Re T}{P}$ $P/\rho^{\delta} = Const.$	Isothermal	$\Delta G_T = \int_a^b \frac{dP}{\rho} = Ln\left(\frac{P_b}{P_a}\right)\frac{(P_b/\rho_b - P_a/\rho_a)}{Ln\left(\frac{P_b/\rho_b}{P_a/\rho_a}\right)}$
	Isentropic	$\Delta H_S = \int_a^b \frac{dP}{\rho} = Ln\left(\frac{P_b}{P_a}\right)\frac{(P_b/\rho_b - P_a/\rho_a)}{Ln\left(\frac{P_b/\rho_b}{P_a/\rho_a}\right)}$
	Bernoulli	$\int_a^b \frac{dP}{\rho} = Ln\left(\frac{P_b}{P_a}\right)\frac{(P_b/\rho_b - P_a/\rho_a)}{Ln\left(\frac{P_b/\rho_b}{P_a/\rho_a}\right)}$
	Any Path	$\Delta H = \int_a^b dU + \int_a^b d\left(\frac{P}{\rho}\right) = C_{V,lm}(T_b - T_a) + \frac{P_b}{\rho_b} - \frac{P_a}{\rho_a}$
Real Fluid $\rho=\frac{z(T,P)\Re T}{P}$ $properties = f(T,P)$ $\Delta H = \Delta H_S / \eta_S$ $\phi_S, \eta_S = f(path)$	Isothermal	$\Delta G_T = (H_b - H_a)_T - T(S_b - S_a)_T$
	Isentropic	$\Delta H_S = (U_b - U_a)_S + ((P/\rho)_b - (P/\rho)_a)_S$
	Bernoulli	$\int_a^b \frac{dP}{\rho} = Ln\left(\frac{P_b}{P_a}\right)\frac{(P_b/\rho_b - P_a/\rho_a)/\phi_S}{Ln\left(\frac{P_b/\rho_b}{P_a/\rho_a}\right)}$
	Any Path	$\Delta H = \int_a^b dU + \int_a^b d\left(\frac{P}{\rho}\right) = U_b - U_a + \frac{P_b}{\rho_b} - \frac{P_a}{\rho_a}$

PTK-806 Balanced Flow Meter, Kinetic and Momentum Correction Factors ©

$u^2/2g_c$ is the kinetic energy of a pound mass of fluid flowing with the kinetic velocity u across the pipe flow area. The kinetic velocity may not be the same as the average flow velocity v determined by mass balance. The relation is $u^2 = \alpha v^2$, where α is the kinetic energy correction factor. α is calculated by the kinetic energy per pound E_K of fluid by,

$$E_K = \frac{\dot{E}_K}{m} = \frac{u^2}{2g_c} = \frac{\alpha v_{avg}^2}{2g_c} = \frac{1}{2g_c}\frac{\langle v_r^3 \rangle}{\langle v_r \rangle} = \frac{1}{2g_c}\frac{\int^A v_r^3 dA}{\int^A v_r dA} = \frac{1}{2g_c}\frac{\int_0^{2\pi}\int_0^R v_r^3 r dr d\theta \Big/ \int_0^{2\pi}\int_0^R r dr d\theta}{\int_0^{2\pi}\int_0^R v_r r dr d\theta \Big/ \int_0^{2\pi}\int_0^R r dr d\theta} \quad \textbf{Equation 65}$$

v_{avg} is calculated from $v_{avg} = m/\rho A$. For this integration, the local average velocity v_r, for axial velocity $\vec{x}$ flow, must be known as a function of radius r and angle θ within the pipe. A similar procedure is used for the momentum correction factor β. The velocity profiles v_r for developed laminar or turbulent flows are shown in the following figure.

Figure 19 - Developed Flow Velocity Distributions and Locations

<table>
<tr><th>Developed-Flow Velocity Distributions</th><th>Developed-Flow Locations</th></tr>
<tr><td>

Laminar:

$$\frac{v_r}{v_{r=0}} = 1 - \left(\frac{r}{R}\right)^2$$

Turbulent, Smooth & Rough:

$$\frac{\kappa(v_r - v_{r=0})}{v_{avg}\sqrt{f/2}} = Ln\left(1 - \frac{r}{R}\right)$$

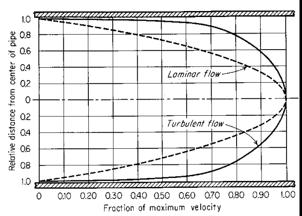

</td><td>

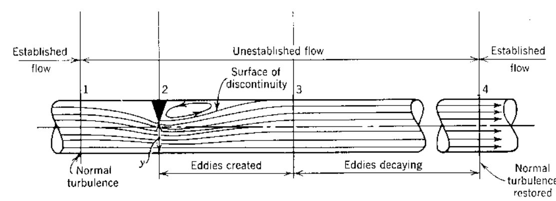

</td></tr>
</table>

For standard head-meter design, fully developed flow is normally taken as 5 to 10 diameters, or more, upstream and downstream of the plate or constriction. An additional 5 to 10 diameters are required upstream for any fittings that may be in the pipe. The locations for established flow are shown as points 1 and 4 in the above figure. The Balanced Flow Meter design provides operations below 2 pipe diameters.

Figure 20 - Universal Velocity Distribution and Effects of Pipe Roughness

<table>
<tr><th>Pipe Universal Velocity Distribution</th><th>Effects of Pipe Roughness</th></tr>
<tr><td>

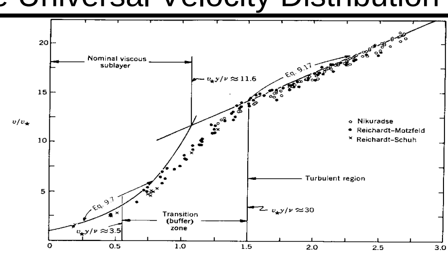

</td><td>

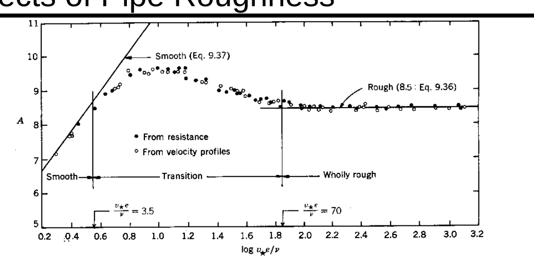

</td></tr>
</table>

Velocity distributions for pipe turbulent fluid flow have been experimentally determined. They follow a universal velocity profile through the viscous sub layer, near the pipe wall, to the turbulent region for any size pipe. The turbulent region dominates the flow area.

The universal velocity distribution is used as the basis for determining profiles in turbulent pipe flows. For laminar and turbulent pipe flows, the length requirements, velocity distributions, average velocity, momentum and kinetic energy correction factors, and Fanning friction factor calculation methods are provided, see next page. On this basis, the momentum and kinetic energy correction factors are determined for the pipe flow areas up and downstream of the Balanced Flow Meter (BFM) Plate for standard designs. The following tables provide a summary of calculated values for smooth pipes with various Reynolds numbers Re and velocity-distribution, power-law exponents n.

Table 7 - Smooth Pipe & Tube Friction Factors and Velocity Ratios for Reynolds Numbers Re

Re	Laminar	Turbulent 4x10^3	10^4	10^5	10^6	10^7
f	0.08 to >1	0.00998	0.00773	0.0045	0.0029	0.00203
$v_{avg}/v_{r=0}$	1/2	0.794	0.814	0.852	0.877	0.895

Table 8 - Kinetic Energy α **and Momentum** β **Correction Factors for Velocity Exponents** n

$1/n$	Laminar 1/2	Turbulent 1/5	1/6	1/7	1/8	1/9
α	2.0	1.106	1.077	1.058	1.046	1.037
β	4/3	1.037	1.027	1.020	1.016	1.013

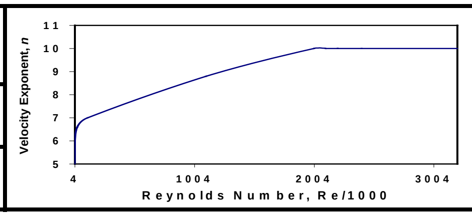

The direct application of these correction factors depends on the tap location. Typical Balanced Flow Meter tap locations are shown on the following table. For pipe taps, this

Table 9 - Typical Balanced Flow Meter Tap Locations

Type of Tap. (Throat tap (s) not listed.)	Distance of upstream tap to front face of plate.	Distance of downstream tap to back face of plate.
Corner	1/4 inch	1/4 inch
Flange	1 inch	1 inch
Vena contracta	1 pipe diameter (actual ID)	0.3 to 0.8 pipe diameters
Pipe	2.5 nominal pipe diameters	8 nominal pipe diameters

direct application may be acceptable. For other pipe tap locations and for flow through the plate, a constrained integration across the flow areas is used. The constraints for each BFM hole of $\kappa\rho A v^{\sigma} =$ constant with a layout of $v_r / v_{r=0} = (1 - r/R)^{1/n}$ are used to minimize discontinuities. Uniform hole-velocities with pipe velocity profiles constrained by mass, momentum, energy and power balances, and as coupled with boundary layer theory, provide the α & β correction factors and power exponent n for each position up or downstream and through the BFM. These methods have been tested and verified.

Results show that the Balanced Flow Meter performance for pressure recovery, accuracy and repeatability are not significantly affected by upstream or downstream disturbances, and fitting L/D distances of two (2) or less may be used.

Table 10 - Velocity Distributions, Correction and Friction Factors for Developed Pipe & Tube Flow

Laminar Flow, $\mathrm{Re} < 2{,}300$	Turbulent Flow, $\mathrm{Re} > 3{,}000$
Length for Fully Developed Flow	
$\frac{L}{D} = 0.06\,\mathrm{Re}$	$\frac{L}{D} = 4.4\,\mathrm{Re}^{1/6}$
Velocity Distribution, Power Law	
$\frac{v_r}{v_{r=0}} = 1 - \left(\frac{r}{R}\right)^2$	$\frac{v_r}{v_{r=0}} \cong \left(1 - \frac{r}{R}\right)^{\frac{1}{n}}$
Average Velocity	
$\frac{v_{avg}}{v_{r=0}} = \frac{1}{2}$	$\frac{v_{avg}}{v_{r=0}} = \frac{2n^2}{(n+1)(2n+1)}$ Universal Velocity Law $\frac{v_{avg}}{v_{r=0}} = \frac{1}{1+3\sqrt{(f/2)/(2\kappa)}}$
Momentum Correction Factor	
$\beta = \frac{4}{3}$	$\beta = \frac{(1+n)^2(2+n)^2}{2(1+2n)(2+n)}$ Universal Velocity Law $\beta = 1 + \frac{5f}{8\kappa^2}$
Kinetic Energy Correction Factor	
$\alpha = 2$	$\alpha = \frac{(1+n)^3(2+n)^3}{4(1+3n)(2+3n)}$ Universal Velocity Law $\alpha = 1 + \frac{f}{8\kappa^2}\left(15 - \frac{9}{\kappa}\sqrt{f}\right)$

<table>
<tr><td colspan="2">Fanning Friction Factor</td></tr>
<tr><td>$f = \frac{16}{\mathrm{Re}}$</td><td>$\frac{1}{\sqrt{f/2}} = \frac{1}{\kappa} Ln\left(\mathrm{Re}\sqrt{\frac{f}{8}} \right) - \frac{3}{2\kappa} + \varepsilon$</td></tr>
<tr><td colspan="2">$\mathrm{Re} \equiv \frac{D\vec{G}}{\mu} \cong const.$, $\vec{G}_{@\, any\, \vec{x}} \equiv m / A = const.$, $v_{\max} @ r = 0$, $\kappa \cong 0.407$, $\varepsilon \cong 5.67$.
Friction factors applicable to smooth pipes and subsonic flows.</td></tr>
</table>

Table 11 - Turbulent Flow Properties for Rough Pipes & Tubes

Velocity Distributions and Velocity Ratio	
Radial Velocity, $v_{\max} @ r=0$	$\frac{v_r}{v_{r=0}} \cong \left(1-\frac{r}{R}\right)^{\frac{1}{n}}$
Average Velocity	$\frac{v_{avg}}{v_{r=0}} = \frac{1}{1+10\kappa\sqrt{(f/2)}} = \frac{2n^2}{(n+1)(2n+1)}$
Friction Factors with Relative Roughness Factor (e/D)	
Turbulent Flow, Fully Rough $(D/e)/(\mathrm{Re}\sqrt{f}) \le 0.01$	$\frac{1}{\sqrt{2f}} = Log\left(\frac{D}{e}\right)+B$
Turbulent Smooth/Rough Transition Flow	$\frac{1}{\sqrt{2f}} = Log\left(\frac{D}{e}\right) - Log\left(\frac{(\varepsilon-1)(D/e)}{\mathrm{Re}\sqrt{f}}+1\right)+B$
$f \pm 1.5\%, 10^8 \ge \mathrm{Re} \ge 10^4, 0.05 \ge e/D \ge 0 \Rightarrow$	$\frac{1}{\sqrt{f}} = -3.6 Log\left[\frac{6.9}{\mathrm{Re}}+\left(\frac{(e/D)}{3.7}\right)^{\frac{10}{9}}\right]$
$\mathrm{Re} \equiv \frac{D\vec{G}}{\mu} \cong const.$, $\vec{G}_{@\,any\,\bar{x}} \equiv m/A = const.$, $\kappa \cong 0.407$, $\varepsilon \cong 5.67$, $B = 2.28$, $Log = Log_{10}$	

Figure 21 - Fanning Friction Factors and Roughness Parameters for Pipes & Tubes, e in feet

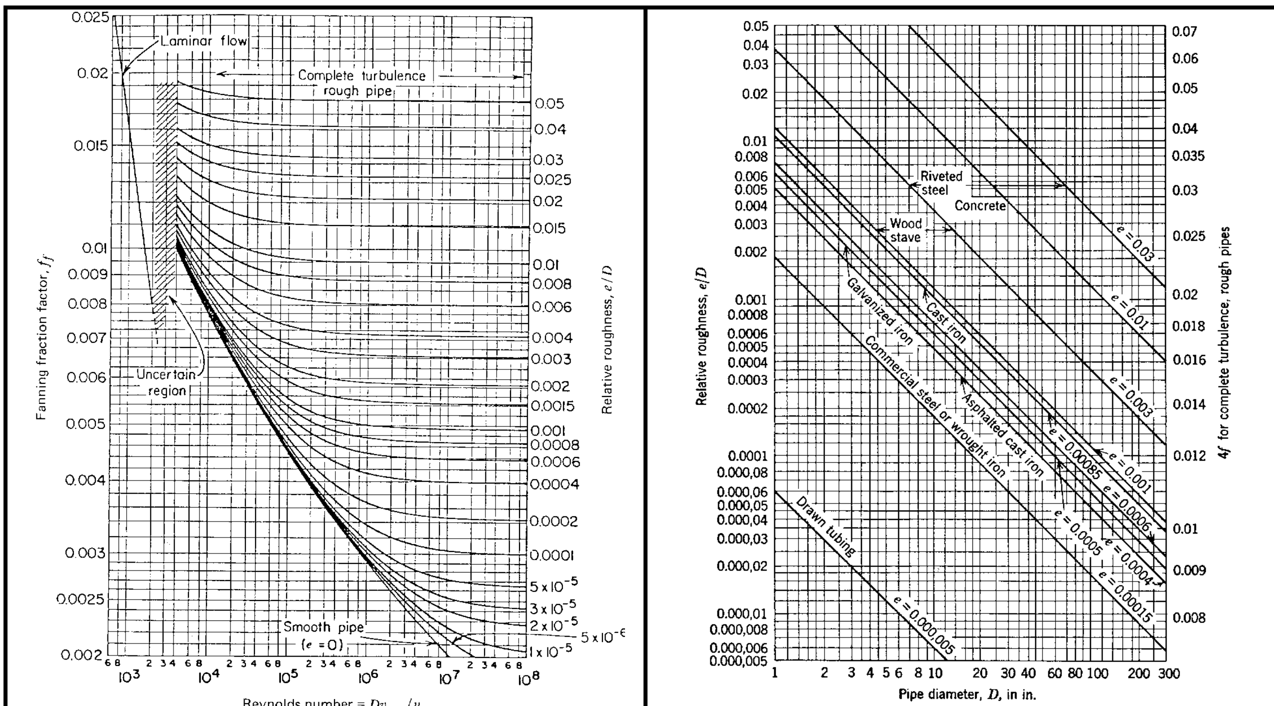

PTK-807 The Balanced Flow Meter Discharge Coefficient ©

The orifice discharge coefficient C_D corrects for the actual flow when compared to the ideal isentropic $(S = Const.)$ flow for the same pressure conditions. It is defined as,

$$C_D \equiv \frac{m_{actual}}{m_{S,ideal}}, \qquad \textbf{Equation 66}$$

and is originally determined by experiment. Accurate values (error <0.25 percent) are provided in numerous publications for a broad arrangement of head-meter configurations with graphs and equations for a large range of flows. The above definition is for any fluid phase. General dimensional analysis shows that for any fluid,

$$\frac{1}{C_D^2} = \frac{\int dP/\rho}{\left(v^2/2g_c\right)} = F\left(\mathrm{Re}, W, M, \beta, e/D, l_1/D, l_2/D\right). \qquad \textbf{Equation 67}$$

Re is the Reynolds number for viscous flow, W is the Weber number for surface tension effects typically for Reynolds numbers below 500 or two-phase flows, M is the Mach number for gas, vapor or liquid compressible flow (from $(dp/d\rho)_S$ for any fluid), β is the beta factor defined by the ratio of diameters $(D_{hole}/D_{pipe})_{ref}$, e is the pipe roughness parameter for velocity profiles and friction factors, and l_1 and l_2 are dimensional characteristics for 1) upstream, downstream lengths, 2) multi-hole pitch and diameters, and 3) pressure and temperature tap locations. The C_D coefficient is related to the velocity-head loss factor k_f by the location dependent (l/D) equation,

$$k_{f,PH} = \left(\frac{1}{(\gamma C_{D,PH})^2} - 1\right)\left(\frac{(1-\beta^4)}{\beta^4}\right)_{to\ plate\ hole} \quad or\ k_{f,PT} = \left(\frac{(1-\beta^2)(1-\beta^4)}{\beta^4 (\gamma C_{D,PT})^2}\right)_{pipe\ taps} \quad \left(Note,\ k_{ff,pipe} = \frac{4fL}{D}\right)$$

Equation 68

The discharge coefficient C_D is used to calculate a corrected flow from the general Bernoulli orifice equation as shown below (shown earlier is a rigorous definition for C_D),

$$m_{actual} = \sqrt{\frac{2g_c J \Delta H_S}{\left(\frac{\alpha + k_f}{(\rho A)_S^2}\right)_b - \left(\frac{\alpha}{(\rho A)_S^2}\right)_a}} = \frac{C_D \gamma A_b}{\sqrt{1-\beta^4}}\sqrt{2g_c \rho_a \Delta P}. \qquad \textbf{Equation 69}$$

For the equation on the right, ΔP is the tap differential pressure, ρ_a is the upstream density, β is the diameter ratio, A_b is the area of the head-meter constriction, and γ is the density-correction factor as used for any compressible fluid. The constant J is the mechanical equivalent of thermal energy and g_c is the Newton's-law conversion factor.

ΔH_S is the enthalpy change, ρ_S is the density, and the S subscript is for a constant entropy path. The enthalpies and densities are calculated from an equation-of-state for the fluid. Upstream pressure and temperature measurements are typically used for inlet enthalpy and density calculations. An outlet pressure or ΔP is used to calculate the down stream enthalpy, temperature and density as based on an isentropic path.

k_f is the velocity head-loss, as developed from the mass, momentum and energy balances, and accounts for frictional head-losses from $(dP_f/\rho)_{LW} = -k_f v dv/g_c$. As $k_f \Rightarrow 0$ the system approaches an ideal flow design since there is no lost-work, LW, fluid energy loss, e.g. $\Delta S = 0$, and the coefficient of discharge $C_D \Rightarrow 1$. With $k_f \neq 0$, k_f is the offset from an ideal meter design. C_D is a measure of the thermodynamic efficiency η_{eff}, as used for turbines, expanders, etc. These relations are given below,

$$C_D = \frac{\rho_{b,f}}{\rho_{b,S}}\left(\frac{\alpha_b}{\alpha_b + k_f}\right)^{1/2} = \frac{\rho_{b,f}}{\rho_{b,S}}\left(\eta_{eff}\right)^{1/2}.\ \ C_D, \eta_{eff} \Rightarrow 1 \textbf{ as } k_f \Rightarrow 0\textbf{, since } \rho_{b,f} \Rightarrow \rho_{b,S} \textbf{, Eq 70}$$

and,

$$m_{actual} = C_D m_{ideal} = \sqrt{\frac{2 g_c J \Delta H_S \eta_{eff}}{\left(\frac{\alpha}{(\rho A)_S^2}\right)_b - \eta_{eff}\left(\frac{\alpha}{(\rho A)_S^2}\right)_a}}. \qquad \textbf{Equation 71}$$

The kinetic energy correction factors α's are calculated from radial velocity distributions and range from 1.0+ to ~1.1 at Reynolds numbers above 60,000. At low Reynolds numbers, these correction factors approach a value of two (2) in the inlet pipe and may significantly influence meter accuracy without proper application. At the vena contracta, with its' uniform velocity profile at high Reynolds numbers, a kinetic energy correction factor of one (1) is normally used and the constriction area is corrected by use of a contraction factor C_c. This gives, $\alpha_b \cong (1/C_{c,\mathrm{Re}=\infty})^2$.

The Bernoulli orifice equation as shown above is for horizontal flow in a pipe or conduit with area change. Corrections for gravitational fields are made by use of the following dimensional equation. For a two-phase fluid, a flow-regime analysis is required to determine the homogeneous enthalpy H, density ρ, and associated kinetic energy correction factor α, typically based on a no-slip interface from transport phenomena.

$$m = \rho_a A_a \sqrt{\frac{\left(2g_c J\Delta H + 2g\Delta Z\cos(\phi)\right)\eta_{eff}}{\left(\left(\frac{1}{C_c\beta^2}\frac{\rho_a}{\rho_b}\right)^2 - \alpha_a\eta_{eff}\right)}} = \frac{C_D\gamma A_b}{\sqrt{1-\beta^4}}\sqrt{\rho_a\left(2g_c\Delta P + 2g\rho_a\Delta Z\cos(\phi)\right)}$$

Equation 72

The following figures provide graphs of flow parameters versus the beta ratio and show the effects of parameter variations on flow rate. The normalized flow rate variations plot show that flow variations are relatively constant for fractional values from ~0.3 to ~0.9. For values above ~0.9, the efficiency, contraction, and kinetic energy effects have the same magnitude value. Fractional values below ~0.3 show an increasing divergence.

Figure 22 - Flow Parameters and Normalized Flow Rate Variations

Flow Parameters	Normalized Flow Rate Variations
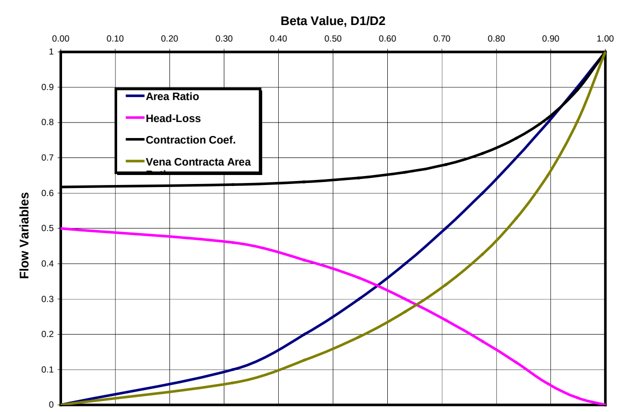	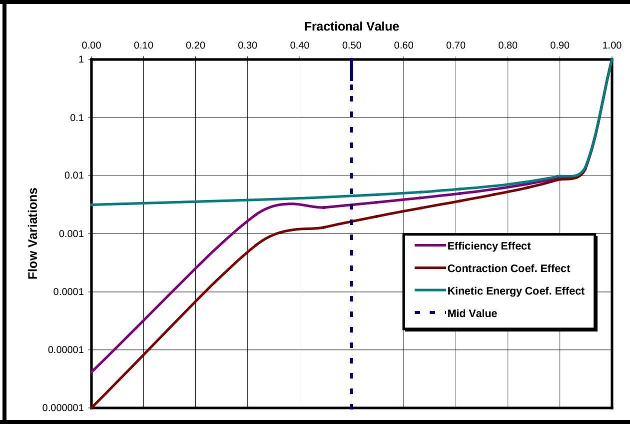

Discharge coefficients are affected by parameter variations as shown above. For improved flow measurement accuracy, the discharge coefficient in the turbulent flow regime can be corrected. The C_D flow adjustment follows the general equation,

$$C_D = C_{D,\mathrm{Re}=\infty} + \frac{b}{\mathrm{Re}_D^n} \cong f(\mathrm{Re},\beta,D).$$

Equation 73

This equation applies to all head-meters, of any fluid and phase. The coefficients $C_{D,\mathrm{Re}=\infty}$, b and n are listed in many publications. As an example, for a venturi meter, b and n are taken as ~zero (0). From testing over a wide range of flows and beta factors, the Balanced Flow Meter (BFM) has similar b and n constants. (However, for the BFM, $C_{D,\mathrm{Re}=\infty} = f(\beta)$ as a secondary affect). The following figures provide graphs of the orifice plate and multi-holed orifice plate discharge coefficients C_D. The multi-holed plate layout is based on a constant pitch to diameter ratio; the BFM is not.

Figure 23 - Square-edged Orifice Plate C_D and Multi-holed Orifice Plate C_D

Square-edged Orifice Plate C_D	**Multi-holed Orifice Plate C_D**
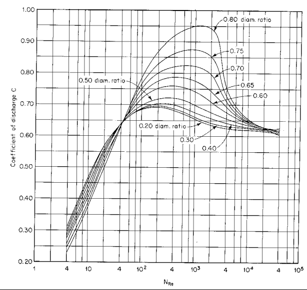	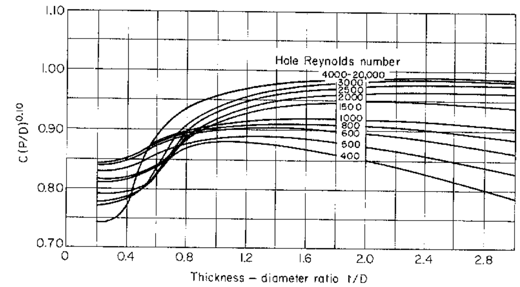

For thin plates $t/D < 0.4$ and for a wide range of beta factors, the Balanced Flow Meter discharge coefficient C_D is constant at ~0.89. The high Reynolds number concentric orifice C_D is ~0.61. The multi-holed thin plate C_D is ~0.74 at high Reynolds numbers. Thick BFM plates, with $t/D > 1$, have C_D's with values close to ~0.99, which is similar for the multi-holed orifice plate. The reason the C_D goes up with plate thickness is that the vena contracta velocity-head is recovered at t/D values greater than one (1). Frictional effects are minimal at thickness to diameter ratios, t/D's, less than seven (7). Please see A+ FLOWTEK technical article PTK-803.

The relation of thermodynamic efficiency and discharge coefficient is provided below. For a discharge coefficient of 0.6, the thermodynamic efficiency is only 36%. This is a high percentage loss of available energy. The BFM efficiency is 80% for a thin plate, and nominally thick-plates provide 95+% thermodynamic energy recovery.

Figure 24 - Head-Meter Thermodynamic Efficiency η_{eff} and Discharge Coefficient C_D Graph

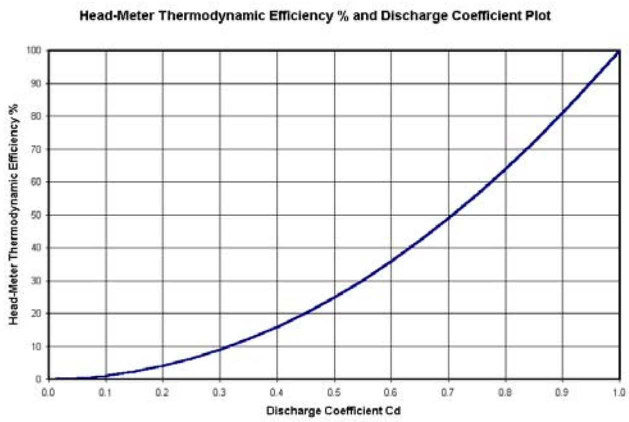

The following table gives discharge coefficients C_D for a range of beta factors. Values for fouled, and upstream and downstream elbow fittings are provided. These are representative values for thin plates. A comprehensive test with detailed results is provided in the NASA Balanced Flow Meter Test Screening Results and Analysis Report, RTP-6-2, as verified by Texas A&M University @ Kingsville. On this basis, the $C_D = f(\mathrm{Re}, \beta)$ corrections are developed. Nominal errors are typically less than 0.25%.

Table 12 - Balanced Flow Meter Calibrations for "Inline" Design Configuration

BETA	0.25	0.500	0.521	0.650	0.500,fouled	0.500,elbow
Avg Cd	0.892	0.882	0.881	0.911	0.824	0.848
Cd Dev	0.032	0.001	0.009	0.010	0.038	0.008
Avg K Val	287.1	16.3	13.2	4.0	15.65	18.63
K Dev	20.8	0.60	0.53	0.16	1.23	0.38

Table 13 - Square-Edged Orifice Sudden Contraction Velocity Head Loss k_f and, Vena-Contracta Contraction Factors C_c at High Reynolds Numbers, Re_∞

Beta Factor $\beta = \frac{D_b}{D_a}$	Area Ratio $\beta^2 = \frac{A_b}{A_a}$	Velocity Head Loss k_f Measured Data	Contraction Factor $C_{c,\mathrm{Re}=\infty} = \frac{A_{vena\ contracta}}{A_b}$
0.000	0.0	0.50	0.617
0.316	0.1	0.46	0.624
0.447	0.2	0.41	0.632
0.548	0.3	0.36	0.643
0.633	0.4	0.30	0.659
0.707	0.5	0.24	0.681
0.775	0.6	0.18	0.712
0.837	0.7	0.12	0.755
0.894	0.8	0.06	0.813
0.949	0.9	0.02	0.892
1.000	1.0	0.00	1.000

Table 14 - Basic Bernoulli Head-Meter Equation and Discharge Coefficient Based on Transport Phenomena

<table>
<tr><th>Orifice and Venturi Meter Basic Bernoulli Head-Meter Equation[1]</th><th colspan="2">Discharge Coefficient Based on Transport Phenomena, BSL, 1960[2]</th></tr>
<tr><td rowspan="4">

$$w = \rho_2 S_2 \sqrt{\frac{-2\alpha_2 \int_1^2 (1/\rho)\,dp}{1 - \frac{\alpha_2}{\alpha_1}\left(\frac{\rho_2 S_2}{\rho_1 S_1}\right)^2 + \alpha_2 e_v}} \qquad (15.4\text{-}$$

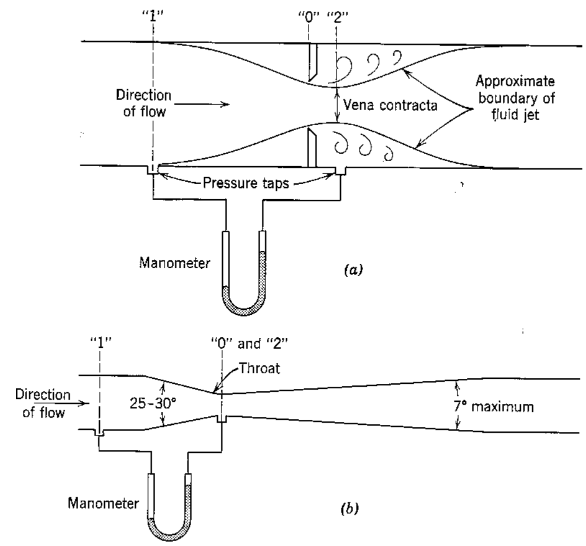

</td><td>

$$C_D = \frac{\sqrt{\dfrac{2g_c J \Delta H_S}{\left(\dfrac{\alpha + k_f}{(\rho A)_S^2}\right)_b - \left(\dfrac{\alpha}{(\rho A)_S^2}\right)_a}}}{\dfrac{\gamma A_b}{\sqrt{1-\beta^4}}\sqrt{2 g_c \rho_a \Delta P}}$$

</td><td>

$$\gamma = \left(\frac{\left(\dfrac{\Delta H}{\Delta P}\right)_S \left(\rho_a\left(1-\beta^4\right)\right)}{\left(\left(\dfrac{\rho_a}{\rho_{b,S}}\right)^2 - \beta^4\right)}\right)^{\frac{1}{2}}$$

</td></tr>
<tr><td colspan="2">

$$C_D = \sqrt{\frac{1-\beta^4\left(\dfrac{\rho_b}{\rho_a}\right)^2}{\left(\alpha + k_f\right)_b - \alpha_a \beta^4 \left(\dfrac{\rho_b}{\rho_a}\right)^2}} \approx Const.$$

</td></tr>
<tr><td colspan="2">

$$C_D \equiv \frac{m_{act}}{m_{ideal}} = \frac{(\rho A v)_{act}}{(\rho A v)_{ideal}} = \frac{\rho_{b,f}}{\rho_{\min,S}}\left(\frac{\alpha}{\alpha + k}\right)_b^{1/2} = \frac{\rho_{b,f}}{\rho_{\min,S}}\left(\eta_{eff}\right)^{1/2}$$

</td></tr>
<tr><td colspan="2">

$$\eta_{eff} = \frac{v_{b,f}^2}{v_{b,ideal}^2} = \frac{(m/\rho)_{b,f}^2}{(m/\rho)_{b,ideal}^2} = \frac{H_b^* - H_{b,f}}{H_b^* - H_{\min,S}} = \frac{\alpha v_{b,f}^2}{\alpha v_{b,f}^2 + k v_{b,f}^2} = \left(\frac{\alpha}{\alpha + k}\right)_b$$

</td></tr>
<tr><td>1) α defined by $Kinetic\ Energy = \dfrac{v^2}{\alpha 2}$</td><td colspan="2">2) Contemporary basis $Kinetic\ Energy = \dfrac{\alpha v^2}{2}$.</td></tr>
</table>

PTK-808 Balanced Flow Meter, Velocity Head Loss Coefficients ©

Velocity head-loss coefficients provide the skin k_{ff} and form k_f frictional permanent pressure loss through pipes and fittings. It is defined by,

$$\frac{h_f}{\left(v^2/2g_c\right)} = \frac{\int \left(dP/\rho\right)_{friction\ loss}}{\left(v^2/2g_c\right)} \equiv k_f \ or\ k_{ff} \text{ ,} \qquad \textbf{Equation 74}$$

where h_f is the frictional head loss, P is the pressure, ρ is the density, v is the velocity, and g_c is Newton's law conversion constant. The utility of velocity head-loss method is shown by the pressure loss that occurs in a pipe entrance to a final velocity distribution in laminar flow. The calculation basis is given in the following table, where the kinetic energy correction factors $\alpha's$ are: a) $\alpha_a = 1$ for uniform flow at the entrance, and b) $\alpha_b = 2$ for fully developed laminar flow. For this configuration, a velocity head loss of one occurs, e.g. $k_f = 1$. For an incompressible Newtonian fluid with a laminar flow-rate between $500 < \mathrm{Re} < 2{,}300$, the frictional head loss is $h_f = \Delta P/\rho = v^2/2g_c$, and one velocity head is lost. Below a Reynolds number of ~500, creeping-flow *may* affect the velocity distributions. Creeping-flow is dominant below a Reynolds number of one.

Table 15 - Derivation of the Velocity Head Loss Coefficient k_f

Velocity Profiles, Pipe Entrance to Developed Laminar Flow	**k_f General Definition**
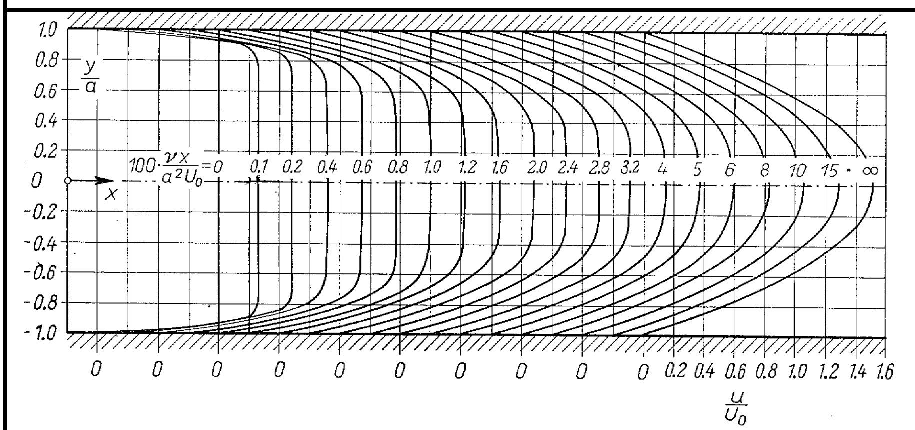	**Isothermal Energy Balance,** $@\ \rho = const.$: $\frac{\Delta P}{\rho} = \left(\alpha_2 - \alpha_1\right)\frac{v^2}{2g_c} \Rightarrow$ $k_f = \left(\alpha_2 - \alpha_1\right) = \left(2-1\right) = 1$ $k_f = \frac{\Delta P/\rho}{v^2/2g_c} = 1$ **One velocity head is lost.**

The general equations for development of the velocity head-loss coefficient k_f are based on the steady-flow mass, momentum, energy and entropy balances. These equations and associated relations, applicable to any fluid, are provided below, (nomenclature is provided in A+ FLOWTEK technical article PTK-800).

Mass:

$$\rho Av = const \ \& \ (\vec{G}A) = const. \qquad \textbf{Equation 75}$$

Momentum:

$$F = -\Delta\left(\frac{1}{g_c} m\beta_{MOM} v + PA\right) + m_{tot}\frac{g}{g_c} \qquad \textbf{Equation 76}$$

Energy:

$$\Delta\left(\frac{\alpha_{KE} v^2}{2g_c J}\right) + \Delta\Phi_{PE} + \int_a^b \frac{dP}{\rho} + E_f = 0 \qquad \textbf{Equation 77}$$

Entropy:

$$\int_a^b TdS = Q + E_f \ \& \ \Delta S = \frac{Q}{T_{ref}} + \frac{E_f}{T_{ref}} \qquad \textbf{Equation 78}$$

Gibbs Fundamental Property Relation:

$$\Delta H = \int_a^b TdS + \int_a^b \frac{dP}{\rho} \qquad \textbf{Equation 79}$$

General Relations:

$$E_f = Lost\ Work(LW) = \int_a^b \frac{dP_f}{\rho} \equiv \left(\frac{k_f v^2}{2g_c}\right)_{form}, = \left(\frac{k_{ff} v^2}{2g_c}\right)_{skin} \qquad \textbf{Equation 80}$$

The combinations of the above equations and relations are used for rigorous calculation of the velocity head-loss coefficient k_f for any fluid and fluid state. Experimental data exists for most fitting designs. This data is used for equation verification, values for correlation constants, and to define applicable flow and Reynolds numbers limits.

The figure on the next page provides skin k_{ff} and form friction k_f representations of the velocity head-loss coefficients. Due to the large eddy effects, and subsequent transformation of velocity head to thermal energy, form friction is generally much larger than skin friction and affects permanent pressure loss to a much higher degree. The factor that most affects accuracy, repeatability and pressure loss in a Bernoulli head meter is eddy turbulence. Eddy turbulence is reduced by limiting flow separation points, into, through, and out of the metering tube or plate. The Balanced Flow Meter (BFM) uniformly distributes the flow across the plate, with the hole-sizes and hole-pitch positions designed to minimize eddy turbulence and shear stress imbalances across the flow area. The BFM design reduces radial velocity, eddy disturbances; and provides a performance comparable to a venturi meter in a single, and thin, multi-holed plate design. It is designed for direct replacement to the orifice plate, and will provide significant flow metering improvements.

Figure 25 - Skin and Form Friction Depictions

Skin Friction Example, k_{ff}	**Form Friction Example,** k_f

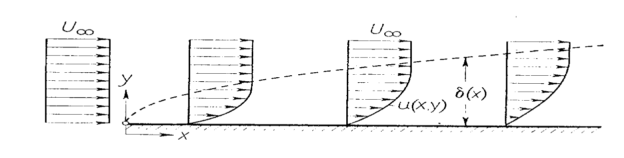

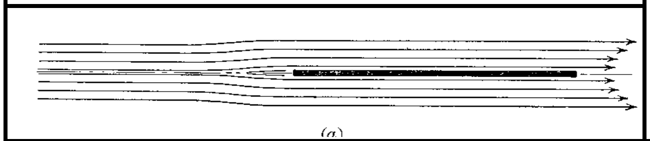

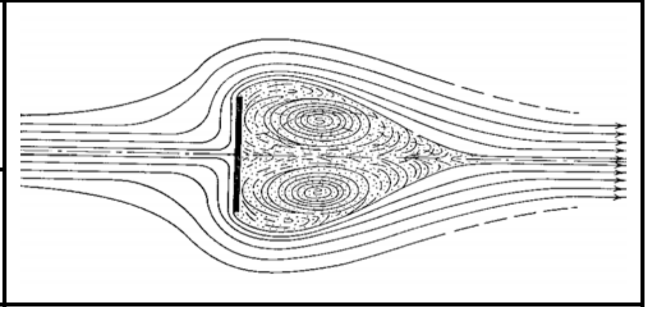

Frictional (and pressure) effects produce a drag on the surfaces as given by,

$$\frac{F_{friction\ drag}}{A_{surface}} = C_f \frac{\rho v^2}{2g_c} \ or \ \frac{F_{total\ drag}}{A_{projected}} = C_d \frac{\rho v^2}{2g_c} \qquad \textbf{Equation 81}$$

The quantity $\rho v^2 / 2g_c$ is the dynamic pressure. The drag force due to friction C_f is caused by the shear stresses at the surface caused by a moving viscous fluid. The total drag C_d on an object may be due to pressure as well as frictional effects. Pressure drag arises from two sources. The first is induced drag; the second is wake drag. As the pressure in the front of the body is greater than the rear, a net rearward force develops. The frictional, or permanent, pressure loss is the result of flow separation and subsequent eddies. A portion of the pressure drag may be recoverable dependent on frictional heating and associated velocity head-loss. C_d values range from ~ 0.1 to 2 for spheres, disks, and cylinders at Reynolds numbers above 500. C_d for a thin plate normal to a wall, such as a thin wedge, is 1.4 above a Reynolds number of 10,000. C_d for a disk is 1.17 for Reynolds numbers above ~500. There is a relation of C_d to C_D.

The Fanning friction factor is C_f. For the surface type skin-friction factor, f, the velocity head-loss coefficient is given by,

$$k_{ff} = \frac{4fL}{D} = \frac{fL}{R_{hydraulic}} = \frac{C_f L}{R_{hydraulic}} \qquad \textbf{Equation 82}$$

The form head-loss coefficients k_f for contraction and expansion type fittings are shown in the following tables. This contraction and expansion basis is used for head-meter analysis as shown in a following table. The procedure provides the velocity head-loss coefficients for any head-meter when the discharge coefficients are known. Other approaches are available for the Balanced Flow Meter design, since the single tube may be replaced by a tube-hole bundle, such as used with shell-and-tube heat exchangers. Design equations for pressure loss are well known with these systems.

The table below shows the velocity head-loss k_f equations and graphs for contraction and expansion type fittings. The equations are based on incompressible fluid flow, but can be extended to any fluid by including a density correction factor. The equations are derived from the momentum and energy balances. Equation forms and constants are verified by experimental data. The equations and associated graphs provide the velocity head-loss coefficients based on the small diameter area or the large pipe area.

Table 16 - Velocity Head-Loss Coefficients k_{ff} for Fittings & Head Meters

Contraction Velocity Head Loss	**Expansion Velocity Head Loss**
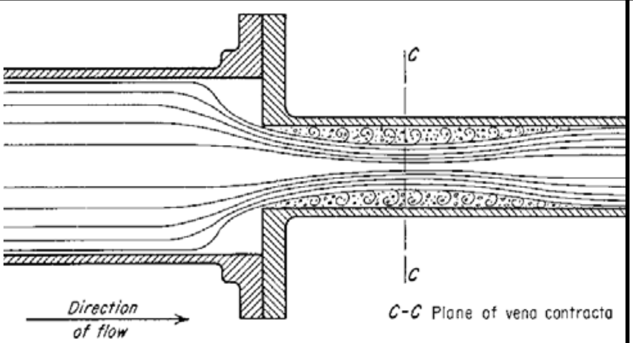	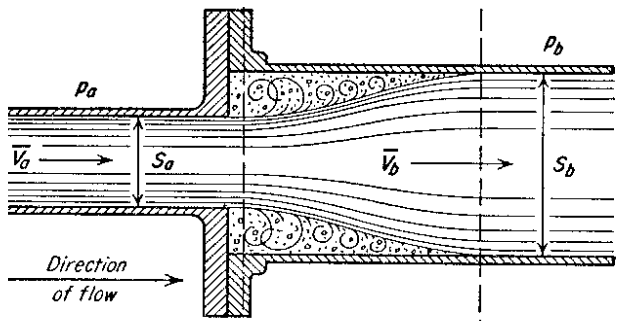
$k_{f,contraction} = \frac{(4-\pi)}{2}(1-\beta^2)$ for $v_{Small\ Area}$ $k_{f,contraction} = \frac{(4-\pi)}{2}\frac{(1-\beta^2)}{\beta^4}$ for $v_{Large\ Area}$	$k_{f,expansion} = (1-\beta^2)^2$ for $v_{Small\ Area}$ $k_{f,expansion} = \left(\frac{1-\beta^2}{\beta^2}\right)^2$ for $v_{Large\ Area}$
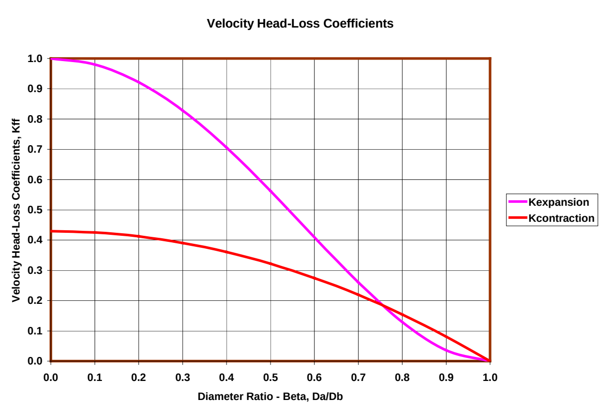 Small Area Velocity Basis	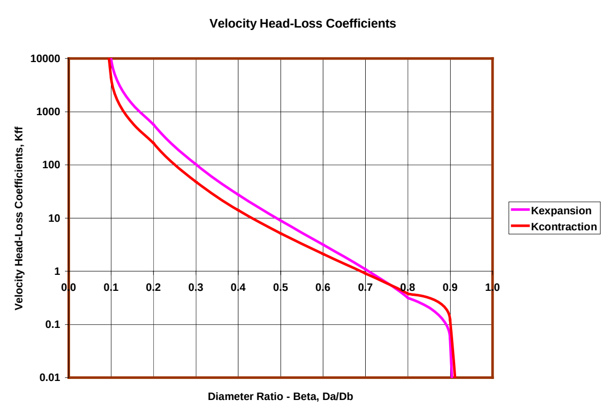 Large Area Velocity Basis

The table below shows the combined equations for a fluid contraction, small area tube flow, and expansion. The model configuration is used for a head-meter, with a contraction, reduced-area flow, and expansion. The approach has been experimentally verified, with use of the flow meter discharge coefficient C_D as a correlating parameter for the orifice, venturi and Balanced Flow Meter.

The relation is,

$$C_D = \frac{\rho_{b,f}}{\rho_{b,S}}\left(\frac{\alpha_b}{\alpha_b + k_f}\right)^{1/2}, \qquad \textbf{Equation 83}$$

and $\frac{1}{C_D^2} = \frac{\int dP_{total}/\rho}{\left(v^2/2g_c\right)}$ & $\frac{\int dP_{friction}/\rho}{(v^2/2g_c)} = k_f$. See the table below, Head Meters with Contraction and Expansion, for relations between C_D and k_f.

Table 17 - Pipe System with Contraction and Expansion Flanges

Piping System Pressure Loss with Contraction & Expansion Fittings

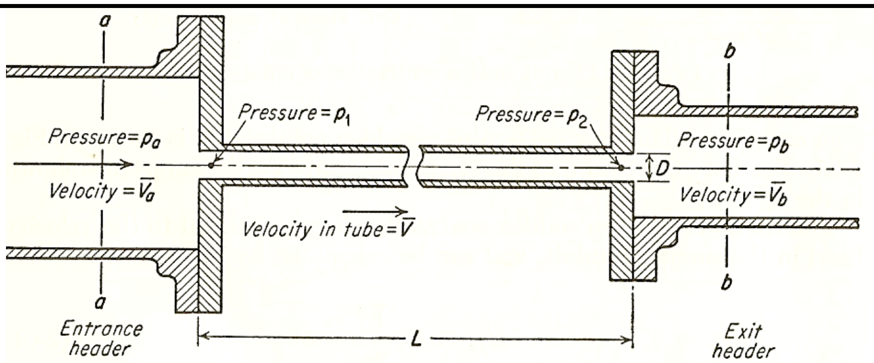

$$\int \frac{dP_{loss}}{\rho} = \left(k_{f,contraction} + 4f\frac{L}{D} + k_{f,expansion}\right)\frac{v_{Tube}^2}{2g_c} \text{ for } v_{Tube}$$

$$\int \frac{dP_{loss}}{\rho} = \left(k_{f,contraction} + 4f\frac{L}{D} + k_{f,expansion}\right)\frac{v_{Pipe}^2}{\beta^4 2g_c} \text{ for } v_{Pipe}$$

Note: The above flange diagrams are not to scale and $A_a = A_b$ for the design configuration and subsequent equations.

The table below provides the relations and graphs for permanent pressure loss in a Bernoulli head meter. The flow metering types shown are the orifice, venturi and Balanced Flow Meter. The coefficients of discharge are based on a pipe tap configuration. Since the coefficients of discharge C_D's are similar for the venturi flow tube and the Balanced Flow Meter, the permanent pressure loss is similar. Additionally, the BFM shows a fifty percent (50%) improvement in pressure recovery over the single-holed orifice plate.

Table 18 - Head Meters with Contraction and Expansion

Head Meter Permanent Pressure Loss with Contraction & Expansion

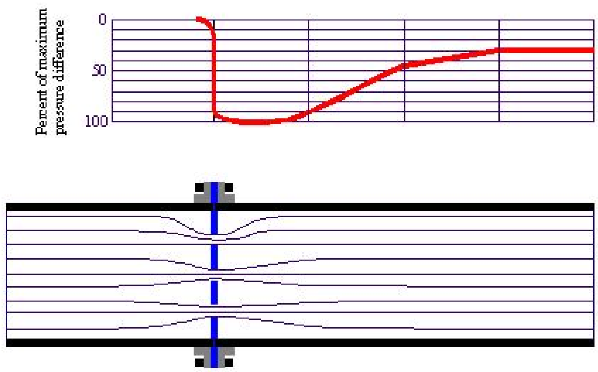

Balanced Flow Meter Pressure Recovery

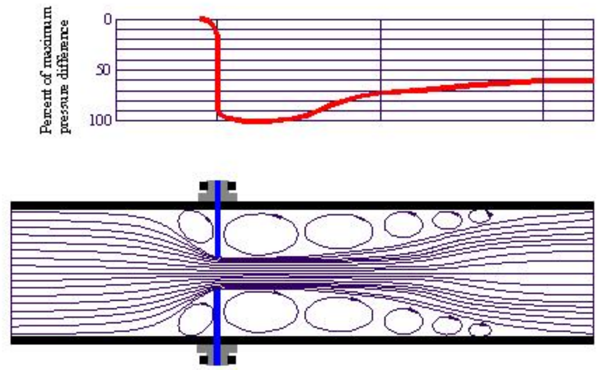

Orifice Meter Pressure Recovery

$$k_{f,PH}=\left(\frac{1}{(\gamma C_D)^2}-1\right)\left(1-\beta^4\right)_{to\ plate\ hole}\ or\ k_{f,PT}=\left(\frac{\left(1-\beta^2\right)\left(1-\beta^4\right)}{(\gamma C_D)^2}\right)_{pipe\ taps}\quad \text{for } v_{Beta}$$

$$k_{f,PH}=\left(\frac{1}{(\gamma C_D)^2}-1\right)\left(\frac{\left(1-\beta^4\right)}{\beta^4}\right)_{to\ plate\ hole}\quad or\ k_{f,PT}=\left(\frac{\left(1-\beta^2\right)\left(1-\beta^4\right)}{\beta^4(\gamma C_D)^2}\right)_{pipe\ taps}\quad \text{for } v_{Pipe}$$

$$C_{contraction,vena-contracta}=C_{D,orifice}=\pi/(\pi+2),C_{D,BFM}=(C_{D,orifice})^{1/4},C_{D,venturi}=(C_{D,orifice})^{1/8}$$

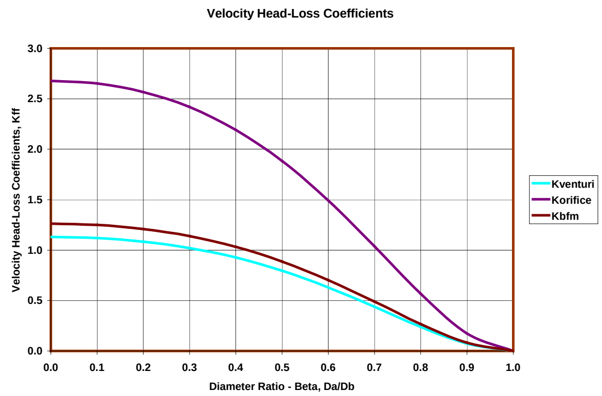

Pipe Taps - Beta Area Velocity Basis

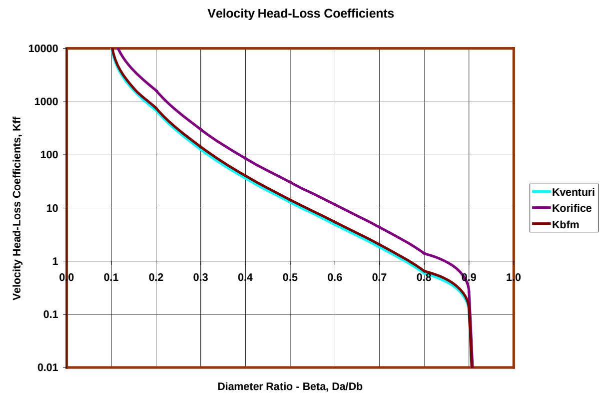

Pipe Taps - Pipe Area Velocity Basis

k_f is determined from measured values based on air testing, ranging from minimum flows to sonic velocities. Values are calculated by an ideal gas compressible fluid equation, verified from the NASA Gas Frictional-Flow Tables. The equation is shown on the next page. Testing results are given in the table below and shown graphically with the figure below.

$$\vec{G}^2 = \left(\frac{m}{A_{Pipe}}\right)^2 = \frac{2g_c\left(1-(\rho_b/\rho_a)^2\right)}{(1-1/\lambda)\left((\rho_b/\rho_a)^2-1\right)/2-2(1+1/\lambda)Ln(\rho_b/\rho_a)+k_f} \qquad \text{Equation 84}$$

Table 19 - Measured and Calculated Velocity Head-Loss k_f for Pipe Taps

Bernoulli Meter Beta, $\beta = D_a/D_b$	0.250	0.500	0.521	0.650
Venturi k_f Calculated, C_D = 0.940	270.6	12.7	10.4	3.0
BFM k_f Measured	287.1*	16.3	13.2	4.0
BFM k_f Calculated, C_D = 0.831	346.4	16.3	13.3	3.9
Orifice k_f Measured	669.4	31.5	25.7	7.4
Orifice k_f Calculated, C_D = 0.598	669.4	31.5	25.6	7.4
Orifice to BFM k_f Ratio Reduction %	233	193	195	185

With the table above, the BFM coefficient of discharge C_D value is 0.831 for a pipe tap configuration. The flange tap C_D value is 0.89+. All k_f values for the BFM and orifice are measured. Values shown for the venturi flow meter are calculated. Density corrections and k_f values for the venturi meter are estimated for a downstream pipe tap location. All k_f values are based on pipe tap permanent pressure losses and the pipe flow area as the velocity reference. Comparisons of the Balanced Flow Meter with the orifice plate show a k_f reduction of ~200%. k_f accuracies are shown below.

Figure 26 - Measured and Calculated Velocity Head-Loss k_f, Orifice and BFM Plate

Orifice Measured and Calculated k_f	BFM Measured and Calculated k_f

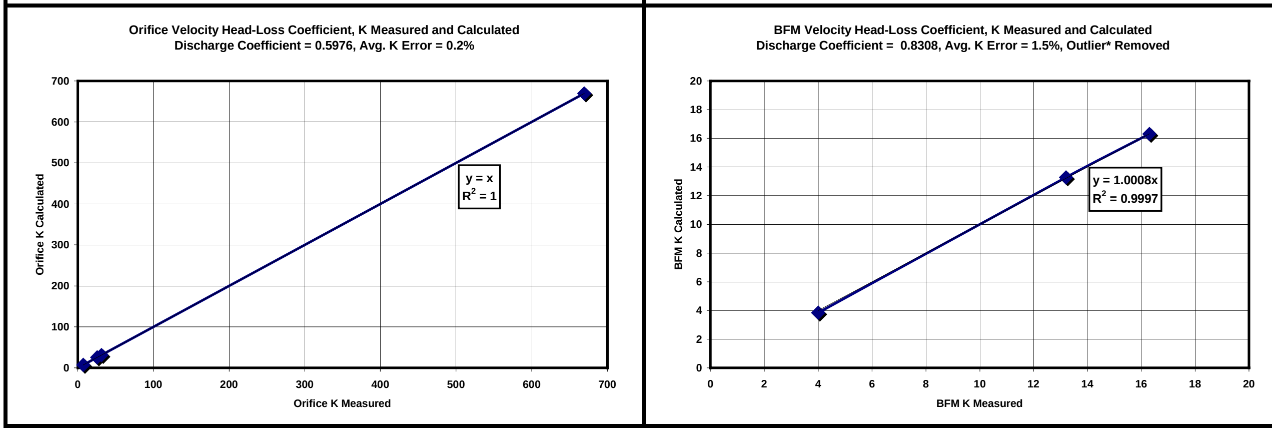

Precise equations for the multi-holed plates follow those used with tube bundles in shell-and-tube heat exchangers, which are well known. This BFM model representation is shown in the following diagrams for the inlet (contraction) and outlet (expansion) zones.

Figure 27 - Tube Bundle Representation of the BFM Configuration

Inlet Contraction	**Outlet Expansion**
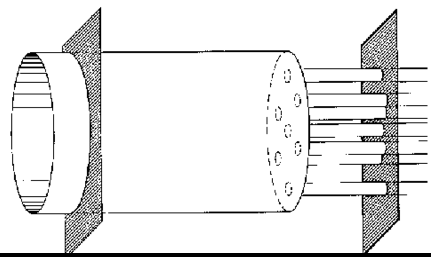	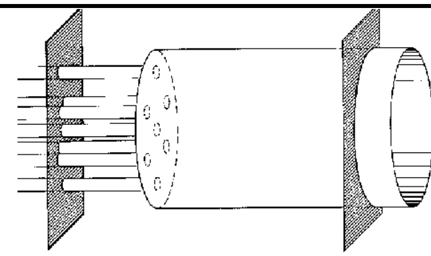

The BFM design based on this model accommodates all beta factors and Reynolds numbers above 500, e.g. $\mathrm{Re} > 500$. The BFM design equations are given by,

Inlet Contraction Design Equation:

$$k_{f,contraction} = \frac{K_3^3}{fnc(\gamma^2)}\left(1 - 2\beta\frac{K_3^2}{K_3^3} + \beta^2\left(2\frac{K_4^2}{K_3^3} - \frac{K_4^3}{K_3^3}\right)\right) \qquad \textbf{Equation 85}$$

Outlet Expansion Design Equation:

$$k_{f,\exp ansion} = \frac{K_1^3}{fnc(\gamma^2 C_D^2)}\left(1 - 2\beta\frac{K_1^2}{K_1^3} + \beta^2\left(2\frac{K_2^2}{K_1^3} - \frac{K_2^3}{K_1^3}\right)\right) \qquad \textbf{Equation 86}$$

where $\beta = D_b / D_a$, and $K^2 = \beta_{MOM}$ & $K^3 = \alpha_{KE}$. As given, the K^i factors are the kinetic and momentum correction factors. Values for the K^i's are determined from the multi-hole layout equations for linear shear stress matching $(\tau_r = r\tau_R / R_{Hyd})$, with hole-radii and hole-pitch distances constrained (as with a tube-bundle layout). Flow mal-distribution relations are applicable to the BFM model as applied to a tube bundle. $\kappa\rho A v^\sigma$ equaling a constant for each hole provides the hole sizing relation. This relation *balances* the velocity, momentum, or kinetic energy *flow* through each hole. Hole sizing and hole-layout optimization is then performed with the general Bernoulli equation,

$$\int\frac{dP}{\rho} + \frac{\Delta\alpha v}{2g_c} + \frac{g}{g_c}\Delta Z = \left(k_{f,contraction} + k_{f,hole} + k_{f,\exp ansion}\right)\frac{v_{Pipe}^2}{\beta^4 2g_c}, \qquad \textbf{Equation 87}$$

to minimize mal-distribution, friction and form drag losses. For $\mathrm{Re} > 500$, this approach reduces the pressure loss by minimizing radial and axial eddy formations and associated adverse shear stresses.

PTK-809 Balanced Flow Meter, Modified Iterative Measurement Test (MIMT©) Statistical Basis and Analysis ©

Foreword

The QMC MIMT© Program for Windows is an advanced data and measurement error detection program solving linear and non-linear data-reconciliation / gross-error-detection problems. The MIMT© algorithm is copyrighted under the American Institute of Chemical Engineers, and is distributed exclusively for QMC and A+ FLOWTEK clientele.

For a given set of measured data, a reconciled data set is generated, i.e., consistent with applicable constraints, such as material balance or model, based requirements. It generates a list of measurements or calculated values, suspected of gross error, and estimates the correct values of the suspect measurements and values. Included in this analysis are total material balances, temperatures, pressures, physical properties, etc. for chemical processes or plants, steam-metering systems in plants and refineries, and natural gas distribution systems. It is applicable to any data set where measured and model constrained calculated variables are related by systems of linear or non-linear algebraic equations.

The QMC MIMT© Program for Windows may also be applied to a single head-meter or Balanced Flow Meter installation when multiple temperature, pressure and/or differential pressure measurements are supplied. All measured values, calculated flows, and associated physical properties can be corrected and errors significantly reduced, if not eliminated, with this MIMT© approach.

Mass Balance

Mass (and energy) balance is a basis for robust flow measurement error-analysis. The mass balance equation is,

$$\sum \textit{Mass Inputs} - \sum \textit{Mass Outputs} = 0 \qquad \textbf{Equation 88}$$

With the difference in the above equation not zero, one or more of the flow rates are in error. Measured flow rates are never exactly precise and flow rate data will typically yield an inconsistent mass balance. The problem is to determine whether the discrepancy is due to normal measurement errors, which are random, or to gross errors caused by malfunctioning instruments. If gross errors are present, it is necessary to identify and correct them; smaller errors can be reconciled by a statistical procedure.

Data Reconciliation

If the measured flow rates contain random errors only, the approach is to generate a consistent mass balance from apparently conflicting data. Since mass balance equations are linear, the flow data can be reconciled by means of a constrained linear least-squared-error procedure.

The problem in mathematical form is to minimize the sum of the normalized squared errors,

$$\phi(X_i) = \sum \frac{(X_i - X_i^*)^2}{\sigma_i^2}.$$ **Equation 89**

Subject to the constraints imposed by j mass (or model based) balance equations of the form,

$$\Psi_j(X_i) = \sum_i a_{ij} X_i = 0.$$ **Equation 90**

Where X_i is the ith corrected measurement, X_i^* is the ith observed measurement, σ_i^2 is the error variance of the ith measurement, Ψ_j is the balance constraint for the jth balance equation, and a_{ij} is the coefficient of X_i in the jth balance equation. The value of a_{ij} is +1 for an input stream, and -1 for an output stream.

The method of LaGrange is used to obtain the X_i values. This involves solving a set of simultaneous equations,

$$\frac{\partial}{\partial X_i}[\phi(X_i) + \sum_j \lambda_j \psi_j(X_i)] = 0,$$ **Equation 91**

$$\frac{\partial}{\partial \lambda_j}[\phi(X_i) + \sum_j \lambda_j \psi_j(X_i)] = \psi_j(X_i) = 0,$$ **Equation 92**

λ is a LaGrangian multiplier.

Any technique for solving the above equations will yield a set of adjusted flow rates (X_i) that will satisfy the mass-balance equations for all the nodes, i.e. systems. To apply LaGrange's method, it is necessary to know the error variance for each measurement, σ_i^2. The value of σ_i^2 for each measuring instrument is estimated independently, typically from the manufacturer's specification, together with the engineer's knowledge of how the instrument actually performs.

Gross-Error Detection

While LaGrange's method will always yield a good mass balance, the adjusted flow rates will be erroneous if there are gross errors in the data. Therefore, such errors have to be identified and bad measurements removed before proceeding with data-reconciliation.

Most methods for gross-error detection involve the use of statistical tests on the basis that random errors in the data are normally distributed. Considered are two general types of statistical tests:

1. Methods for analyzing least-squares residuals. The approach is to adjust the data using a least-squared-error analysis and then calculate a set of residuals,

$$\ell_i = X_i - X_i^*. \quad \textbf{Equation 93}$$

The outliers among the ℓ_i values are those that exceed some number of standard deviations, $\sigma =$ 1.96 for a 95% confidence level. Thus, a given residual is an outlier if the following is true:

$$\frac{\ell_i}{\sigma_{\ell,i}} > 1.96, \text{ or } \frac{\ell_i}{\sigma_{\ell,i}} < -1.96. \quad \textbf{Equation 94}$$

where $\sigma_{\ell,i}$ is the standard deviation of the residual (the residuals are random variables, like the X_i values). The outliers are the results of gross errors.

2. Methods for analyzing nodal imbalances. The nodal imbalance is the left-hand side of the mass balance equation. This value is divided by the nodal standard deviation, σ_j which is the square root of the nodal variance:

$$\sigma_j^2 = \sum_i \sigma_i^2 \quad \textbf{Equation 95}$$

Here, the summation extends over all the streams connected to node *j*. The resulting normalized statistic is denoted δ_j,

$$\delta_j = \frac{\sum_i a_{i,j} X_i}{\sigma_j}. \quad \textbf{Equation 96}$$

For a 95% confidence level, there are one or more gross errors in the measurements associated with node j when,

$$\delta_j > 1.96\text{, or } \delta_j < 1.96\text{.} \qquad \textbf{Equation 97}$$

Modified Iterative Measurement Test, MIMT©

Error detection methods have two principal drawbacks,

1. The least-squares procedure tends to spread the error over all the data so even the best measurements can have high residuals. When these residuals fail the test for outliers, the corresponding measurements are erroneously identified as having gross errors.
2. There is no provision to prevent unrealistic flow rates from being computed. If the algorithm fails to identify all the gross errors, the data-reconciliation procedure may generate negative flow rates, or absurdly large positive ones, for some of the streams.

The modified iterative measurement test, MIMT©, is designed to overcome these two problems. The test for outliers is applied in a stepwise fashion. After the least-squares calculation, the one measurement corresponding to the worst significant outlier is identified as having a gross error. This measurement is removed from the data set by nodal aggregation, and the least-squares analysis is repeated on the reduced data set to obtain residuals for the next round of tests. If unrealistic flow rates result when a particular measurement is removed, that measurement is put back in the calculation and the next-worst outlier is removed instead. When there are no more outliers among the remaining residuals, the iterations are terminated.

Example of MIMT© Gross-Error Detection

The following table provides a set of measurements that contain both random and gross errors. These data were developed by superimposing random and gross errors onto a perfect mass balance. The stream numbers are shown in column 1. The measured values with gross errors are shown in column 2. The third column gives the reconciled flow rates obtained using the modified iterative measurement test. The algorithm correctly identified all three gross errors, and correctly reconciled the flow rates, including the ones that had been grossly wrong. The flow rate for Stream 2, for instance, was adjusted downward by 40%. The sum of the absolute values of the errors is only 30.50 in the reconciled data, vs. 252.58 in the raw data; the MIMT© method reduced the error by 88%.

Table 20 - Example of MIMT© Error Detection with Data Reconciliation

		Reconciled Values		
Stream Number	**Measured Value**	**With Error-Detection**	**Without Error-Detection**	**Deviation %**
1	289.94	294.25	296.55	+ 1
2	85.41	51.77	83.43	+ 63
3	113.86	118.45	111.17	- 6
4	120.81	116.56	109.28	- 6
5	241.81	242.47	213.12	- 12
6	248.39	248.18	256.77	+ 3
7	245.53	246.39	254.97	+ 3
8	1.79	1.79	1.79	0
9	4.55	4.55	4.57	+ 0.4
10	1.89	1.89	1.90	+ 0.5
11	83.09	83.12	73.31	- 12
12	71.30	71.01	73.27	+ 3
13	67.90	132.32	108.98	- 18
14	203.55	202.41	212.54	+ 5
15	202.19	199.67	182.59	- 9
16	90.07	187.35	169.67	- 9
17	12.31	12.32	12.92	+ 5
18	104.31	103.66	83.70	- 19
19	35.52	35.49	32.80	- 8
20	5.48	5.47	5.40	- 1
21	274.32	268.28	238.37	- 11
22	37.49	37.33	37.03	- 1
23	298.31	311.08	280.80	- 10
24	8.33	8.33	8.29	- 0.5
25	193.42	192.25	200.02	+ 4

The fourth column in the above table illustrates the affect when data reconciliation is performed without first identifying the gross errors. The sum of the absolute values of the errors is 269.90, which is greater than the error in the raw data. In extreme cases, with this approach, the adjusted flow rates may include such absurdities as negative flow rates, or flow rates beyond the range of the meter. Thus, misapplying a least-squares data-reconciliation can be worse than useless and provide misleading values and results. The MIMT© method eliminates these affects.

MIMT© Performance

The performance of five well-known and industrially applied error detection algorithms with a steam-metering system has been tested. The data were created by computer, using a random-number generator to superimpose errors on flow rate data that were balanced to begin with. One hundred such cases were created. The percentage of measurements containing gross errors was permitted to be as high as 25%; the magnitude of the gross errors ranged from about 10% to 100% of the true flow rate.

The modified iterative measurement test MIMT© method identified over 80% of the gross errors, made few erroneous identifications, and reduced the total error by more than 60%. No other method tested provided this consistency, accuracy increase or identified the gross errors dependably. The MIMT© method is reliable and effective for detecting gross errors in data sets subject to linear constraints. Additionally, the modified iterative measurement test MIMT© has the advantage of being much faster than other methods. The average computing times per run were 3 seconds for the MIMT©, and more than 40 seconds for the other methods.

A number of chemical process companies are using MIMT© as an aid to process analysis, control, leak detection and inventory accounting. The modified iterative measurement test MIMT© method is effective at detecting gross errors and reconciling data. It is sufficiently robust to be used in an industrial and "real-time" environment. The methods have been extended to non-linear systems, such as those involving component mass balances, energy balances, physical property verification and sensor measurements with model based constraints.

Advantages of MIMT©

As has been seen throughout the last several decades, all chemical plants have bad flow meters. Often the percentage of bad meters is as high as 25%. Without Error Detection & Data Reconciliation, plant personnel live with these problems because they have no way of knowing which meters are bad. These bad meters result in inventory problems or accountability problems, such as not knowing where the fluids are going or why the inventory does not balance. When problems occur in the plant, since the meters are bad, it is difficult to tell what is happening. Therefore, the resolution of the real problem takes additional time and loss of profit. Often metering problems can cost several thousand dollars per day. Once the QMC MIMT© Program is applied, the problems can be corrected in one day.

The QMC MIMT© Program also enables one to find and pinpoint leaks and losses. It identifies the bad meters/sensors, and calculates what the bad meters/sensors should be reading, termed data reconciliation. Gross errors are pinpointed and corrected. Minor errors are corrected statistically based on weighted flow meter error analysis and mass balance constraints.

The five main applications of the QMC MIMT© Program are:

1. On Demand Material Balancing - This mode allows the user the ability to check material balances, for example, when an accounting error is suspected or for trouble shooting purposes. Instrument technicians can also use this mode to verify flow meter calibrations and for routine maintenance and operational purposes.

2. Automatic Daily Error Detection - Every 24 hours, or other time interval, a report identifying erroneous meters will print to your print queue. This report will also provide the erroneous meters' corrected values and a complete set of reconciled flows.

3. Reconciliation of Historical Data - Historical data used to train artificial neural network models or process simulations must not contain data that has gross errors in it. A year of plant data can be error corrected and data reconciled in less than a day.

4. Advanced Process Control - Advanced Process Control (APC) cannot function correctly with bad measurements. The leading cause of down time or failure of APC projects is bad metering.

5. On Line Optimization - On-line optimization programs require "clean" data, i.e., data that does not contain gross errors. Running the QMC MIMT© Program prior to the optimization program eliminates bad results and incorrect optimum conditions.

6. Balanced Flow Meter - With multiple pressure, differential pressure and temperature sensors, the MIMT© algorithm may be applied to a single head meter with the use of the following equations. Any sensor measurement, flow measurement and physical property(s) errors will be significantly reduced if not eliminated.

Table 21 - Bernoulli Head-Meter Steady State, Mass Momentum, Energy and Rate Equations

Equation Basis	Inlet Point a	Inlet to Outlet Point a to Point b	Outlet Point b
Base Bernoulli Head-Meter		$m = \frac{C_D \gamma A_b}{\sqrt{1-\beta^4}} \sqrt{2 g_c \rho_a \Delta P}$	
Mass Balance	$m = \rho A v$	$\rho A v = \rho A v$	$m = \rho A v$
	$\vec{G} = \rho v = m / A$	$A\vec{G} = A\vec{G}$	$\vec{G} = \rho v = m / A$
Momentum Balance		$m = \sqrt{\frac{\Delta P A}{\Delta\left(\frac{\beta_{mom}}{1/\rho A}\right)}}$	

Energy Balance	$m = \rho A \sqrt{\left(\frac{2 g_c J \Delta H^T}{\alpha} \right)}$	$m = \sqrt{\frac{2 g_c \ J \Delta H}{\Delta \left(\frac{\alpha_{ke}}{(\rho A)^2} \right)}}$ $m = \sqrt{\frac{2 g_c \ J \Delta H_S}{\Delta \left(\frac{\alpha_{ke} + k}{(\rho A)^2} \right)}}$	$m = \rho A \sqrt{\left(\frac{2 g_c J \Delta H^T}{\alpha} \right)}$ $m = \rho A \sqrt{\left(\frac{2 g_c J \Delta H_S}{k} \right)}$
Energy-Rate Constraint		$m = \frac{\Delta \left(\alpha \vec{G}^3 / (\rho A)^2 \right)}{2 g_c J \Delta H}$ $m = \frac{\Delta \left((\alpha + k) \vec{G}^3 / (\rho A)^2 \right)}{2 g_c J \Delta H_S}$	
Equation of State Constraint	$\left(\frac{P \alpha (\vec{G} / \rho)^3 / A^2}{(z \Re T)(2 g_c J)} + PQ \left(\frac{c_V}{zR} + 1 \right) \right)_a - \left(\frac{P \alpha (\vec{G} / \rho)^3 / A^2}{(z \Re T)(2 g_c J)} + PQ \left(\frac{c_V}{zR} + 1 \right) \right)_b = 0$ $\rho = \frac{z(T,P) \Re T}{P}$ & $v = \frac{\vec{G} z(T,P) \Re T}{P}$ *at any a or b, &* $\vec{G} \equiv m / A$ $H_S^T = (H_S + \alpha v^2 / 2 g_c)_a = (H_S + (\alpha + k + 4 f / LD) v^2 / 2 g_c + g Z / g_c)_{b,c} = Const$ $\Delta H^T = H^T - (H_S + \alpha v^2 / 2 g_c)_a =$ $H^T - (H_S + (\alpha + k + 4 f / LD) v^2 / 2 g_c + g Z / g_c)_{b,c} = ... = H^T - Const$ $P = z(T,P) \rho(T,P) \Re T$ & $H(T,P) = U(T,P) + P / \rho(T,P)$		

Table 22 - Balanced Flow Meter Discharge Coefficient

Equation Basis	Equation
Base Discharge Coefficient	$C_D = \frac{\sqrt{\frac{2 g_c J \Delta H_S}{\left(\frac{\alpha + k_f}{(\rho A)_S^2} \right)_b - \left(\frac{\alpha}{(\rho A)_S^2} \right)_a}}}{\frac{\gamma A_b}{\sqrt{1 - \beta^4}} \sqrt{2 g_c \rho_a \Delta P}}$
Fluid Density Correction Expansion Factor	$\gamma = \left(\frac{\left(\frac{\Delta H}{\Delta P} \right)_S \left(\rho_a \left(1 - \beta^4 \right) \right)}{\left(\left(\frac{\rho_a}{\rho_{b,S}} \right)^2 - \beta^4 \right)} \right)^{\frac{1}{2}}$

Discharge Coefficient Base Factors	$C_D = \sqrt{\dfrac{1-\beta^4\left(\dfrac{\rho_b}{\rho_a}\right)^2}{\left(\alpha+k_f\right)_b - \alpha_a\beta^4\left(\dfrac{\rho_b}{\rho_a}\right)^2}} \approx Const.$
Discharge Coefficient Calibration Curve	$C_D = C_{D,\mathrm{Re}=\infty} + \dfrac{b}{\mathrm{Re}_D^n}$
Discharge Coefficient Base Factors and Relations	$C_D \equiv \dfrac{m_{act}}{m_{ideal}} = \dfrac{(\rho A v)_{act}}{(\rho A v)_{ideal}} = \dfrac{\rho_{b,f}}{\rho_{\min,S}}\left(\dfrac{\alpha}{\alpha+k}\right)_b^{1/2} = \dfrac{\rho_{b,f}}{\rho_{\min,S}}\left(\eta_{eff}\right)^{1/2}$
Thermodynamic Efficiency Constraint	$\eta_{eff} = \dfrac{v_{b,f}^2}{v_{b,ideal}^2} = \dfrac{(m/\rho)_{b,f}^2}{(m/\rho)_{b,ideal}^2} = \dfrac{H_b^* - H_{b,f}}{H_b^* - H_{\min,S}} = \dfrac{\alpha v_{b,f}^2}{\alpha v_{b,f}^2 + k v_{b,f}^2} = \left(\dfrac{\alpha}{\alpha+k}\right)_b$

Table 23 - Fluid Flow Parameters

Equation Basis	Equation
Velocity Distribution	$\frac{v_r}{v_{r=0}} = 1 - \left(\frac{r}{R}\right)^2$
	$\frac{\kappa(v_r - v_{r=0})}{v_{avg}\sqrt{f/2}} = Ln\left(1 - \frac{r}{R}\right)$ $\frac{v_r}{v_{r=0}} \cong \left(1 - \frac{r}{R}\right)^{\frac{1}{n}}$
Average Velocity	$\frac{v_{avg}}{v_{r=0}} = \frac{1}{2}$
	$\frac{v_{avg}}{v_{r=0}} = \frac{1}{1+10\kappa\sqrt{(f/2)}} = \frac{2n^2}{(n+1)(2n+1)}$
Momentum Correction Factor	$\beta = \frac{4}{3}$
	$\beta = \frac{(1+n)^2(2+n)^2}{2(1+2n)(2+n)}$
Kinetic Energy Correction Factor	$\alpha = \frac{(1+n)^3(2+n)^3}{4(1+3n)(2+3n)}$

Table 24 - Friction Factors with Relative Roughness Factor

Turbulent Flow, Fully Rough $(D/e)/(\mathrm{Re}\sqrt{f}) \le 0.01$	$\frac{1}{\sqrt{2f}} = Log\left(\frac{D}{e}\right) + B$
Turbulent Smooth/Rough Transition	$\frac{1}{\sqrt{2f}} = Log\left(\frac{D}{e}\right) - Log\left(\frac{(\varepsilon-1)(D/e)}{\mathrm{Re}\sqrt{f}} + 1\right) + B$
$f \pm 1.5\%, 10^8 \ge \mathrm{Re} \ge 10^4, 0.05 \ge e/D \ge 0 \Rightarrow$	$\frac{1}{\sqrt{f}} = -3.6 Log\left[\frac{6.9}{\mathrm{Re}} + \left(\frac{(e/D)}{3.7}\right)^{\frac{10}{9}}\right]$
$\mathrm{Re} \equiv \frac{D\vec{G}}{\mu} \cong const.$, $\vec{G}_{@\,any\,\vec{x}} \equiv m/A = const.$, $\kappa \cong 0.407$, $\varepsilon \cong 5.67$, $B = 2.28$, $Log = Log_{10}$	

PTK-810 Balanced Flow Meter Temperature Expansion ©

Temperature Expansion

When the temperature of a body is increased, the average distance between atoms increases. This leads to an expansion of the whole solid body as the temperature is increased. The change in any linear dimension of the solid, such as its length, width, or thickness, is called a linear expansion. If the length of the linear dimension is l, the change in length from a change in temperature ΔT is Δl. Base on experimental data, with small temperature changes, ΔT, the change in length Δl is proportional to the temperature change ΔT and to the original length l,

$$\Delta l = \alpha\, l\, \Delta T \text{ ,} \qquad \textbf{Equation 98}$$

where α, called the coefficient of linear expansion, has different values for different materials. Rewriting this formula gives,

$$\alpha = \frac{1}{l}\frac{\Delta l}{\Delta T}, \qquad \textbf{Equation 99}$$

and α is the fractional change in length per degree temperature change.

On the microscopic level, thermal expansion is an increase in the average separation between the atoms in the solid. The potential energy curve for two adjacent atoms in a crystalline solid as a function of their internuclear separation is an asymmetric curve. As the atoms move, close together, the separation decreases from the equilibrium radius. Strong repulsive forces come into play and the potential curve rises steeply $(F = -dU/dr)$. As the atoms move farther apart, the separation distance increase from the equilibrium value and somewhat weaker attractive forces take over. The potential curve rises more slowly in this region.

If the potential energy curve were symmetric about the equilibrium separation, then no matter how large the amplitude of the vibration becomes the average separation would correspond to the equilibrium separation. Thermal expansion is a direct consequence of the deviation from symmetry (that is, the asymmetry) of the potential energy curve characteristic of solids.

Some crystalline solids in certain temperature regions may contract as the temperature rises. The above analysis remains valid where compression (i.e., longitudinal) modes of vibration exist and dominate. Solids may vibrate in shear-like (i.e., transverse) modes as well and these modes of vibration will allow the solid to contract as the temperature rises, the average separation of the planes of atoms decrease. For certain types of crystalline structure and in certain temperature regions, these transverse modes of vibration may predominate over the longitudinal ones giving a net negative coefficient of thermal expansion.

For many solids, called isotropic, the percent change in length for a given temperature change is the same for all lines in the solid. The expansion is analogous to a photographic enlargement, except that a solid is three-dimensional. A flat plate with a hole punched in it, $\Delta l / l \left(= \alpha \Delta T\right)$ for a given ΔT is the same for the length, the thickness, the face diagonal, the body diagonal, and the hole diameter. Every line, whether straight or curved, lengthens in the ratio α per degree temperature rise. The equivalence to a photographic enlargement is shown below.

Figure 28 - Thermal Expansion Proportional Scaling In All Dimensions

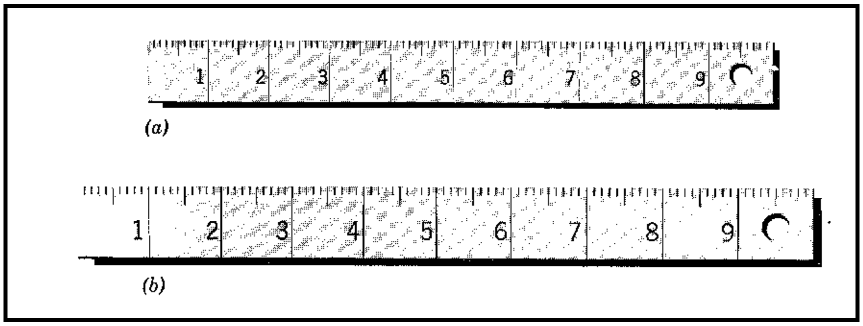

The figure above shows the same steel ruler at two different temperatures. On expansion, every dimension is increased by the same proportion; the scale, the numbers, the hole, and the thickness are all increased by the same factor. The expansion shown, from (a) to (b), is exaggerated, for it would correspond to an imaginary temperature rise of about 100,000 °C.

<u>Thermal Expansion Factors</u>
At flowing conditions, the pipe diameter will increase or decrease in size with pressure and temperature from the value measured at a reference temperature, usually 68°F (15.5°C). The effect due to pressure is usually considered negligible and only the thermal effect is normally considered. If pressure effects are considered important, please contact A+ FLOWTEK.

The sizing, flow rate, and differential pressure equations are for the flowing beta β and diameters d and D at flowing temperature. The diameters at the measured (bench) temperature of 68°F (20°C) are subscripted as d_{meas} and D_{meas}, respectively.

The pipe and primary element (plate) material expands or contracts with flowing temperature changes. The pipe and bore diameters are measured at room temperature but will be larger or smaller when used at other temperatures. These dimensions are used in the dimensional term $d^2 / \sqrt{1-\left(d/D\right)^4}$ and in the beta-ratio dependent terms for the discharge coefficient and the gas expansion factor. The pipe diameter at flowing conditions is calculated by

$$D = F_{\alpha D}\ D_{meas} = \left[1 + \alpha_P \left(T_F - 68\right)\right] D_{meas}$$ **Equation 100**

D_{meas} is the measured pipe diameter in inches at a reference temperature of 68°F (15.5°C). $F_{\alpha D}$ is the pipe material's thermal expansion correction and α_P is the coefficient of thermal expansion for the pipe material in in/(in °F).

Similarly, the bore diameter(s) is corrected for the flowing temperature by

$$d = F_{\alpha d}\ d_{meas} = \left[1 + \alpha_{PE}\left(T_F - 68\right)\right] d_{meas}$$ **Equation 101**

where d_{meas} is the measured bore diameter in inches at a reference temperature of 68°F (15.5°C), $F_{\alpha d}$ is the thermal expansion correction factor and α_{PE} is the coefficient of thermal expansion for the primary element material in in/(in °F).

The orifice is manufactured and measured at approximately 68°F; this measured diameter is determined by combining the equations as

$$d_{meas} = \frac{d}{F_{\alpha d}} = \frac{\beta D}{F_{\alpha d}}$$ **Equation 102**

where by definition the equivalent bore diameter at the flowing temperature is $d = \beta D$. For the Balanced Flow Meter, the equivalent bore diameter is reported in the A+ FLOWTEK Sizing Program and the beta factor β is used for setting the hole-layout.

The following tables give the linear expansion coefficients values and equations for many pipe and plate materials.

Table 25 - Coefficient Of Thermal Expansion Materials Listings

Material	Coefficient of thermal expansion α, in/(in·°F)	α', mm/(mm·°C)
Plain carbon steel (SAE 1020)		
70–600°F (21–315°C)	0.0000067	0.000012
−300–70°F (−185–21°C)	0.0000047	0.000009
Stainless steels		
301 70–600°F (21–314°C)	0.0000097	0.0000175
−300–70°F (−185–21°C)	0.0000076	0.0000137
304 70–600°F (21–315°C)	0.0000095	0.0000171
−300–70°F (−185–21°C)	0.0000074	0.0000133
310 70–600°F (21–315°C)	0.0000090	0.0000162
−300–70°F (−185–21°C)	0.0000070	0.0000126
316 70–600°F (21–315°C)	0.0000096	0.0000173
−300–70°F (−185–21°C)	0.0000071	0.0000128
330 70–600°F (21–315°C)	0.0000089	0.0000160
−300–70°F (−185–21°C)	0.0000058	0.0000104
347 70–600°F (21–315°C)	0.0000097	0.0000175
−300–70°F (−185–21°C)	0.0000075	0.0000135
Hastelloy B 32–212°F (0–100°)	0.0000056	0.0000101
Hastelloy C	0.0000063	0.0000113
Inconel X, annealed	0.0000067	0.0000120
Haynes Stellite 25 (L605)	0.0000076	0.0000137
Copper (ASTM B152, B124, B133)	0.0000093	0.0000167
Yellow brass (ASTM B36, B134, B135)	0.0000105	0.0000189
Aluminum bronze (ASTM B169 Alloy A)	0.0000092	0.0000166
Beryllium copper 25 (ASTM B194)	0.0000093	0.0000167
Cupronickel 30%	0.0000085	0.0000154
K-Monel	0.0000074	0.0000133
Nickel	0.0000083	0.0000149
Pyrex glass 32–580°F (0–300°C)	0.0000002	0.0000004
Titanium 70–212°F (20–100°C)	0.0000047	0.0000085
Tantalum 70–212°F (20–100°C)	0.0000036	0.0000065

Table 26 - Thermal Expansion Equations of Selected Materials

Equations for mean coefficient of thermal expansions for U.S. units from 70°F to temperature and SI units from 21°C to temperature

Carbon steel: carbon-moly, low-carbon steels (<3 Cr)

$$\alpha_{in/(in\cdot°F)} = 5.877 \times 10^{-6} + 2.538 \times 10^{-9} T_F - 2.575 \times 10^{-13} T_F^2 - 2.042 \times 10^{-16} T_F^3$$

$$\alpha_{mm/(mm\cdot°C)} = 10.725 \times 10^{-6} + 8.171 \times 10^{-9} T_{°C} - 1.671 \times 10^{-12} T_{°C}^2 - 2.065 \times 10^{-15} T_{°C}^3$$

Stainless steels

300 Series

$$\alpha_{in/(in\cdot°F)} = 8.949 \times 10^{-6} + 2.009 \times 10^{-9} T_F - 1.043 \times 10^{-12} T_F^2 + 3.381 \times 10^{-16} T_F^3$$

$$\alpha_{mm/(mm\cdot°C)} = 16.223 \times 10^{-6} + 6.307 \times 10^{-9} T_{°C} - 5.940 \times 10^{-12} T_{°C}^2 + 3.589 \times 10^{-15} T_{°C}^3$$

400 Series

$$\alpha_{in/(in\cdot°F)} = 5.073 \times 10^{-6} + 2.151 \times 10^{-9} T_F - 6.526 \times 10^{-13} T_F^2 + 3.920 \times 10^{-17} T_F^3$$

$$\alpha_{mm/(mm\cdot°C)} = 9.255 \times 10^{-6} + 6.841 \times 10^{-9} T_{°C} - 3.825 \times 10^{-12} T_{°C}^2 + 4.517 \times 10^{-16} T_{°C}^3$$

†Ranges of 70 to 600°F (21–315°C) unless otherwise noted.

The following figure graphically provides the $F_{\alpha d}$ and $F_{\alpha D}$ corrections. The values from these graphs are used for thermal expansion dimensional corrections for the Balanced Flow Meter plate and pipe.

Figure 29 - Thermal Expansion Plots of Common Steels

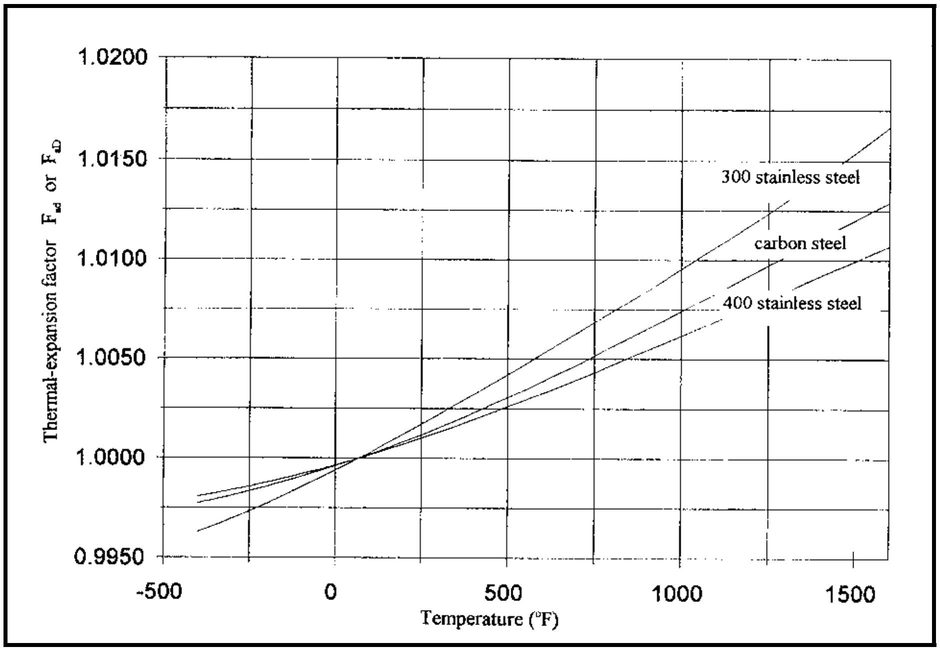

The above values, equations and figures are used to correct the flowing temperature β from the pipe and plate manufactured temperature and vice versa.

For plates and pipes made of the same material <u>no</u> beta-ratio (β) thermal expansion correction is required. For the typical plate design of 304 or 316 stainless steel with a carbon steel pipe, the ratio of $F_{\alpha d} / F_{\alpha D}$ is typically close to one (1) in the temperature region of most industrial applications. The A+ FLOWTEK Balanced Flow Meter Sizing Program calculates the measured hole diameters based the 300 stainless steel series basis.

For highly accurate applications, < 0.25%, the thermal correction ratio should be applied from real time temperature measurements. A fluid density correction should also be applied. The flowing fluid density correction is typically most important when compared to the pipe/plate thermal expansion ratio correction.

PTK-811 Balanced Flow Meter Low Reynolds Number Corrections ©

Foreword

For fluid-flow processes, equation adjustments are required for the laminar, transition, and turbulent flow regimes. The orifice or venturi equation, as derived from the Bernoulli equation, is typically based on fully developed turbulent flow. However, for Reynolds numbers below 30,000 to 60,000 correction factors are required to adequately describe the Bernoulli head meter. These effects are reviewed and equations are provided to correct for low Reynolds number operations with the Balanced Flow Meter.

Engineering Bernoulli Equation

The steady state *engineering Bernoulli equation* for flow systems of any steady state, thermodynamic path and flow regime is given by,

$$\Delta\left(\frac{\alpha v^2}{2g_c}\right)+\Delta\frac{gZ}{g_c}+\int\frac{dP}{\rho}+W_{shaft}+LW_{friction}=0 \qquad \text{Equation 103}$$

For a head meter, such as an orifice, venturi, or Balanced Flow Meter, the generalized orifice equation is used as derived from the Bernoulli equation,

$$m=\frac{C_D\gamma A_b}{\sqrt{1-\beta^4}}\sqrt{2g_c\rho_a\Delta P}\equiv Orifice\ Equation \qquad \text{Equation 104}$$

The discharge coefficient C_D is used to correct for losses from frictional effects and to correct for low Reynolds numbers, where the kinetic energy correction factors α,s are not one (1). A more general equation is,

$$m=\frac{C_V C_C\gamma A_b}{\sqrt{\alpha_b-\alpha_a C_C^2\beta^4}}\sqrt{2g_c\rho_a\Delta P} \qquad \text{Equation 105}$$

For an orifice plate, C_V is the velocity coefficient and C_C is the contraction coefficient. The kinetic energy correction factors are for the upstream position, α_a, and downstream position, α_b.

Orifice Contraction and Velocity Coefficients

In the fully developed turbulent flow regime, the contraction coefficient C_C is given by,

$$C_C=\left(1+\frac{(1-\beta^4)}{(1+C_D)}\right)^{-1} \qquad \text{Equation 106}$$

The beta factor β is the orifice hole to pipe diameter ratio, $D_{Orifice}/D_{Pipe}$, and the discharge coefficient C_D for any beta factor is,

$$C_D = \frac{\pi}{\pi + 2} \qquad \text{Equation 107}$$

The orifice velocity coefficient C_V is given by,

$$C_V = \left(\frac{C_D}{C_C}\right)_{\beta=0} \left(1 - C_D^4 \beta^4\right)^{\frac{1}{2}} \qquad \text{Equation 108}$$

On this basis,

$$C_D = \left(\frac{C_D}{C_C}\right)_{\beta=0} \left(1 - C_D^4 \beta^4\right)^{\frac{1}{2}} \left(\frac{(1-\beta^4)}{(1/C_C^2 - \beta^4)}\right)^{\frac{1}{2}} \qquad \text{Equation 109}$$

Plots of these factors for measured and calculated orifice plate values are shown below,

Table 27 - Orifice Plate Flow Correction Factors at High Reynolds Numbers

Velocity Coefficient C_V	Contraction Coefficient C_C
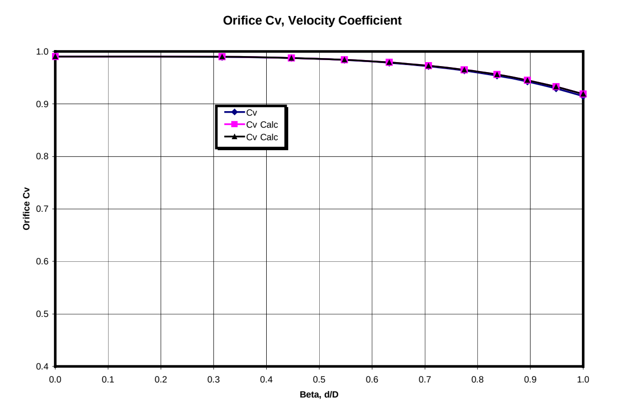	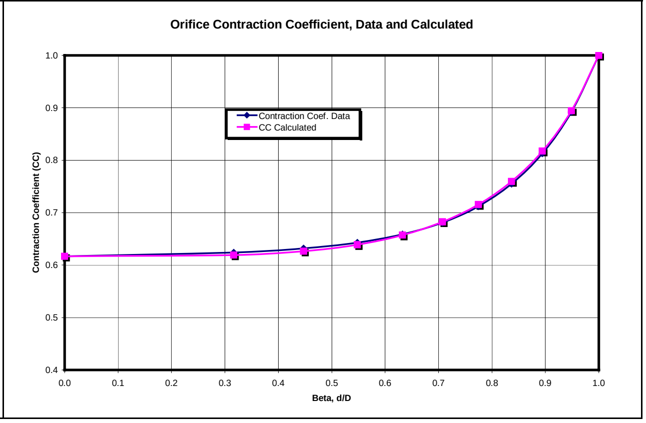

Kinetic Energy Correction Factor

The kinetic energy correction factor corrects the average pipe velocity for the actual velocity profile. The velocity profile in developed flow is dependent on the friction factor f. The kinetic energy correction factor α is given by,

$$\alpha = 1 + \frac{f}{8\kappa^2}\left(15 - \frac{9}{\kappa}\sqrt{f}\right), \qquad \text{Equation 110}$$

for turbulent flow, and $\alpha = 2$ for laminar flow.

Reynolds Number Correction, Contraction Factor and Contraction Coefficient
The contraction coefficient is a function of Reynolds number. The Reynolds number correction factor for an orifice is given by,

$$F_{\mathrm{Re}} = 1/(1 + 2000/(\mathrm{Re} - 100)),$$ Equation 111

as shown in the following figure.

Figure 30 - Orifice Contraction Correction Factor

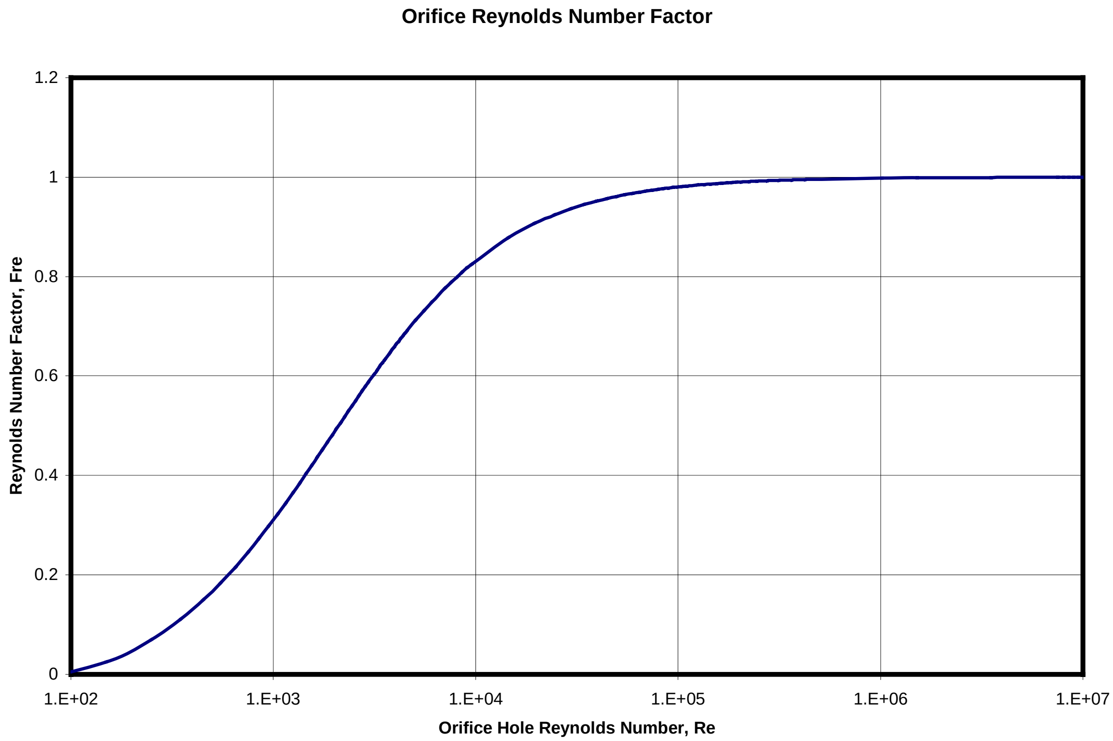

The orifice contraction factor exponent C_f corrects the contraction factor as a function of beta factor. The regressed equation is,

$$C_f = 29.442\beta^4 - 35.747\beta^3 + 15.731\beta^2 - 2.5684\beta + 0.5323$$ Equation 112

The following figure provides a plot of the contraction factor exponent C_f as a function of beta factor, and regression results. As shown, the R squared value is one (1).

Figure 31 - Contraction Factor Exponent

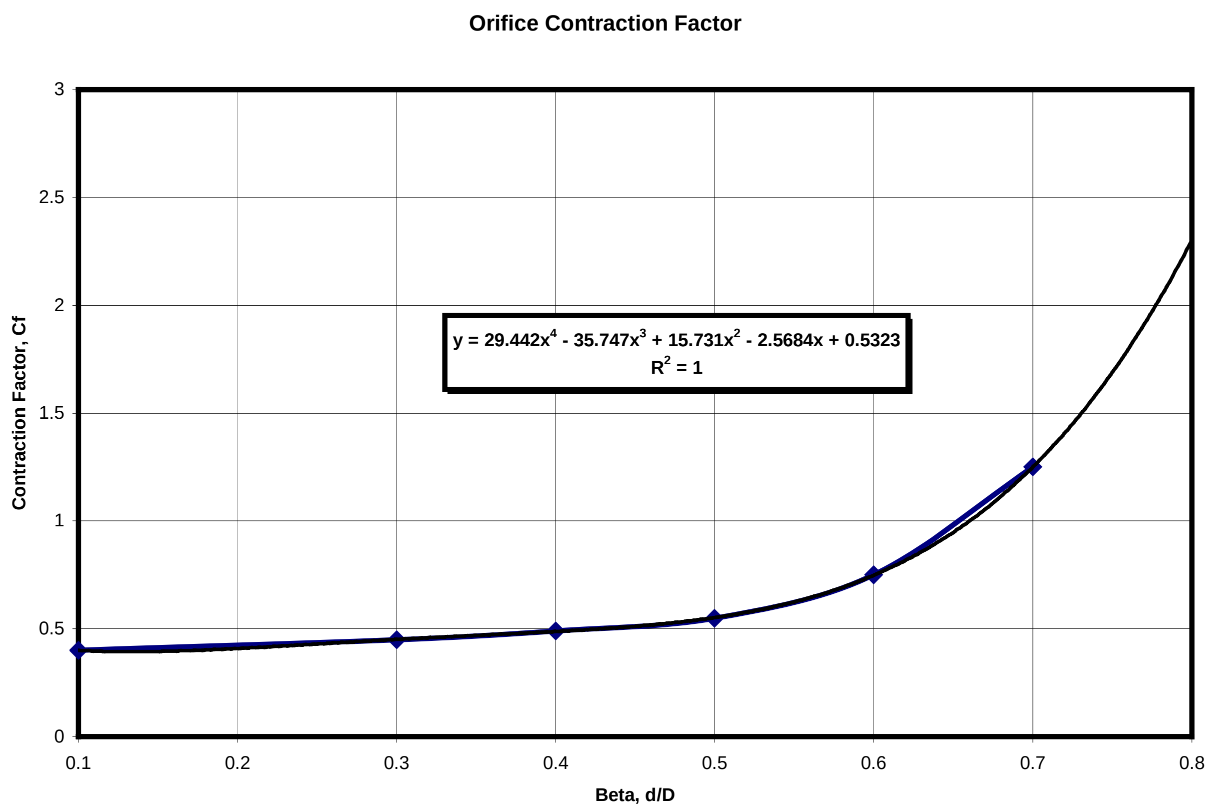

With these factors, the orifice contraction coefficient, as a function of Reynolds number is given by,

$$C_C = \left(1 + \frac{(1-\beta^4)}{F_{\mathrm{Re}}^{C_f}(1+C_D)}\right)^{-1} \qquad \text{Equation 113}$$

<u>Discharge Coefficient Calculation Method</u>

The general calculation method for the discharge coefficient C_D is given by,

$$C_D = \frac{C_V C_C \left(1-\beta^4\right)^{\frac{1}{2}}}{\left(\alpha_b - \alpha_a C_C^2 \beta^4\right)^{\frac{1}{2}}} \qquad \text{Equation 114}$$

and $C_D/(1-\beta^4)^{1/2}$ includes the velocity of approach. This method applies to any head meter, including the orifice, venturi, or Balanced Flow Meter. With $\alpha_a = \alpha_b = 1$ and with the contraction coefficient equal to a value of one, $C_C = 1$, the discharge coefficient C_D is equal to the velocity coefficient C_V, e.g. $C_D = C_V$. For other conditions the following method applies:

The velocity coefficient C_V is determined from,

$$C_V = \left(\frac{C_D}{C_C}\right)_{\beta=0} \left(1 - C_D^{4/m} \beta^{4/m}\right)^{\frac{m}{2}},$$ Equation 115

and the contraction coefficient is given by,

$$C_C = \left(1 + \frac{(1-\beta^4)}{F_{\mathrm{Re}}^{C_f}(1+C_D)}\right)^{-m}.$$ Equation 116

For an orifice $(m = 1)$,

$$C_{D,O} = \left(\frac{\pi}{\pi + 2}\right)_{m=1}^{m},$$ Equation 117

for the venturi $(m = 1/8 ... 1/n')$,

$$C_{D,V} = \left(\frac{\pi}{\pi + 2}\right)_{m=1/8(or\, 1/n')}^{m},$$ Equation 118

and for the Balanced Flow Meter $(m = 1/4)$,

$$C_{D,BFM} = \left(\frac{\pi}{\pi + 2}\right)_{m=1/4}^{m}.$$ Equation 119

<u>Discharge Coefficient Plots</u>

With these Reynolds number correction factors, the discharge coefficients can be estimated. The following figures show the discharge coefficients for an orifice plate, venturi and Balanced Flow Meter as a function of Reynolds number. These figures may be used to estimate the discharge coefficients for Reynolds numbers less than 30,000 to 60,000. Surface tension may affect the discharge coefficient below a Reynolds number of about 300. For fluid flow systems where surface tension is not important, the discharge coefficients as shown on the following figures may be extrapolated (or calculated) for Reynolds number values below 300. A hole-tap is recommended for these fluid measurement systems. The hole-tap approach directly measures the Bernoulli effect. For any flow condition and design, field calibration is recommended.

Figure 32 - Orifice Discharge Coefficients, Velocity of Approach Included

Measured Discharge Coefficient	Calculated Discharge Coefficient
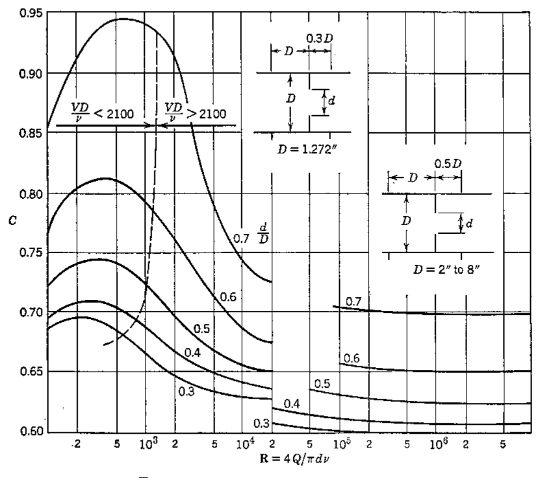	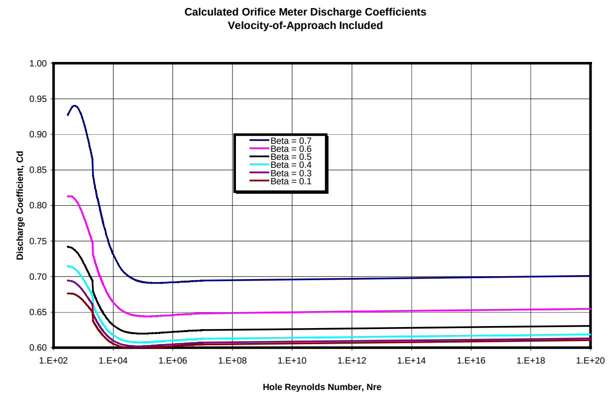

Note: The Reynolds Number range is enlarged in this figure to show the limit as $\mathrm{Re} \Rightarrow \infty$. At low Reynolds numbers, the measured and calculated values are within experimental error.

Figure 33 - Venturi Discharge Coefficients, Velocity of Approach Not Included

Measured Discharge Coefficient	Calculated Discharge Coefficient
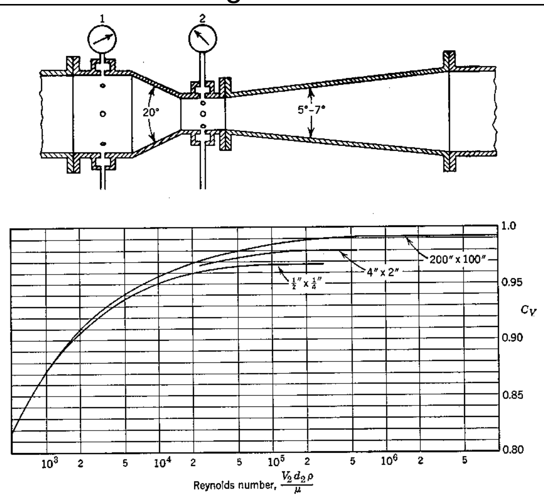	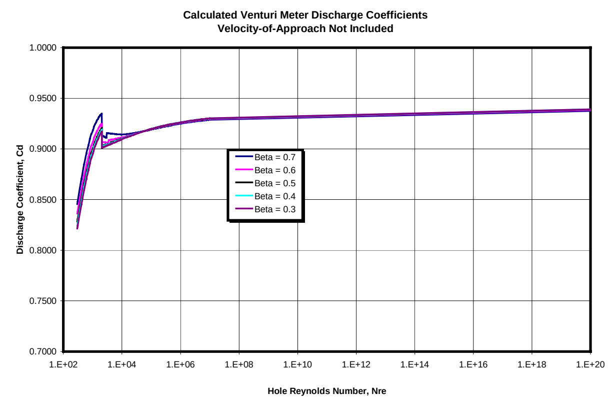

Note: The Reynolds Number range is enlarged in this figure to show the limit as $\mathrm{Re} \Rightarrow \infty$. At low Reynolds numbers, the measured and calculated values are within experimental error.

Figure 34 - Calculated Orifice Meter Discharge Coefficients, Velocity-of-Approach Included

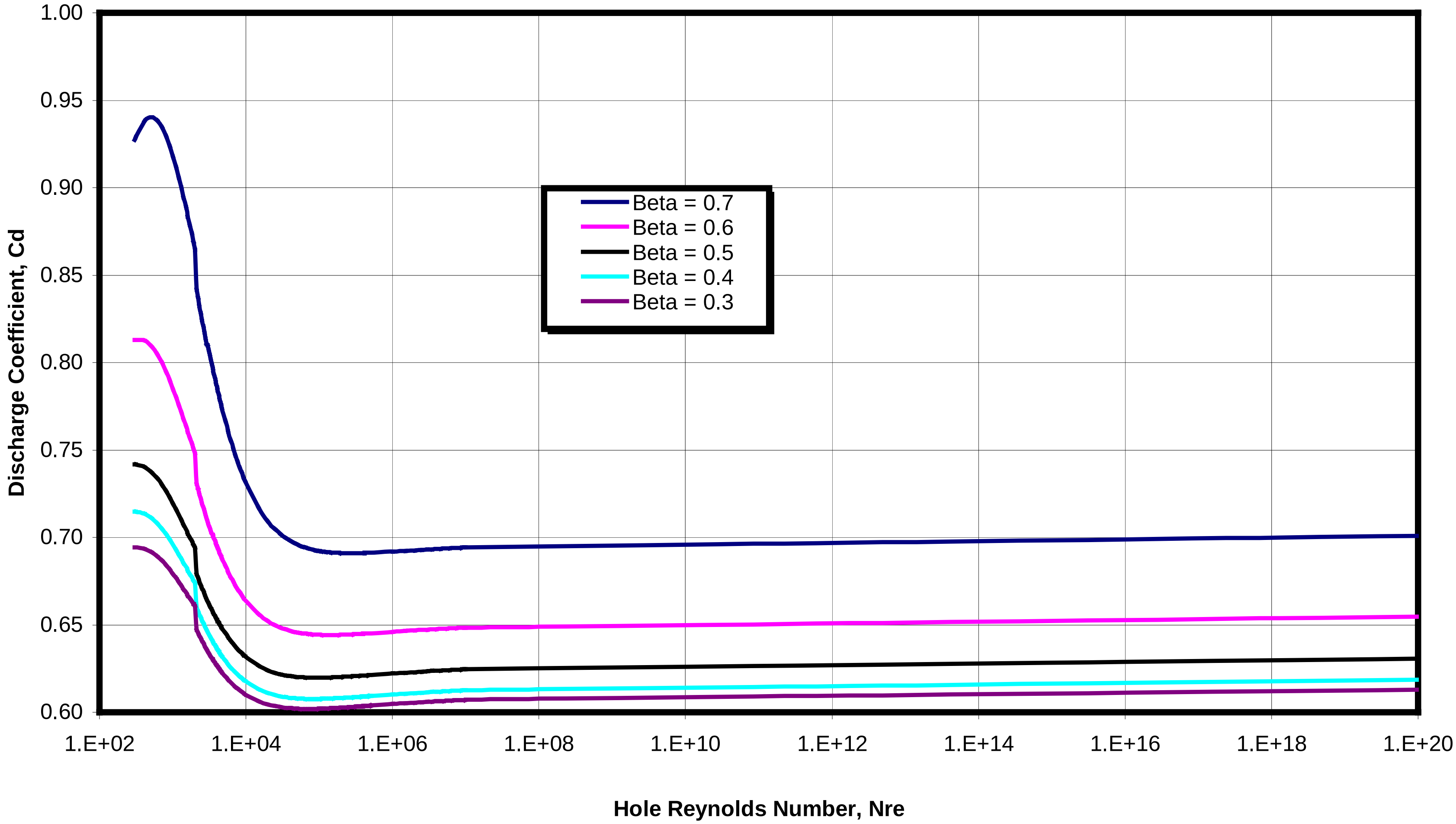

Figure 35 - Calculated Orifice Meter Discharge Coefficients, Velocity-of-Approach Not Included

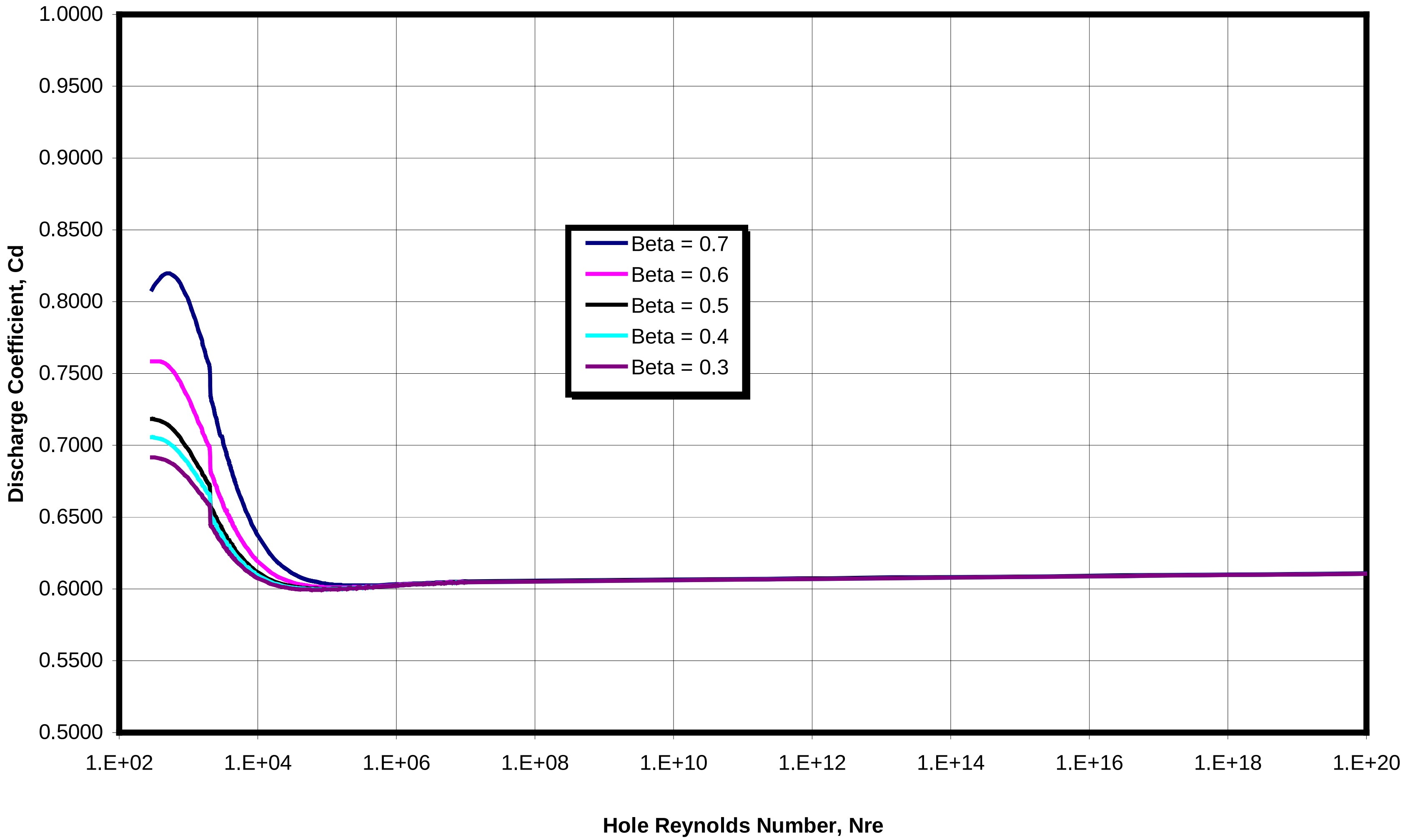

Figure 36 - Calculated Venturi Meter Discharge Coefficients, Velocity-of-Approach Included

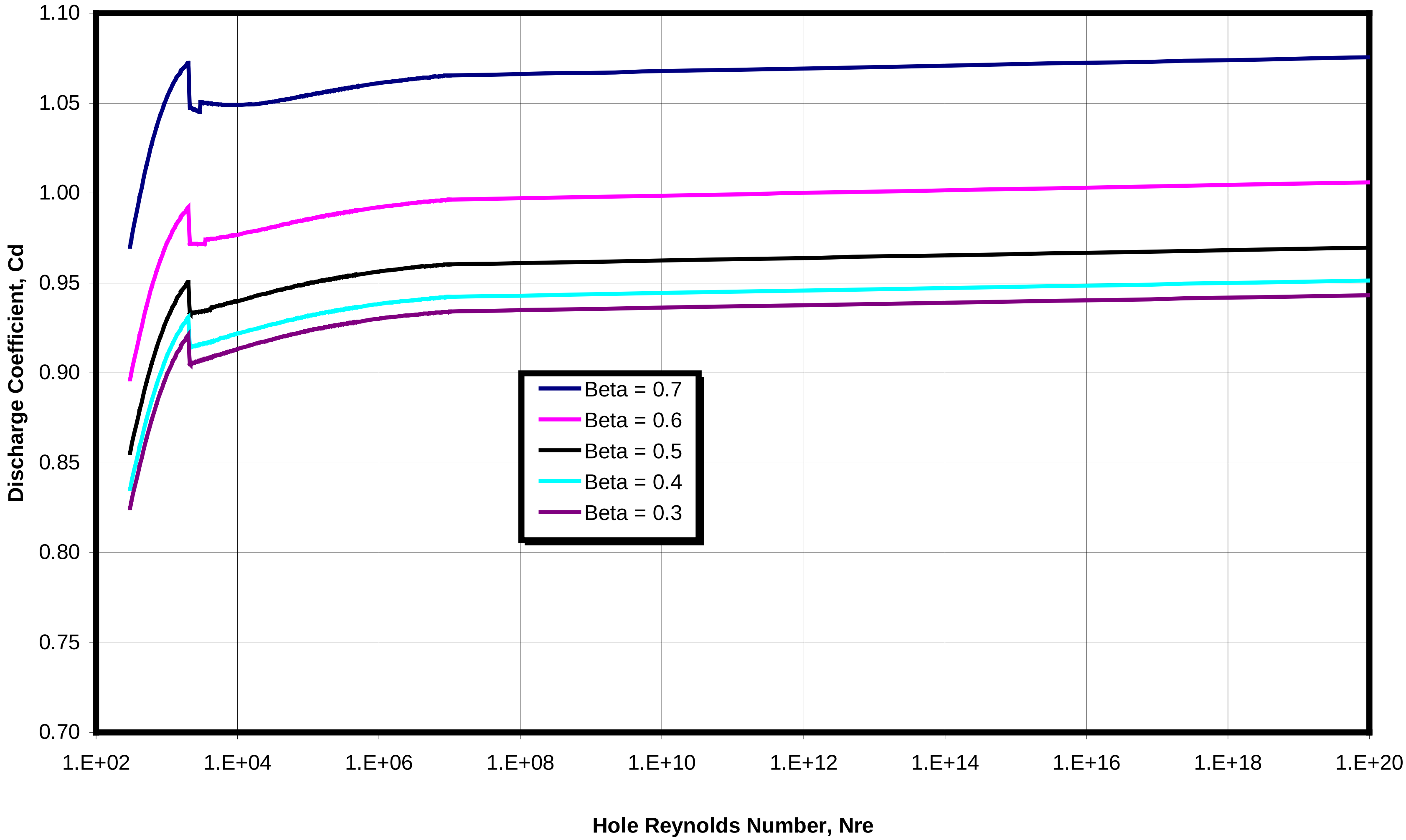

Figure 37 - Calculated Venturi Meter Discharge Coefficients, Velocity-of-Approach Not Included

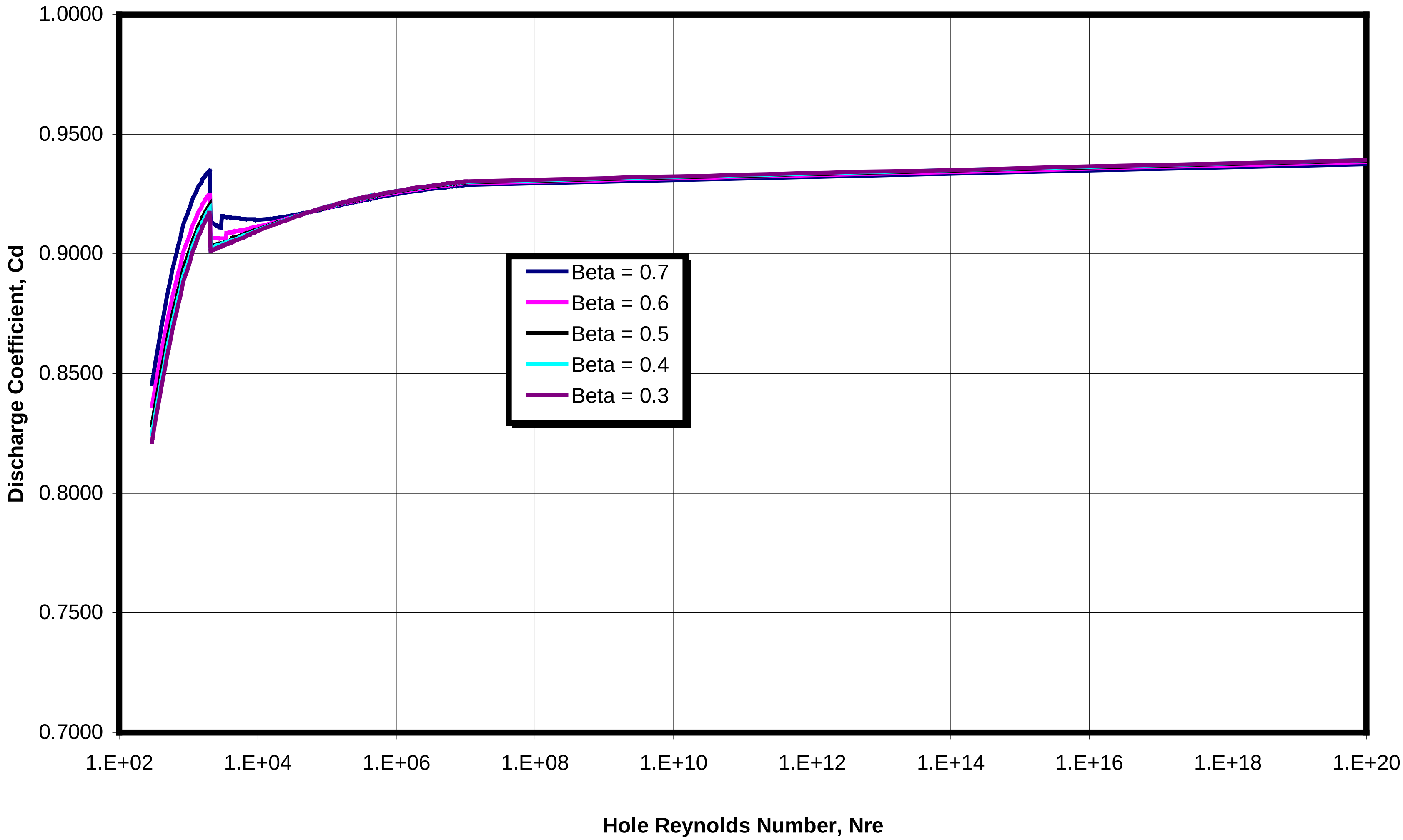

Figure 38 - Calculated Balanced Flow Meter Discharge Coefficients, Velocity-of-Approach Included

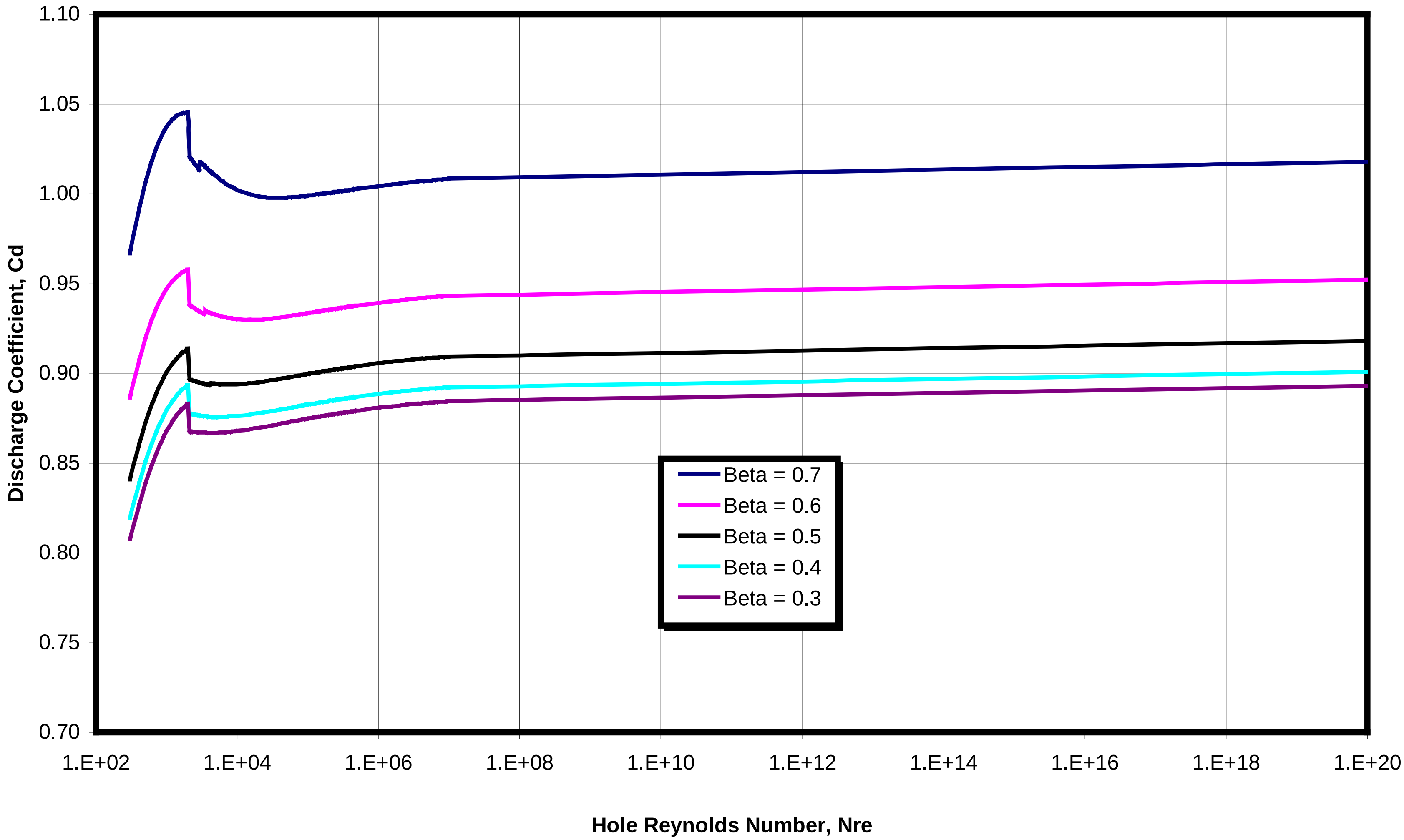

Figure 39 - Calculated Balanced Flow Meter Discharge Coefficients, Velocity-of-Approach Not Included

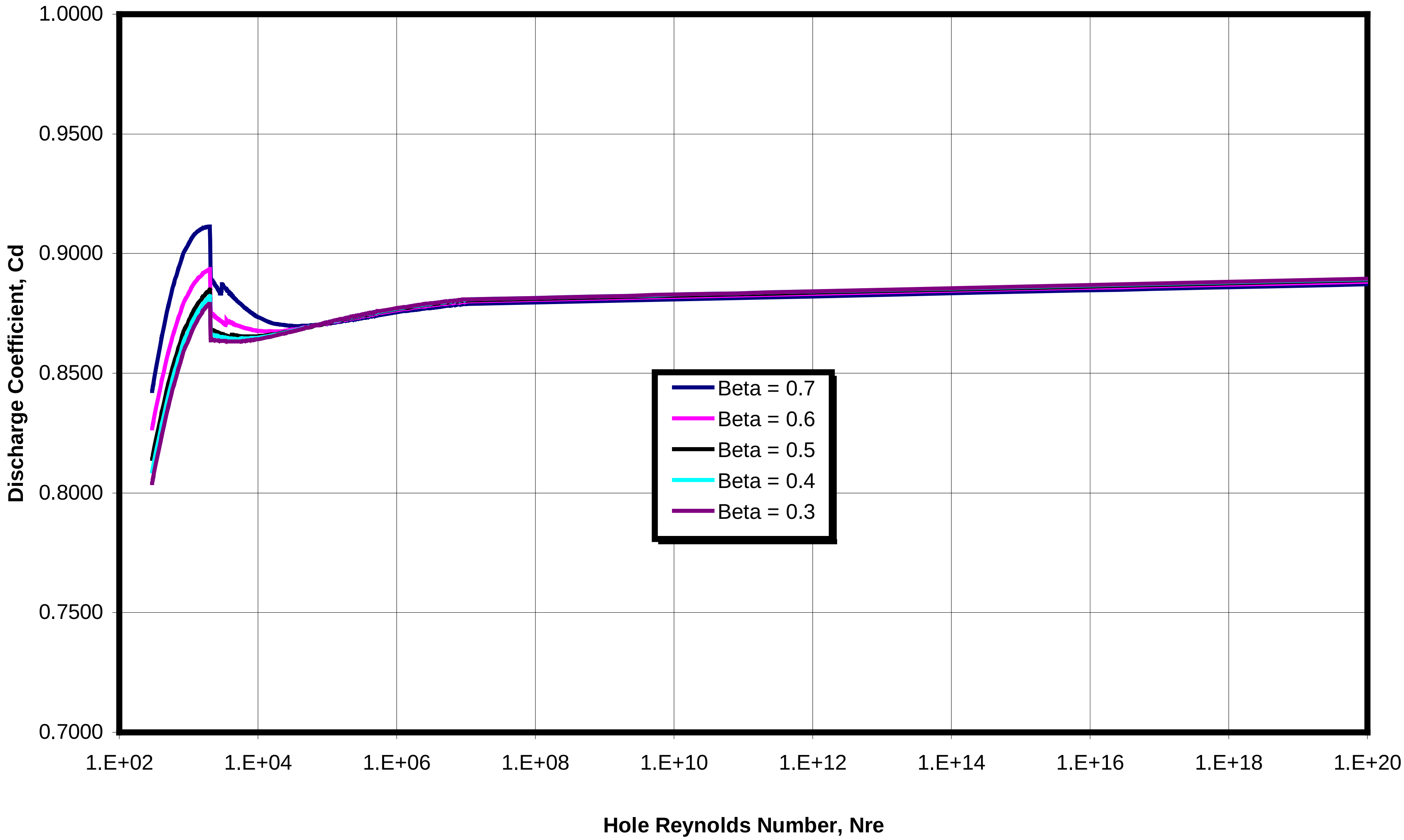

Acknowledgement

The author is grateful to NASA/Marshall Space Flight Center and Dr. William A. Heenan, Dean of Engineering, Texas A&M University-Kingsville and A+ FLOWTEK Vice President, for their support in the development of the Balanced Flow Meter. Dr. Heenan is the co-developer of the MIMT© algorithm.

References

1 Unit Operations of Chemical Engineering, 2nd Edition, McCabe & Smith
2 Unit Operations of Chemical Engineering, 3rd Edition, McCabe & Smith
3 Unit Operations of Chemical Engineering, 5th Edition, McCabe, Smith & Harriott
3a Unit Operations of Chemical Engineering, 5th Edition, McCabe & Smith, 1956
4 Engineering Thermodynamics, Reynolds & Perkins
5 Chemical Engineering Thermodynamics, Balzhiser, Samuels and Eliassen
6 Thermodynamics of Engineering Science, Soo
7 Thermodynamics, Principles of, Sorensen
8 Properties of Gases and Liquids, The, 2nd Edition, Reid and Sherwood
8a Properties of Gases and Liquids, The, 2nd Edition, Reid and Sherwood
9 Thermodynamics and Its Applications, 2nd Edition, Modell & Reid
10 Tubular Exchanger Manufacturers Association, Standards of, 6th Edition, TEMA
11 Heat Transmission, 3rd Edition, McAdams
12 Process Heat Transfer, Kern
13 Applied Heat Transfer, Ganapathy
14 Industrial Heat Transfer, Hutchinson
15 Heat Transfer, Handbook of, Rohsenow & Hartnett
16 Process Heat Transfer, Hewitt, Shires & Bott
17 Heat Transfer, Lindon C. Thomas
18 Fluid Mechanics and Heat Transfer, Kay
19 Heat Transfer, 3rd Edition, Brown & Marco
20 Thermal Network Modeling Handbook, NASA Contract 9-10435
21 Heat Exchangers, Design of, Chemical Engineering, Lord, Minton & Slusser
22 Elementary Fluid Mechanics, 4th Edition, Vennard
23 Fluid Mechanics for Chemical Engineers, 2nd Edition, de Nevers
24 Petroleum Refinery Engineering, 4th Edition, Nelson
25 Plant Design and Economics for Chemical Engineers, 4th Edition, Peters & Timmerhaus
26 Perry’s Chemical Engineers' Handbook, 5th Edition
27 Perry's Chemical Engineers' Handbook, 6th Edition
28 Perry's Chemical Engineers' Handbook, 7th Edition
29 Compressor Selection for the Chemical Process Industries, Chemical Engineering, January 20, 1975, McGraw-Hill
30 Can You Rerate Your Centrifugal Compressor? Chemical Engineering, January 20, 1975, McGraw-Hill Inc.
31 Properties of Gases and Liquids, The, 5th Edition, Poling, Prausnitz & O’Connell, McGraw-Hill
32 Probability and Statistics, Spiegel

33 Statistics, 3rd Edition, Spiegel & Stephens

34 Weibull Handbook, The New, 3rd Edition, Abernathy

35 Machinery Malfunction Diagnosis and Correction, Vibration Analysis and Troubleshooting for the Process Industries, Robert C. Eisenmann, Sr., P.E., Robert C. Eisenmann, Jr., Prentice Hall, 1998

36 Chemical Properties Handbook: Physical, Thermodynamics, Environmental Transport, Safety and Health Related Properties for Organic and Inorganic Chemical, Carl L. Yaws, McGraw-Hill, October 1998

37 Statistics, Schaum's Outline Theory and Problems of, 2nd Edition, Murray R. Spiegel, Ph.D., McGraw-Hill, 1988

38 Statistical Design and Analysis of Experiments with Applications to Engineering and Science, Robert L. Mason, Richard F. Gunst, James L. Hess, John Wiley & Sons

39 Polymerization, Principles of, 2nd Edition, George Odian, John Wiley & Sons, 1981

40 Polymerization, Rubbers, Plastics, and Fibers, Fundamental Principles of, G. F. D'Alelio, John Wiley & Sons, 1952

41 Pyrolysis: Theory and Industrial Practice, Lyle F. Albright, Billy L. Crynes, William H. Corcoran, Academic Press, 1983

42 Coke Formation on Metal Surfaces, Lyle F. Albright, R. T. K. Baker, American Chemical Society, 1982

43 Modeling and Simulation in Chemical Engineering, Roger G. E. Franks, John Wiley & Sons, 1972

44 Polymer Science, Textbook of, 3rd Edition, F.W. Billmeyer, Jr., John Wiley & Sons, 1984

45 Hydrogenation Catalysts, Robert J. Peterson, Noyes Data Corporation, 1977

46 Ethylene Producers Conference, Proceedings of the 5^{th}, Vol. 2, March 29 - April 1, 1993, American Institute of Chemical Engineers, 1994

47 Polymer Chemistry, Principals of, Paul J. Flory, Cornell University Press, 1953

48 Polymer Chemistry, Introduction to, Raymond B. Seymour, McGraw-Hill, 1971

49 Gases, Liquids and Solids, D. Tabor, Penguin Books Ltd., 1969

50 Chemical Kinetics, 3rd Edition, Keith J. Laidler, Harper & Row, 1987

51 Manufacturing Processes, 6th Edition, Begeman, Amstead, John Wiley & Sons, 1957

52 Petroleum Refining

53 Furnace Operations

54 Separation Process Technology, Handbook of

55 Basic Electrical Engineering

56 Separation Techniques for Chemical Engineers, Handbook of, 2nd Edition

57 Advanced Engineering Mathematics, 3rd Edition

58 Mathematical Tables and Formulas, Handbook of, 5th Edition

59 Process Instruments and Controls Handbook
60 Physical Chemistry, 2nd Edition
61 Physical Properties of Hydrocarbons, Volume 1
62 Physical Properties of Hydrocarbons, Volume 2
63 Understanding Statistical Process Control
64 Chemical and Catalytic Reaction Engineering
65 Engineering Fundamentals, Handbook of, 2nd Edition
66 Engineering Optimization Methods and Applications, G.V. Reklaitis, An. Ravindran, K.. Ragsdell
67 Physical Chemistry, Outlines of
68 Chemical Thermodynamics, A Course of Study
69 Separation Processes, 2nd Edition
70 Modeling and Simulation, Proceedings of the IASTED International Conference, MS‘94
71 Gas-Liquid and Gas-Liquid-Solid Reactor Engineering, The First International Conference On, Volume 47, #13/14
72 Equilibrium Stage Processes, Design of
73 Petroleum Refining Processes, Handbook of
74 Process Modeling, Simulation and Control for Chemical Engineers, 2nd Edition
75 Engineering Mathematics Handbook, 2nd Edition
76 Momentum, Heat, and Mass Transfer, Fundamentals of, 3rd Edition
77 Process Dynamics, Modeling, and Control
78 High Polymers, Analytical Chemistry of Polymers, Part I, Volume XII, Analysis of Monomers and Polymeric Materials, Plastics - Resins - Rubbers - Fibers
79 Mathematics - It’s Magic and Mastery
80 Environmental Engineering, Standard Handbook of
81 Noise Control Solutions for the Chemical & Petroleum Industry
82 Refrigeration and Air Conditioning, Mechanical Engineering
83 Chemistry and Physics, Handbook of,
84 Applied Mathematics in Chemical Engineering, 2nd Edition
85 Distillation Control
86 Chemical Reaction Engineering, 2nd Edition
87 Distillation Operations
88 Neural Networks for Optimization and Signal Processing
89 Chemical Data Guide for Bulk Shipment by Water
90 Heat Transfer, Elements of, 3rd Edition
91 Numerical Analysis, Schaum’s Outline Theory and Problems of
92 Engelhard Catalysts
93 Numerical Methods, Software and Analysis
94 Applied Numerical Methods

95 Flow of Fluids Through Valves, Fittings, and Pipe by Crane
96 Modeling, Simulation and Control in the Process Industry, Proceedings of the IASTED International Conference
97 Distillation Engineering
98 Expert Systems
99 Applied Numerical Methods with Personal Computers
100 Physics, Parts I & II
101 Chemical Principles, 2nd Edition
102 Understanding Industrial Designed Experiments, 2nd Edition
103 Numerical Methods with FORTRAN IV Case Studies
104 Air Conditioning System Design, Handbook of
105 Navco Piping Data
106 Plane and Spherical Trigonometry
107 Hazardous Waste Incineration, Handbook of
108 Chemical Reaction Engineering, Fundamentals of, 2nd Edition
109 Steam - Its Generation and Use, 37th Edition
110 Geometry, 2nd Edition
111 Air Pollution Control, A Design Approach
112 Control Systems, Continuous and Discrete
113 Statistical Process Control for Quality Improvement
114 Chemical Hazard Analysis Procedures, Handbook of
115 Engineering Mechanics of Deformable Bodies, 2nd Edition
116 Thermodynamics, Introduction to, Classical & Statistical, 2nd Edition
117 Differential Equations, Schaum's Outline Theory and Problems of
118 Mechanics molecular Physics Heat and Sound
119 Corrosion Inhibitors, Recent Developments
120 Elementary Differential Equations, 4th Edition
121 Organic Chemistry, 3rd Edition
122 Biochemical Engineering Fundamentals, 2nd Edition, James E. Bailey, David F. Ollis
123 Processes for Major Addition - Type Plastics and their Monomers
124 Micro-Organisms, Introduction to
125 Kinetic Theory of Gases, An Introduction to the
126 Physicochemical Processes for Water Quality Control
127 Strength of Materials
128 Concepts in Physics
129 Gaseous State, The
130 Catalytic Hydrogenation
131 Encyclopedia of Science Industry and Technology

132 Thermodynamics
133 Applied Mathematics, Handbook of, 4th Edition
134 Elementary Differential Equations
135 Vector Mechanics for Engineers: Dynamics
136 College Chemistry with Qualitative Analysis
137 Numerical Recipes, The Art of Scientific Computing
138 Nuclear Physics, Progress in, Volume 2
139 Thermodynamic Fundamentals for Engineers with Problems and Solutions
140 Physical Methods in Chemical Analysis, Volume III
141 Fundamental Physics, 2nd Edition
142 National Electrical Code
143 American Civil Engineers' Handbook, Volume 1, 5th Edition
144 Electricity for Air Conditioning and Refrigeration Technicians
145 Great Ideas of Modern Mathematics: Their Nature and Use
146 Transport Phenomena
147 Surface Water Quality Modeling and Control, Principals of
148 Environmental Control
149 Electrical Engineering, Introduction to
150 College Calculus with Analytic Geometry, 2nd Edition
151 Differential and Integral Calculus, Schaum's Outline Theory and Problems of
152 Modern Refrigeration and Air Conditioning
153 AIChE Reprints, 88th National Meeting, AIChE
154 Plane Trigonometry, 2nd Edition
155 Thermodynamic Properties of Minerals and Related Substances
156 Calculation & Shortcut Desk Book
157 Analytical Chemistry, Fundamentals of, 3rd Edition
158 Fixed-Bed Reactor Design and Diagnostics
159 Farris Safety and Relief Valves
160 Visual Display of Quantitative Information
161 Structured Programming, Fundamentals of
162 AMPL - A Modeling Language for Mathematical Programming
163 AIChE Extended Abstracts, Annual Meeting, AIChE, 1992
164 Refinery Operating Costs, Guide to
165 Flow Data Reference Book, ABB Kent-Taylor
166 Polyred, Computer-Aided Polymerization Reactor Design
167 Route Surveying and Design, 4th Edition
168 ISA Instrumentation and Control, Advances In, Volume 47, Part 1, ISA 1992
169 ISA Instrumentation and Control, Advances In, Volume 47, Part 2, ISA 1992
170 Water, the Universal Solvent

171 AIChE Separations Technologies: New Developments and Opportunities, First Separations Division Topical Conference on, AIChE, 1992
172 Industrial Computing Conference, Proceedings of the, Volume 2, ICS/92
173 Flow Solutions, ABB Instrumentation
174 Transwedge, Severe Service for Liquids, Gas, Steam, and Slurries, Rawson
175 Engineering Data Book, GPSA, Volume I, 10th Edition
176 Engineering Data Book, GPSA, Volume 2, 10th Edition
177 Modeling, Simulation, and Optimization of Chemical Processes, Special Summer Program, MIT, 1992
178 Disposal of Refinery Wastes, Manual on, Volume on Atmospheric Emissions
179 Disposal of Refinery Wastes, Manual on, Volume on Solid Wastes
180 Disposal of Refinery Wastes, Manual on, Volume on Liquid Wastes
181 Carbon Adsorption, Process Design Manual
182 Phosphorus Removal, Process Design Manual
183 Vogt, F-11
184 Vogt, F-12
185 Ethylene Forum, 8th
186 Upgrading Existing Wastewater Treatment Plants, Process Design Manual
187 Oil Industry Terms & Phrases, Handbook of, 5th Edition, Langenkamp
188 Ullmann's Encyclopedia of Industrial Chemistry 5e Vol B1 - Fundamentals of Chemical Engineering
189 Properties of Gases and Liquids, The, 3rd Edition, Reid, Prausnitz, Sherwood
190 Physical Properties of Polymers, 2nd Edition, Mark, Eisenberg, Graessley, et al
191 Properties of Gases and Liquids, The, 4th Edition, Reid, Prausnitz, Poling
192 Polymer Solutions - An Introduction to Physical Properties
193 Process Modeling, Simulation and Control for Chemical Engineers, 1st Edition
194 Process Systems Analysis and Control, Coughanowr and Koppel
195 Chemical Engineering Thermodynamics, Introduction to, Smith and Van Ness
196 Momentum, Heat and Mass Transfer, Bennett and Myers
197 Petroleum Refining Processes, Handbook of, 2nd Edition, Myers
198 Petroleum Reservoir Engineering, 1960, Amyx, Bass & Whiting
199 Petroleum Chemistry and Refining, Speight
200 Noise - A Comprehensive Survey from Every Point of View, 1935, McLachlan
201 Mathematical Tables, Pryde
202 Molecular Thermodynamics of Fluid-Phase Equilibria, 3rd Edition, Prausnitz etal
203 Computer Calculations for High-Pressure Vapor-Liquid Equilibria
204 Engineering Data Book, GPSA, 12th Edition, Volume I, & CD-ROM set, FPS Version
205 Engineering Data Book, GPSA, 12th Edition, Volume2
206 Chemical Process Equipment: Selection and Design, Stanley M. Walas

207 Engineering Data Book, GPSA, 9th Edition, Volume I
208 Technical Data Handbook, The Hartford Steam Boiler Insp & Ins Co., 2nd Edition,1984
209 Mathematical Ideas, 6th Edition, Miller, Heeren, Hornsby
210 Fundamentals of College Algebra, Swokowski, 7th Edition
211 Fundamentals of College Algebra, Study Guide and Solutions Manual, Cole
212 Economics Today, 8th Edition, Miller
213 Mathematical Applications, Harshbarger / Reynolds
214 Physical Chemistry, Kittsley, 3rd Edition
215 General Chemistry & General Chemistry with Qualitative Analysis, 5th Edition
216 General Chemistry & General Chemistry with Qualitative Analysis, 5th Edition, Inst Manual
217 General Chemistry & General Chemistry with Qualitative Analysis, 5th Edition, Test Bank
218 How to Think Like Einstein, Scott Thorpe
219 How to Think Like Leonardo da Vinci, Michael J. Gelb
220 Mathematical Applications, Instructor's Guide, Harshbarger / Reynolds
221 Solar Energy Thermal Processes, John Duffie; William Beckman
222 Passive Solar Energy, Bruce Anderson; Malcolm Wells
223 Thermodynamics, 2nd Edition, Reynolds
224 Fluid Mechanics, 5th Edition, Streeter
225 Elementary Fluid Mechanics, 6th Edition, Vennard & Street, Wiley
226 Thermodynamics, 2nd Edition, Holman
227 Fluid Mechanics, 5th Edition, Frank M. White w CD
228 Flow Measurement Engineering Handbook, 3rd Edition, Miller
229 Engineering Thermodynamics, Jones & Hawkins, 1960
230 Chemical Thermodynamics - Basic Theory and Methods, Klotz, 1950
231 Chemical Engineering, Volume 1, Fluid Flow, Heat Transfer & Mass Transfer, Coulson 1959
232 Chemical Engineering, Volume 2, Unit Operations, Coulson & Richardson, 1959
233 Chemical Engineering Thermodynamics, Introduction to, 4th Edition, Smith & Van Ness, 1987
234 Chemical Engineering Thermodynamics, Introduction to, 6th Edition, Smith & Van Ness & Abbott, 2001
235 Plant Design and Economics for Chemical Engineers, 2nd Edition, Peters & Timmerhaus, 1968
236 Fire Protection Handbook, Vol 1, Sections 1-7, 19th Edition, 2003, NFPA FPH1903
237 Fire Protection Handbook, Vol 2, Sections 8-14, 19th Edition, 2003, NFPA FPH1903
238 ASME Metals Engineering - Design - ASME Handbook, 1953

239 Petroleum Refining, Technology and Economics, 2nd Edition, Gary & Handwerk 1984
240 Piping Engineering, 3rd Edition, 1975
241 Petroleum Production Engineering - Oil Field Development, 3rd Edition, Uren, 1946
242 Industrial Heat Exchangers - A Basic Guide, 2nd Edition, Walker
243 Reaction Kinetics for Chemical Engineers, 1959
244 Chemical Reaction Engineering - An Introduction to the Design of Chemical Reactors, 4th Edition, Levenspiel, 1966
245 Fluid Mixing, A Guide to, by Oldshue and Herbst, 1990
246 Solar Ephemeris and Surveying Instrument Manual, 1962
247 Fluid Mechanics for Chemical Engineers, 3rd Edition, de Nevers, 2005
248 Boundary Layer Theory, Schlichting, 1955

APPENDIX A

UNITS, DIMENSIONS AND DIMENSIONAL ANALYSIS

Appendix A - Units, Dimensions and Dimensional Analysis

Any physical quantity consists of two parts: 1) A unit, which tells what the quantity is and gives the standard by which it is measured and, 2) a number which tells how many units are needed to make up the quantity, e.g., 8 feet means that a definite length has been measured. The standard length is called the foot and there are eight one-foot units laid end to end that cover the distance. Physical quantities are divided into two groups, termed primary and secondary quantities. A minimum list of primary quantities for all engineering is length, mass, time, temperature and quantity of electric charge. Force and heat may also be added to this list. Secondary units are derived from the primary unit quantities.

The units and dimensions of three common mechanical properties, force, mass and weight, are commonly used. Mass is the quantity conserved in all non-nuclear unit operations; material balances are in terms of mass, not weight. The amount of mass is not affected by body forces, such as gravitational. Weight is often used for both force and mass. Relations exist among these quantities, and units and dimensions must be addressed correctly in engineering formulas and calculations. Force F, body mass M and acceleration a are related by

$$F = kMa. \qquad \textbf{Equation 120}$$

Mass is defined as,

$$M = \lambda(g_c / g) \qquad \textbf{Equation 121}$$

where λ is the weight of fluid.

Several systems of units and dimensions are defined and used for the quantities in engineering equations. The various systems differ in the numbers and choice of the fundamental quantities, and in the choice of standard units for the fundamental units. One such system is the centimeter-gram-second (cgs) system. Another is the foot-pound-second (fps) system. The fps units are also called English units. In the fps system, two units, mass and force, have the same name, termed the pound. The lb-mass is designated lb and the lb-force is lb_f.

In the cgs system, only three fundamental mechanical quantities, mass, length and time are used. Force is then a derived or secondary unit. It is defined by making the constant k dimensionless and by choosing its numerical value as unity. To complete this system, mass is measured in grams, length in centimeters and time in seconds. The mks and SI (Systeme International d'Unites) systems are closely related to the cgs system and use mass measured in kilograms, length in meters, and time in seconds. The constant k is also dimensionless and equal to unity.

In the fps system, force is a fundamental quantity along with mass, length and time. These four mechanical units are used as the primary quantities. The constant k is a dimensional quantity with a numeric value fixed with a numeric size of 1/32.174. The value of 32.174 is designated as g_c. This value for the gravitational constant g_c is chosen since it is the average acceleration of gravity at sea level. The units of g_c are ft-lb/lb$_f$-sec^2 and g_c is the Newton's Law conversion factor.

For comparison of the cgs/mks/SI and fps units, two common forms are used with mechanical energy: 1) The kinetic energy of translation of a body and 2) the potential energy of a body at a distance above the earth's surface or any arbitrary datum plane. Mechanical energies in the cgs system are in ergs, Newtons for the mks and SI systems, and are ft-lb$_f$ in the fps system. For a body mass of M, Z as its distance above a datum plane, u as its kinetic velocity, and g as the local acceleration of gravity, the kinetic and potential energies in the dimensional systems are given in the table below.

Table 28 - Potential and Kinetic Energies

Potential and Kinetic Energies		
Energy	cgs/mks/SI units	fps units
Potential	MgZ	MgZ / g_c
Kinetic	$Mu^2 / 2$	$Mu^2 / 2g_c$

The fps or cgs/mks/SI units are employed dependent on the technical reference for the primary mechanical quantities. Equations in the fps system are converted to the cgs/mks/SI systems by deleting g_c; correspondingly, the cgs/mks/SI systems are converted to the fps system by adding g_c.

Dimensional Analysis

Dimensional analysis is based on the fact, if a theoretical equation exists among variables affecting a physical process, the equation must be dimensionally homogeneous. Because of this requirement, it is possible to group many factors into a smaller number of dimensionless groups of variables. The numerical values of these groups, in any given situation, are independent of the dimension system used, and the groups themselves rather than the separate factors appear in the final equation.

Dimensionless groups may be formed by analyzing the dimensions of the terms appearing in the differential equations governing the various operations. Such a procedure emphasizes the physical significance of the dimensionless groups and guards against inadvertent omission of important variables. Some dimensionless groups occur with such frequency that they have been given names and special symbols. The group $dv\rho / \mu$, for example, is called the Reynolds number N_{Re}, and the group $c_p \mu / k$ the Prandtl number N_{Pr}.

The numerical value of a dimensionless group for a given case is independent of the units chosen for the primary quantities provided consistent units are used within the group. The following provides a listing of dimensionless groups used with fluid systems.

Table 29 - Dimensionless Groups

Symbol	Name	Definition
C_D	Drag coefficient	$2g_c F_D / u^2 \rho A_p$
f	Fanning friction factor	$-\Delta P\, g_c d / 2L_p u^2$
j_H	Heat transfer factor	$(h / c_p G)(c_p \mu / k)^{2/3} (\mu_w / \mu)^{0.14}$
j_M	Mass transfer factor	$(k / G_m)(\mu / D_m M)^{2/3}$
N_{Fo}	Fourier number	$kt / c_p \rho A^2$
N_{Fr}	Froude number	u^2 / gL
N_{Gr}	Grashof number	$L^3 \rho^2 \beta g\, \Delta T / \mu^2$
N_{Gz}	Graetz number	mc_p / kL
N_{Ma}	Mach number	u / a
N_{Nu}	Nusselt number	hd / k
N_{Pc}	Peclet number	LGc_p / k
N_{Po}	Power number	$Pg_c / \rho n^3 d^5$
N_{Pr}	Prandtl number	$c_p \mu / k$
N_{Re}	Reynolds number	dG / μ
N_{Sc}	Schmidt number	$\mu / D_m M$
N_{Sh}	Sherwood number	kd / D_m

APPENDIX B

TOTAL MASS AND ENERGY EQUATIONS OF STEADY FLOW

7561 FM 1960 East, Suite 313, Humble, Texas 77346 Phone 832.257.3818
Consultant@APlusFlowTek.com www.APlusFlowTek.com

Appendix B - Total Mass and Energy Equations of Steady Flow

The most important processes in unit operations are fluid flow processes, in which fluids flow into, through, and out of pieces of equipment. Accurate and general equations based on the laws of conservation of mass and energy applies directly to flow-systems.

Steady Flow Process

In a steady flow process, the flow rates and the properties of flowing materials such as temperature, pressure, composition, density and velocity, at each point in the apparatus including all entrance and exit ports, are constant with time. These quantities can and usually do vary from point to point in the system; at any one location, they do not change. Because of this constancy of local conditions, there is no accumulation or depletion of either mass or energy within the apparatus. In all material and energy balances the following simple expression applies,

input = output.

Energy Balance for a Single Stream Process

For a steady flow process in which a single stream of fluid material is treated, consider the unit operation as shown in the figure below. The equipment is <u>any</u> device through which a fluid is passing.

Figure 40 - Diagram for a Steady Flow Process

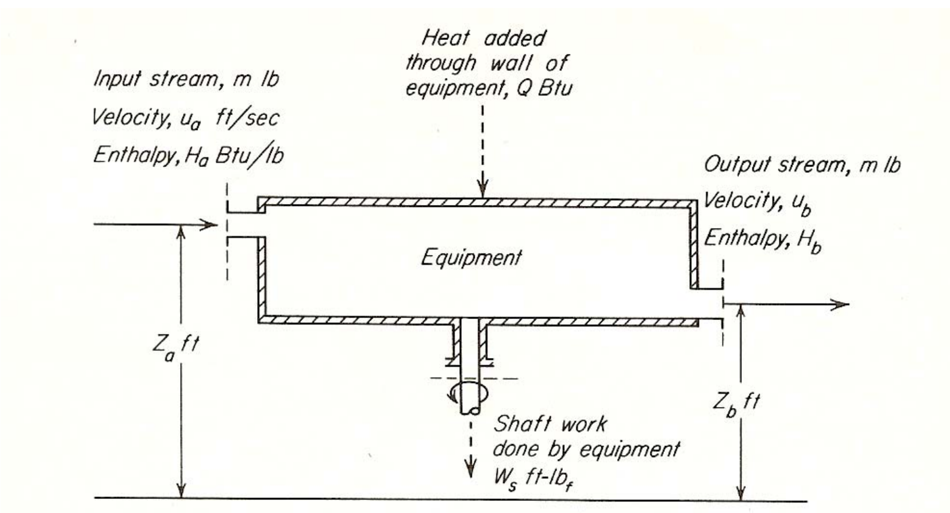

The fluid is flowing through the system at constant mass rate with a flow of m lb-mass/time of material. The entering stream has a kinetic velocity of u_a ft/sec and is Z_a ft above a horizontal datum from which heights are measured. Its thermodynamic energy, or enthalpy, is H_a Btu/lb. The enthalpy is a function of the stream's thermodynamic pressure and temperature and is related to the fluid's internal energy (U) and mechanical (P/ρ) energy by, $H = U + P/\rho$. The corresponding quantities for the leaving stream are u_b, Z_b, and H_b. Heat, with the amount Q Btu/time, is being transferred through the boundaries of the equipment to the material flowing through. If the equipment includes a turbine, the equipment may do work by means of a turning shaft. If the unit includes a pump, work from the outside must be done on the equipment, again through the mechanism of a turning shaft. Work effects of this kind are called shaft work, W_s. Shaft work is equal to W_s ft-lb$_f$/time, which is the amount of work being done on the outside by the equipment. For this process, the following equation that is derived from technical thermodynamics applies,

$$m\left[\frac{u_a^2 - u_b^2}{2g_c J} + \frac{g(Z_b - Z_a)}{g_c J} + H_b - H_a\right] = Q - \frac{W_s}{J}. \qquad \textbf{Equation 122}$$

The constant J is the mechanical equivalent of heat, in ft-lb$_f$/Btu, and g and g_c have their usual meanings.

Limitations and Restrictions

Limitations and restrictions of the above equation are:

1. Changes in electrical, magnetic, surface and mechanical-stress energies are not taken into account. Except in rare situations, these are absent or unimportant.

2. To apply the above equation to a specific situation, a precise choice of the boundaries of the equipment must be made. The inlet and outlet streams must be identified, the inlet and outlet ports located, and rotating shafts noted. All heat-transfer areas between the equipment and its surroundings must be located. The boundaries of the equipment and the cross sections of all shafts and inlet and outlet ports form the control surface. This must be a closed envelope, without gaps. The above equation applies to the equipment and material inside the control surface. The control surface of the process of the figure shown above is bounded by the walls of the equipment, the cross sections of the shaft and the inlet and outlet ports.

3. The constant J is a universal constant, the value of which depends only on the units chosen for heat and work. The fps value of J is 778.26 ft-lb$_f$/Btu.

4. For the equation as shown, the heat effect Q is, by convention, positive when heat flows from the outside of the control surface into the equipment and negative when heat flows in the opposite direction. The shaft work W_s is taken as positive when the work is done on the outside of the control surface by the equipment and is negative when the work is supplied to the equipment from outside the control surface. Work required by a pump located within the control surface is negative. Both Q and W_s are net effects on the system. The signs of Q and W_s may be changed dependent on the sign convention used since the values are net effects.

5. No term appears in the above equation for friction or other energy losses. Friction is an internal transformation of mechanical energy into heat and occurs inside the control surface. These effects are included in the other terms of the equation.

Enthalpy

The quantities H_a and H_b in the above equation, the enthalpies of the inlet and outlet streams, respectively, are physical properties of the material. The enthalpy of a unit mass of a pure single-phase substance is a function of pressure and temperature. With a mixture, the enthalpy of a unit mass of a single-phase fluid is a function of pressure, temperature and composition. With a known and constant composition through the equipment, (such as with no chemical reaction) the enthalpy reduces to a function of temperature and pressure only. As with friction or other energy losses, the condition of chemical reaction is included in the other terms of the equation and the composition, temperature and pressure of the fluid at the inlet and at the outlet require measurement.

Bernoulli Equation for Flow Measurement

The total energy equation, without heat or work interaction $(W_s = Q = 0)$ and when the inlet and outlet elevation planes are at the same reference elevation $(Z_a = Z_b)$ is:

$$m\left[\frac{u_a^2 - u_b^2}{2g_c J} + H_a - H_b\right] = 0 \text{.} \qquad \textbf{Equation 123}$$

From the mass balance at steady flow, it can be shown that there is a density ρ and average velocity v, such that

$$(\rho A v)_{a,b} = m_a = m_b = Const \text{.} \qquad \textbf{Equation 124}$$

In the above equation, ρ_a or ρ_b is the average density at the inlet or outlet, ν_a or ν_b is the average velocity, and A_a or A_b is the flow area at the inlet or outlet respectively. The average velocity v is related to the kinetic energy velocity u by a common factor α, the kinetic energy correction factor, by the following relationship,

$$\alpha\, v^2 = u^2 . \qquad \textbf{Equation 125}$$

The mass flow rate through <u>any</u> apparatus, with the restraints as specified, is provided by substitution of the above relationships into the total energy equation. The mass flow rate is then determined by,

$$m = \rho_a\, A_a \sqrt{\frac{2g_c\, J\left(H_a - H_b\right)}{\alpha_a\left(\frac{\alpha_b}{\alpha_a}\left(\frac{\rho_a\, A_a}{\rho_b\, A_b}\right)^2 - 1\right)}} . \qquad \textbf{Equation 126}$$

This equation is a thermodynamic form of the Bernoulli equation. The basis is very general, adiabatic flow in a horizontal plane. Proper design and utilization provides extremely accurate flow measurement. The kinetic energy correction factor is determined by integration of the velocity profile across the flow area. The numbers approach a value of one (1) for uniform velocity or for moderate to high Reynolds numbers in fully developed boundary layer pipe-flow. The enthalpy and density at the inlet and outlet are determined from the measured thermodynamic pressure and temperature at the inlet and outlet, since for enthalpy $H = f_H(T,P)$ and for density $\rho = f_\rho(T,P)$.

The Bernoulli equation is subject to the constraints of the mass, momentum, energy, and power balances for steady flow systems. It is also subject to the thermodynamics of state. As an example, from the power balance and thermodynamics of state,

$$\left(\varpi\left(\frac{\alpha v^2}{2g_c J} + U + z\Re T\right)\right)_a - \left(\varpi\left(\frac{\alpha v^2}{2g_c J} + U + z\Re T\right)\right)_b = 0 \qquad \textbf{Equation 127}$$

where v is calculated from the equation of continuity. $\Re$ is calculated from the ideal gas constant R as,

$$\Re = R / M_W \qquad \textbf{Equation 128}$$

M_W is the fluid's molecular weight. The compressibility factor is calculated from,

$$z = P / \rho \Re T$$ **Equation 129**

and the flow factor ϖ is calculated from,

$$\varpi = PAv / z\Re T = PQ / z\Re T$$ **Equation 130**

where Q is the volumetric flow rate.

These equations were developed across the piece of flow equipment. Macroscopic balances with respect to the fluid are also repeated which provides another grouping of mass, momentum, energy, and power balances, with thermodynamics of state equations. The thermodynamics of state are provided by the Extended Lee-Kesler Equation-of-State (ELK-EoS).

On the macroscopic basis, additional state variables are constant. The variables for transport systems are enthalpy H for insulated systems and Gibbs free enthalpy G for isothermal systems. The isothermal system is defined as one in which heat absorbed or generated does not cause appreciable temperature change.

For these systems, the total enthalpy H^* or total Gibbs free enthalpy G^* is constant down the flow measurement device. This provides a cross checking procedure from the a, b, c, etc., locations of the flow tube and within various locations of the flow tube, such as a to b, c to a, b to c, etc. Additionally, with the total enthalpies known, the flow rate at a particular location (a, b, c, etc.) can be determined at that location without any additional information.

All equations with associated parameters and variables may then be solved by a global optimization procedure such as MIMT© to minimize flow measurement errors with respect to pressure and temperature measurements as positioned down the flow tube. This is the basis for high accurate flow measurement systems as developed in the fluid flow industry. This general approach and procedure may be extended to all unit operations, such as pipes, valves, pumps, compressors, turbines, mixers, reactors, etc., within the process industry. This method and procedure extends and significantly improves the global optimization procedure for unit operation analysis, and is attributed to the development of the ELK-EoS and MIMT©.

The basis for accurate flow measurement requires a reliable physical property method to determine density and thermodynamic properties, and requires good design to ensure proper measurement of the true thermodynamic pressure and temperature. These measurements are to be de-coupled of kinetic, potential or other dynamic head and thermal response effects. With precise area measurements and known mechanical and fluid-flow design, any flow measurement error can be traced to pressure measurement, temperature measurement or physical properties.

The thermodynamic form of the Bernoulli flow equation is rigorous and can be used for any real-fluid flow measurement within the restraints as listed. Corrections for out-of-plane gravitational fields or variable, directional accelerations are made by re-positioning the pressure tap locations or by use of the following equation,

$$m = \rho_a \; A_a \sqrt{\frac{2g_c \;\; J\left(H_a - H_b\right) + 2g(Z_a - Z_b)\cos(\phi)}{\alpha_a\left(\dfrac{\alpha_b}{\alpha_a}\left(\dfrac{\rho_a \; A_a}{\rho_b \; A_b}\right)^2 - 1\right)}} \,.$$ **Equation 6**

With a two-phase fluid supplementary analysis is required for determining the enthalpy H, density ρ, and kinetic energy correction factor α. The enthalpy, $H = f_H(T, X)$ or $f_H(P, X)$, and density, $\rho = f_\rho(T, X)$ or $f_\rho(P, X)$, are functions of T or P, and X, where X is the amount vaporized. The amount vaporized, X, may be measured or calculated since it is related to the entropy, which is evaluated from additional thermodynamic and transport relations. The kinetic energy correction factor can be determined from two-phase flow analysis methods, e.g., annular, wave, slug or homogeneous two-phase flow regimes.

APPENDIX C

PHYSICAL PROPERTIES

Volumetric and Thermodynamic Properties Relation

Volumetric and thermodynamic properties of a pure substance (or fluid mixture) are related. From volumetric data, across a wide range of temperatures and pressures for gases, vapors, and liquids, there are relations for calculation of the thermodynamic properties of the substance. Volumetric data can be measured or determined with the "Law of Corresponding States".

A simple volumetric measurement method is to place a known amount of mass (or moles, $moles = mass / molecular\ weight$) into a small capsule for which the volume is accurately known for all pressure and temperatures. With heating or cooling, the temperature can be adjusted. At the steady state measured temperature, an average (gravity adjusted) pressure is measured. From these measurements, an Equation-of-State (EoS) can be developed of the form,

$$P = f_p(T, (\rho = m/Vol)) \qquad \textbf{Equation 131}$$

where T is the temperature, P is the pressure, m is the mass or moles in the capsule, and Vol is the volume of the capsule. The above equation is developed for diverse amounts of known mass (or moles) charged into the small capsule. With the measured data, a new variable, called the compressibility factor z, can be determined from the measured data. The compressibility factor is defined as,

$$z = \frac{P}{\rho RT}. \qquad \textbf{Equation 132}$$

In the above equation, R is the ideal gas constant when the density units are on a molar basis.

The compressibility z represents a departure from the Ideal Gas Equation-of-State (IG EoS) since $z = 1 = P/(\rho RT)$ for an ideal gas. The departure function is,

$$(1-z) = \left(\frac{P}{\rho RT}\right)_{IdealGas} - \left(\frac{P}{\rho RT}\right)_{Measured} = \frac{P}{RT}\left(\frac{1}{\rho_{IdealGas}} - \frac{1}{\rho_{Measured}}\right). \qquad \textbf{Equation 133}$$

With the equation $P = f_P(T, (V = 1/\rho))$ and the departure function $(1-z)$, the thermodynamic departure functions (Helmholtz free energy A, internal energy U, entropy S, and enthalpy H) are defined, and calculated at constant temperature by the following relations:

$$\frac{A^\circ - A}{RT} = \int_V^\infty (1-z)\frac{dV}{V} + Ln(z)$$ **Equation 134**

$$\frac{U^\circ - U}{RT} = \int_V^\infty T\left(\frac{\partial Z}{\partial T}\right)_V \frac{dV}{V}$$ **Equation 135**

$$\frac{S^\circ - S}{R} = \frac{U^\circ - U}{RT} - \frac{A^\circ - A}{RT}$$ **Equation 136**

$$\frac{H^\circ - H}{RT} = \frac{U^\circ - U}{RT} + (1-z)$$ **Equation 137**

In the above equations B° refers to the ideal gas state for any property B. The internal energy U, entropy S, and enthalpy H between any two states of pressure and temperature are calculated by,

$$U(T,P)_b - U(T,P)_a = -(U^\circ - U)_b + \int_{T_a}^{T_b} C_V^\circ dT + (U^\circ - U)_a$$ **Equation 138**

$$S(T,P)_b - S(T,P)_a = -(S^\circ - S)_b + \int_{T_a}^{T_b} \frac{C_P^\circ dT}{T} - R\ln\left(\frac{P_b}{P_a}\right) + (S^\circ - S)_a$$ **Equation 139**

$$H(T,P)_b - H(T,P)_a = -(H^\circ - H)_b + \int_{T_a}^{T_b} C_P^\circ dT + (H^\circ - H)_a.$$ **Equation 140**

For an ideal gas, $\frac{dU}{dP} = 0$, $C_P^\circ = C_V^\circ + R$ and $C_P^\circ \neq f(P,\ for\ any\ pressure)$.

The thermodynamic path follows $(B^{\circ}-B)_a$ at constant T_a from P_a to 0 pressure, the ideal gas enthalpy change from T_a to T_b, and then $(B^{\circ}-B)_b$ at constant T_b from 0 to P_b pressure.

This powerful approach provides a rigorous and fundamental evaluation of all thermodynamic properties directly from only the fluid's volumetric and ideal gas properties. Volumetric and ideal gas properties are normally obtained from elementary measurements or can be estimated from well-known and accurate methods such as the Law of Corresponding States.

Law of Corresponding States

The basis for the pressure-volume-temperature relationships of constant component gases, vapors and liquids is the thermodynamic proof that for each substance there exists a unique relation among pressure P, temperature T, and specific volume V for any single phase. This thermodynamic postulate is not derived from the Gibbs phase rule, but from the fundamental Gibbs equation relating internal energy U, entropy S, temperature T, and volume V,

$$dU_{fluid} = T_{fluid}\ dS_{fluid} - P_{fluid}\ dV_{fluid}\ .$$ **Equation 141**

Methods for determination of the pure component volumetric, thermodynamic and transport behavior of liquids, vapors, gases and their mixtures as a function of temperature and pressure are derived from the "Law of Corresponding States". This approach asserts that dimensionless physical properties of materials follow universal variations with dimensionless variables of state. The general and specific forms are derived from molecular theory.

The properties P, V (or ρ), and T are necessary system parameters. Characterizing parameters in the appropriate intermolecular potential function are also necessary; for non-polar molecules, parameters are usually chosen to represent the collision diameter σ and the minimum potential energy $\in_0$. For polar molecules, in additional to σ and $\in_0$, the dipole moment μ, the quadrupole moment Q, and the polarizability α are direct choices. Additionally, some variable characteristic of the shape (or nonsphericity) is required; following the suggestion of Bird and Brock, the elliptic eccentricity β is chosen. Finally, the molecular mass m, Planck's constant h, and Boltzmann's constant k complete the list. The base relationship is,

$$\phi_1(P,V,T,\sigma,\in_0,\mu,Q,\alpha,\beta,m,h,k) = 0\ .$$ **Equation 142**

Bird and Brock suggest an arrangement in terms of dimensionless groups,

$$\phi_2(PV/kT, V/\sigma^3, kT/\in_0, \mu^2/\in_0 \sigma^3, Q^2/\in_0 \sigma, \alpha\sigma^3, h/(\sigma(m\in_0)^{1/2}), \beta) = 0 .$$ **Equation 143**

Upon using simplifications, neglecting the quantum group, and applying dimensional analysis, the following equation is obtained,

$$\phi_3(z, P/P_c, T/T_c, \mu^2/V_c kT_c, Q^2/V_c^5 kT_c, \alpha/V_c, \beta) = 0 .$$ **Equation 144**

The above three equations are the basic relations for all the corresponding state correlations.

This is the basis for the departure from an ideal gas condition at the specified pressure and temperature for determining the actual molar (or mass) density. The departure from an ideal gas state is $(1-z)$, where z is the fluid compressibility factor. An Equation-of-State (EoS) calculates the compressibility factor $z = \frac{PV}{RT}$ and pressure $P = f_P(T,(V = 1/\rho))$. All thermodynamic properties can be determined rigorously with the departure function $(1-z)$, density ρ, and their variations along fixed paths (defined by "natural properties", such as $\left(\frac{\partial A}{\partial V}\right)_T = P$) and ideal gas properties.

<u>Compressibility and Volumetric Properties</u>

The non-ideality of a fluid as expressed by the compressibility factor z is,

$$z = \frac{P}{\rho RT} = f_z(T,P) = f_z(T,\rho) .$$ **Equation 145**

R is the ideal gas constant. P and T are the pressure and temperature, respectively. The molar-density ρ is the defined by

$$\rho = Lim\left(\frac{\Delta mole}{\Delta Vol}\right)_{\Delta Vol \Rightarrow \delta} .$$ **Equation 146**

The compressibility is applicable, by the defining equation, to any continuous state. The value of R depends on the units of the variables used. For an ideal gas $z^{\circ} = 1.0$. For real gases, z is somewhat less than one (< 1.0) except at high-reduced temperatures $(T/T_{critical})$ and pressures $(P/P_{critical})$ where values are greater than one (>1.0). For liquids between the boiling and melting points (i.e. solids), z is small (~<0.1). $Z_{critical}$ is typically between 0.15 and 0.4 at the vapor-liquid critical point of $T_{critical}$, $P_{critical}$ and $\rho_{critical}$.

Calculation of the compressibility z is by the Extended Lee-Kesler Equation-of-State (ELK-EoS) as jointly developed and co-patented with NASA/MSFC, Patent Number 11 /152,810. The basis of this EoS is a modified Taylor series expansion that includes the deviation functions of argon with octane and water, and uses the acentric factor (ω), radius-of-gyration (σ), and a Q factor (Θ) as correlating parameters. A similar ELK-EoS relation applies to the transport properties, i.e. acoustic velocity, viscosity, thermal conductivity and surface tension.

Fluid property comparisons are based on the Yaws physical property database, containing over 1700 organic and inorganic materials. Results demonstrate that for a large number of components the volumetric and thermodynamic fluid properties can be evaluated with relative errors typically within 3 to 5 percent over a wide range of operating conditions. For the gas viscosity, relative errors are within 5 percent over the entire range of Yaws Data Base temperatures for over 1700 organic and inorganic compounds (over 4,400 data points). This accuracy range is of the same magnitude as the original experimental data. Improved accuracies will result with improved data. For high accuracy, the Q factor (Θ) may be adjusted to experimental data and calibrated as $\Theta = f_{\Theta}(T_{reduced}, P_{reduced}) = f_{\Theta}(T_{reduced}, \rho_{reduced})$. With this adjustment factor, the volumetric, thermodynamic, and transport property accuracy can be of the same order of magnitude as any provided experimental data.

By utilization of a modified Taylor series expansion, the ELK-EoS for compressibility is,

$$z_{fluid} = z^{(0)} + z^{(1)} + z^{(4)} - \left(\Theta/\Theta^{(0)}\right)\left(z^{(1)} - z^{(2)} - z^{(3)} + z^{(4)}\right).$$ **Equation 147**

The reference Q factor ($\Theta^{(0)}$) value is 1.16395. $z^{(0)}$ is the compressibility of the simple fluid and the $z^{(i)}$'s represent the deviation functions defined by,

$$z^{(1)} = ((\omega - \omega^{(0)})/(\omega^{(R)} - \omega^{(0)}))\,(z^{(R)} - z^{(0)})$$ **Equation 148**

$$z^{(2)} = ((\sigma - \sigma^{(0)})/(\sigma^{(R)} - \sigma^{(0)}))\,(z^{(R)} - z^{(0)})$$ **Equation 149**

$$z^{(3)} = ((\omega - \omega^{(0)})/(\omega^{(W)} - \omega^{(0)}))\,(z^{(W)} - z^{(0)})$$ **Equation 150**

$$z^{(4)} = ((\sigma - \sigma^{(0)})/(\sigma^{(W)} - \sigma^{(0)}))\,(z^{(W)} - z^{(0)}).$$ **Equation 151**

The correlating factors are listed in the following table.

Table 30 - ELK EoS Correlating Factors

Component	Superscript	Acentric Factor, ω	Radius-of-Gyration, σ	Q Factor, Θ
Argon	(0)	-0.004605018	1.076	1
Octane	(R)	0.397732487	4.546	1
Water	(W)	0.3214248	0.615	1

The compressibility factor $z^{(0)}$ of a simple fluid, such as argon, the reference fluid octane $z^{(R)}$, and water $z^{(W)}$ are represented by the twelve (12) constant Modified Benedict-Webb-Ruben (MBWR) equation-of-state,

$$\begin{aligned} z &= (P_r V_r / T_r) = 1 + B/V_r + C/V_r^2 + D/V_r^5 \\ &\quad + c4/(T_r^3 V_r^2)(\beta + \gamma / V_r^2)\exp(-\gamma / V_r^2) \end{aligned}$$ **Equation 152**

where

$$B = b1 - b2/T_r - b3/T_r^2 - b4/T_r^3$$ **Equation 153**

$$C = c1 - c2/T_r + c3/T_r^3$$ **Equation 154**

$$D = d1 + d2/T_r$$ **Equation 155**

$$V_r = 1/\rho_r.$$ **Equation 156**

The ELK-EoS MBWR constants are given in the following table for the three specified fluids. The argon and octane constants are the same as provided by Lee-Kesler for their simple and reference fluids. The water constants are derived from the ASME Steam Tables for both water and steam.

Table 31 - ELK-EoS MBWR Constants

Constant	Argon	Octane	Water
b_1	0.1181193	0.2026579	0.1263781
b_2	0.265728	0.331511	0.1786672
b_3	0.15479	0.027655	0.1308736
b_4	0.030323	0.203488	0.1944523
c_1	0.0236744	0.0313385	-0.00355054
c_2	0.0186984	0.0503618	-0.000736033
c_3	0	0.016901	0.017420037
c_4	0.042724	0.041577	0.006247606
$d_1 \times 10^4$	0.155488	0.48736	0.131647
$d_2 \times 10^4$	0.623689	0.0740336	-0.0391698
β	0.65392	1.226	6.6484506
γ	0.060167	0.03754	0.01861792

Thermodynamic Properties

The thermodynamic and thermodynamic departure functions derived from the compressibility relation are identical to those as originally developed by Lee-Kesler. These thermodynamic functions are as follows:

Fugacity Coefficient

$$Ln(f/P) = z - 1 - Ln(z) + B/V_r + C/(2V_r^2) + D/(5V_r^5) + E$$ **Equation 157**

where

$$E = c4/(2T_r^3\gamma)\left\{\beta + 1 - (\beta + 1 + \gamma/V_r^2)\exp(-\gamma/V_r^2)\right\}$$ **Equation 158**

Enthalpy Departure

$$(H - H^\circ)/RT_c = \{T_r\ z - 1 - (b2 + 2b3/T_r + 3b4/T_r^2)/(T_r V_r) - (c2 - 3c3/T_r^2)/2T_r V_r^2) + d2/(5T_r V_r^5) + 3E\}$$ **Equation 159**

Entropy Departure

$$(S-S^\circ)/R+Ln(P/P^\circ)=Ln(z)-(b1+b3/T_r^2+2b4/T_r^3)/V_r \\ -(c1-2c3/T_r^3)/(2V_r^2)-d1/(5V_r^5)+2E \qquad \textbf{Equation 160}$$

Isochoric Heat Capacity Departure

$$(C_v-C_v^\circ)/R=2(b3+3b4/T_r)/(T_r^2V_r)-3c3/T_r^3V_r^2)-6E \qquad \textbf{Equation 161}$$

Isobaric Heat Capacity Departure

$$(C_p-C_p^\circ)/R=(C_v-C_v^\circ)/R-1-T_r((\partial P_r/\partial T_r)_{Vr})^2/(\partial P_r/\partial V_r)_{Tr} \qquad \textbf{Equation 162}$$

and

$$(\partial P_r/\partial T_r)_{Vr}=(1/V_r)\{1+(b1+b3/T_r^2+2b4/T_r^3)/V_r \\ +(c1-2c3/T_r^3)/V_r^2+d1/V_r^5 \\ -2c4/(T_r^3V_r^2)[(\beta+\gamma/V_r^2)\exp(-\gamma/V_r^2)]\} \qquad \textbf{Equation 163}$$

$$(\partial P_r/\partial V_r)_{Tr}=-(T_r/V_r^2)\{1+2B/V_r+3C/V_r^2+6D/V_r^5 \\ +c4/(T_r^3V_r^2)[3\beta+\{5-2(\beta \\ +\gamma/V_r^2)\}\gamma/V_r^2]\exp(-V_r^2)\} \qquad \textbf{Equation 164}$$

where $P^\circ=1$ atm, $H^\circ=$the ideal-gas enthalpy, $S^\circ=$the ideal-gas entropy, $C_v{}^\circ=$ideal-gas constant volume specific heat, and $C_P{}^\circ=$ideal-gas constant pressure specific heat, all at the reduced temperature, T_r.

ELK-EoS Calculation Procedure

The following procedure is used to calculate the volumetric or any of the thermodynamic departure functions (X):

1. Determine the molar volume of the simple fluid, reference fluid and water at the given reduced temperature and pressure from the MBWR compressibility equation.

2. Calculate the departure functions for the volumetric or thermodynamic property of interest, $X^{(0)}$, $X^{(R)}$ and $X^{(W)}$ from the appropriate thermodynamic departure function

3. With the fluids acentric factor and radius-of-gyration, calculate the volumetric or thermodynamic deviation function $X^{(1)}$ through $X^{(4)}$ using the following deviation functions:

$$X^{(1)} = ((\omega - \omega^{(0)})/(\omega^{(R)} - \omega^{(0)}))(X^{(R)} - X^{(0)})$$ **Equation 165**

$$X^{(2)} = ((\sigma - \sigma^{(0)})/(\sigma^{(R)} - \sigma^{(0)}))(X^{(R)} - X^{(0)})$$ **Equation 166**

$$X^{(3)} = ((\omega - \omega^{(0)})/(\omega^{(W)} - \omega^{(0)}))(X^{(W)} - X^{(0)})$$ **Equation 167**

$$X^{(4)} = ((\sigma - \sigma^{(0)})/(\sigma^{(W)} - \sigma^{(0)}))(X^{(W)} - X^{(0)})$$ **Equation 168**

4. The volumetric or thermodynamic property can then be calculated from,

$$X_{fluid} = X^{(0)} + X^{(1)} + X^{(4)} - (\Theta/\Theta^{(0)})(X^{(1)} - X^{(2)} - X^{(3)} + X^{(4)})$$ **Equation 169**

A value of one (1) is normally used for the fluid's Q factor (Θ) unless specific data indicates otherwise. For improved precision in density and thermodynamic property determination, the Q factor (Θ) values are included in the Yaws database for selected components and at various reduced temperatures and pressures. When using these supplied Q factors the volumetric (and associated state functions) errors are zero on the liquid saturation curve, from the melting temperature to the critical point. Alternatively, an average Q factor (Θ) value may be used since the standard deviation across a wide range of reduced temperatures is typically low. For the thermodynamic and vapor pressure fluid properties, a Q factor (Θ) value of one (1) is typically acceptable for engineering applications.

The enthalpy change from state a to state b $(H_b - H_a)$ is calculated from,

$$H_b - H_a = RT_c H^d(T_b, P_b) + \int_{T_a}^{T_b} C_P^\circ dT - RT_c H^d(T_a, P_a)$$ **Equation 170**

where $H^d(T,P) = ((H - H^\circ)/RT_c)_{fluid}$ as given above, and the superscript ° is the ideal gas reference condition. The ideal gas C_P°-A$_i$ values are provided in the Yaws database as a polynomial of form $C_P^\circ = \sum_{i=1}^{J} A_i T^i$. Similar approaches are used for the other thermodynamic properties. For reaction systems, the above enthalpy equation must be altered to include the heat of formation. For Gibbs or Helmholtz free energy reaction equilibrium calculations, the absolute entropy of formation must be included for the entropy relation.

Certain flow system designs provide a reversible conversion of velocity to enthalpy as given by $dH = udv/g_c$, where u is the kinetic velocity. This equation is based on the total energy balance, in differential form, with the restrictions as previously listed. The thermodynamic equivalent for a reversible enthalpy change is $dH = VdP$. Integration and solving for the average specific-volume gives $V_{avg} = 1/\rho_{avg} = v^2/(2g_c \Delta P)$. This relation is based on the zero velocity stagnation enthalpy, which is a constant for adiabatic flow through a horizontal pipe and/or through valves and fittings. This density/specific-volume relationship provides redundant volumetric verification that can be used to verify all-fluid thermodynamic properties in flow systems. Pressure taps located in high-flow and stagnation zones can be readily incorporated into the hardware for any head-meter flow system.

Transport Properties

With the transport properties the correlating parameters are given by the same X_{fluid} equations as given above with the following modifications for properties evaluation:

1. For the simple fluid, reference fluid and water the respective transport property is evaluated at the reference temperature as calculated by:

$$T^{(j)} = T_c^{(i)}(T/T_c^{(j)}).$$ **Equation 171**

2. A log reduced transport property is based on:

$X^{(0)} = Ln(f(T^{(0)}))$, for the simple fluid **Equation 172**

$X^{(R)} = Ln(f(T^{(R)}))$, for the reference fluid **Equation 173**

$X^{(W)} = Ln(f(T^{(W)}))$, for water. **Equation 174**

3. These equations are used in the formulas as provided above, with specific correlating factors for the transport property of interest.

APPENDIX D

THERMODYNAMICS OF FLUID FLOW

Appendix D - Thermodynamics of Fluid Flow

Fluid Physical Properties as Thermodynamic State Properties

Fixed state properties connecting any number of thermodynamic paths are independent of the path. The path determines the energy interaction of the system with the environment, typically heat Q or work W. Physical properties, such as density ρ, temperature T, pressure P, viscosity η, etc., are state properties. Any state property that can be expressed uniquely as a function of these properties is itself a state property. All thermodynamic properties, such as enthalpy H, entropy S, internal energy U, etc., are functions of temperature and pressure alone, and are variables of state. Any state variable can be determined by $B = f_B(T,P)$. For temperature T, pressure P, or density ρ, one of many forms for the state representation is:

$$T = (\partial U/\partial S)_V, \quad P = -(\partial U/\partial V)_S, \; \& \quad 1/\rho = V = (\partial H/\partial P)_S \qquad \textbf{Equation 175}$$

The measured values of temperature, pressure or density are simply a measurement of the respective slopes, or derivatives, of other state properties. As an example, the density of any constant composition fluid can be determined by taking the enthalpy derivative with respect to pressure, at constant entropy, from an equation of state, at the corresponding system temperature and pressure. Since enthalpy and entropy are functions of temperature and pressure only, density and density variations can be determined at any state within a process.

The uniqueness of this equation of state approach provides redundancy, consistency and measurement validation. It also provides closure to the mass, momentum and energy balances as the fluid (system) flows from state a to state b. With fluid flow systems, certain properties are conserved with respect to a reference thermodynamic state, which can be represented by the thermodynamic convenience functions.

Thermodynamic Convenience Functions

The following equation is the Gibbs fundamental property relationship and represents the third of the three basic equations of thermodynamics. (For fluid flow analysis, the energy and entropy balances are the other two equations coupled with an equation-of-state and the mass and momentum balances.) The Gibbs equation relates the fundamental physical properties of internal energy U, specific volume V, pressure P, entropy S and temperature T, to one another when the system is defined as the fluid. Since it relates only the state functions to each other it is an exact differential equation with extremely powerful mathematical properties in the analysis of fluid flow systems. When put in the form of PdV, other work terms, such as magnetic, electric, gravitation, kinetic, etc., can be added to the fundamental property relationship. These added terms do not affect the basic physical property relationships.

$$dU_{syst} = T_{syst}\ dS_{syst} - P_{syst}\ dV_{syst}$$ **Equation 176**

It is possible to express all thermodynamic relations in terms of the fundamental properties U, V, P, S, and T. However, with fluid flow analysis, certain properties are conserved when following a thermodynamic path from state a to state b. These properties are convenience functions and provide unique relationships as groupings of new mathematical variables.

The enthalpy convenience function is defined as

$$H = U + PV \quad or \quad dH = TdS + VdP\ .$$ **Equation 177**

The Helmholtz free energy A, and the Gibbs free energy, or Gibbs free enthalpy G, are defined respectively as:

$$A = U - TS \quad or \quad dA = -SdT - PdV$$ **Equation 178**

and

$$G = H - TS \quad or \quad dG = -SdT + VdP\ .$$ **Equation 179**

The internal energy U, enthalpy H, Helmholtz free energy A, and Gibbs free enthalpy G provide unique properties when other functions of state are constrained to fixed values. As examples, for an isentropic process,

$$(\partial H / \partial P)_S = V$$ **Equation 180**

and for an isothermal process,

$$(\partial G / \partial P)_T = V\ .$$ **Equation 181**

Integration of the enthalpy term for an isentropic pressure change gives,

$$\int_a^b (VdP)_S = \int_a^b (\partial H / \partial P)_S\, dP_S = \int_a^b (dH)_S = \Delta H_S$$ **Equation 182**

Integration of the Gibbs free enthalpy term for an isothermal pressure change gives,

$$\int_a^b (VdP)_T = \int_a^b (\partial G/\partial P)_T \, dP_T = \int_a^b (dG)_T = \Delta G_T \,.$$ **Equation 183**

From the Gibbs free enthalpy property relation, the equation for specific volume is,

$$(\partial G/\partial P)_T = V$$ **Equation 184**

from which a new property is defined as the fugacity f.

Where,

$$dG_T = RTd(Ln(f)) \; or \; \Delta G_T = Ln(f_b / f_a) \,.$$ **Equation 185**

The fugacity thermodynamic-property function is defined as

$$f \to P \quad as \quad P \to 0$$ **Equation 186**

$$\frac{f}{P} \to 1 \quad as \quad P \to 0$$ **Equation 187**

and

$$RT\left(\frac{\partial In \; f}{\partial P}\right)_T = V = 1/\rho \,.$$ **Equation 188**

For fluids, other than an ideal gas or incompressible liquid, the fugacity representation for density provides improvements in state property calculations when compared to the density. As an example, for saturated liquids and vapors,

$$G_i^{Liquid} = G_i^{Vapor}$$ **Equation 189**

where G_i is the chemical potential for the particular component. The fugacity representation is,

$$f_i^{Liquid} = f_i^{Vapor} \,.$$ **Equation 190**

Therefore, for any single component or fluid mixture at the saturation point or within the vapor/liquid envelope, the component fugacity function provides a constant value whereas the density may change by factors of several magnitudes. The fugacity approach provides a constraining-constant factor for rigorous analysis of saturated and two-phase fluid systems.

Reversible and Irreversible Processes

A reversible process requires that the change of states from a to b may be reversed from b to a. Any thermodynamic process or path that does not meet these conditions is called an irreversible process.

Entropy S is used as a measure of this irreversibility and since it is a thermodynamic function of state, its value can be determined. There are two forms in flow systems that generate an entropy change. The first is energy transfer Q from the fluid system to its surroundings; the second is due to frictional effects, termed lost mechanical work LW. The Q and LW can be determined as separate terms from knowledge of the fluid flow process and subsequently related individually to the entropy S.

An irreversible process always involves the degradation of energy potential without producing the maximum amount of work or a corresponding increase in another energy potential other than temperature. An irreversible process includes the flow of a viscous fluid through a pipe and fittings where the system is defined as a fluid.

The irreversible degradation of an energy potential in fluid flow processes results from frictional effects or from an imbalance of mechanical-energy potentials. The imbalance occurs when the rate of the process does not allow molecular adjustment of the system. Most fluid flow processes operate at a rate much slower than the molecular processes. Fluid flow analysis is referred to as a quasi-static or quasi-equilibrium and is amenable to analysis by a reversible process technique. The dissipation of a shock wave is an example of mechanical-molecular energy non-uniformity. However, even this process can be adequately evaluated with thermodynamic principles. Frictional losses are evaluated to a high degree of accuracy with mechanical-thermodynamic principles.

Any frictional process is irreversible. However, when the fluid is defined as the system, there may not be degradation of particular convenience-function energy potential. Therefore, even if a process is irreversible, there may be reversible state components within the process that provides a powerful analysis tool. As an example, for an adiabatic and isolated (no Q and W_s) process with frictional lost work LW affects,

$$H^* = H + \sum energy\ potentials + \sum frictional\ lost\ work = const \text{.} \qquad \textbf{Equation 191}$$

Bernoulli Equation or Mechanical Energy Balance

For the flow of fluid through a piece of process equipment, such as a pipeline, pump or expander, the first law differential energy balance is,

$$\left(H+\frac{u^2}{2g_c}+\frac{gZ}{g_c}\right)_a \delta m_a-\left(H+\frac{u^2}{2g_c}+\frac{gZ}{g_c}\right)_b \delta m_b+\delta Q-\delta W_s= d\left[M\left(U+\frac{u^2}{2g_c}+\frac{gZ}{g_c}\right)\right].$$ **Equation 192**

The entropy balance is,

$$\Delta(\delta mS)+\int_{surface\,area}\frac{\delta\, qdA}{T}+\int_{volume}\frac{\delta\, lw\, dV}{T}=d(MS)_{syst}.$$ **Equation 193**

For a steady state system, the energy and entropy balances become,

$$\Delta\left(H+\frac{u^2}{2g_c}+\frac{gZ}{g_c}\right)_a m+Q-W_s=0$$ **Equation 194**

$$-TdS+\delta LW+\delta Q=0.$$ **Equation 195**

Taking differentials and equating the energy and entropy balances with the Gibbs fundamental relation provides,

$$-LW-W_s-\int_{P_1}^{P_2}V\,dP-\Delta\left(\frac{u^2}{2g_c}+\frac{gZ}{g_c}\right)=0.$$ **Equation 196**

The Bernoulli representations for isentropic and isothermal fluid flow systems, respectively are,

$$\Delta H_S+\Delta\left(\frac{u^2}{2g_c}+\frac{gZ}{g_c}\right)+LW=0$$ **Equation 197**

$$\Delta G_T + \Delta\left(\frac{u^2}{2g_c} + \frac{gZ}{g_c}\right) + LW = 0.$$ **Equation 198**

The total enthalpy H_S^* and Gibbs free enthalpy G_T^* "head" representations for these systems are,

$$H_S^* = (H_S + u^2/2g_c + gZ/g_c + \delta LW)_a = (H_S + u^2/2g_c + gZ/g_c + \delta LW)_b = Const$$ **Equation 199**

$$G_T^* = (G_T + u^2/2g_c + gZ/g_c + \delta LW)_a = (G_T + u^2/2g_c + gZ/g_c + \delta LW)_b = Const$$ **Equation 200**

For two-phase flow systems, a fugacity representation can be substituted in the G_T^* equation. This approach provides the necessary equilibrium calculations throughout the saturated and two-phase regions.

APPENDIX E

THE BERNOULLI EQUATION FOR FLUID FLOW MEASUREMENT

Thermodynamics of fluid-flow measurement systems are based on the first and second laws of thermodynamics and the Gibbs fundamental equation. For a steady state, adiabatic fluid-flow system, with no external work, the first law based on an energy balance is,

$$\Delta(H + \alpha v^2 / 2g_c + gZ / g_c)m = 0 \,. \qquad \textbf{Equation 201}$$

The second law based on an entropy balance that includes any lost-work LW is,

$$\partial LW = TdS \,. \qquad \textbf{Equation 202}$$

The Gibbs equation for the fluid is,

$$dU = TdS - PdV \qquad \textbf{Equation 203}$$

and the enthalpy function is,

$$dH = dU + PdV + VdP \,. \qquad \textbf{Equation 204}$$

Combining equations for dH with $V = 1/\rho$ gives,

$$dH = \delta LW + dP / \rho \,. \qquad \textbf{Equation 205}$$

The lost work LW is derived from a momentum balance, and is commonly given by,

$$\int \delta LW = LW = kv_b^2 / 2g_c \,. \qquad \textbf{Equation 206}$$

Where k is the velocity head loss, or number of velocity heads.

The total change in enthalpy is,

$$\Delta H = \frac{kv_b^2}{2g_c} + \int_a^b dP / \rho \,. \qquad \textbf{Equation 207}$$

Substitution into the total energy balance provides the mechanical energy balance, for $Z_b - Z_a = 0$, in the form of the Bernoulli equation,

$$\frac{(k+\alpha_b)v_b^2 - \alpha_a v_a^2}{2g_c} + \int_a^b dP/\rho = 0 \text{.} \qquad \textbf{Equation 208}$$

Applying the equation of continuity $(\rho A v = m)$ and solving for the mass flow rate in the above equation gives the following general representation of the Bernoulli equation for flow through a horizontal head meter,

$$m = \left(\frac{2g_c \int_a^b dP/\rho}{\left(\frac{k+\alpha}{(\rho A)^2}\right)_b - \left(\frac{\alpha}{(\rho A)^2}\right)_a} \right)^{1/2} \text{.} \qquad \textbf{Equation 209}$$

The enthalpy H representation is,

$$m = \left(\frac{2g_c \Delta H}{\left(\frac{k+\alpha}{(\rho A)^2}\right)_b - \left(\frac{\alpha}{(\rho A)^2}\right)_a} \right)^{1/2} = \left(\frac{2g_c \Delta H}{\left(\frac{k+\alpha}{((\partial H/\partial P)_S A)^2}\right)_b - \left(\frac{\alpha}{((\partial H/\partial P)_S A)^2}\right)_a} \right)^{1/2} \textbf{.Equation 210}$$

The Gibbs free enthalpy G representation is,

$$m = \left(\frac{2g_c \Delta G}{\left(\frac{k+\alpha}{(\rho A)^2}\right)_b - \left(\frac{\alpha}{(\rho A)^2}\right)_a} \right)^{1/2} = \left(\frac{2g_c \Delta G}{\left(\frac{k+\alpha}{((\partial G/\partial P)_T A)^2}\right)_b - \left(\frac{\alpha}{((\partial G/\partial P)_T A)^2}\right)_a} \right)^{1/2} \textbf{.Equation 211}$$

The Bernoulli equation for flow through a head meter of any orientation is,

$$m = \left(\frac{2g_c \int_a^b dP/\rho + g/g_c (Z_b - Z_a)}{\left(\frac{k+\alpha}{(\rho A)^2}\right)_b - \left(\frac{\alpha}{(\rho A)^2}\right)_a} \right)^{1/2} \text{.} \qquad \textbf{Equation 212}$$

The enthalpy H representation is,

$$m=\left(\frac{2g_c\,\Delta H+g/g_c(Z_b-Z_a)}{\left(\frac{k+\alpha}{(\rho A)^2}\right)_b-\left(\frac{\alpha}{(\rho A)^2}\right)_a}\right)^{1/2}=\left(\frac{2g_c\,\Delta H+g/g_c(Z_b-Z_a)}{\left(\frac{k+\alpha}{((\partial H/\partial P)_S A)^2}\right)_b-\left(\frac{\alpha}{((\partial H/\partial P)_S A)^2}\right)_a}\right)^{1/2}$$ **Equation 213**

The Gibbs free enthalpy G representation is,

$$m=\left(\frac{2g_c\,\Delta G+g/g_c(Z_b-Z_a)}{\left(\frac{k+\alpha}{(\rho A)^2}\right)_b-\left(\frac{\alpha}{(\rho A)^2}\right)_a}\right)^{1/2}=\left(\frac{2g_c\,\Delta G+g/g_c(Z_b-Z_a)}{\left(\frac{k+\alpha}{((\partial G/\partial P)_T A)^2}\right)_b-\left(\frac{\alpha}{((\partial G/\partial P)_T A)^2}\right)_a}\right)^{1/2}$$ **Equation 214**

where Z_b-Z_a is the vertical distance parallel with the local gravitational field.

Another method is the total head method:

$$H_a^*=(H+\alpha V^2/2g_c)_a=H_b^*=(H+\alpha' V^2/2g_c)_b=Const$$ **Equation 215**

where $\alpha'=k+\alpha$.

For which $H_a^*-H_b^*=0$, and for the a location,

$$m_a=(\rho A((2g_c/\alpha)(H^*-H)^{1/2})_a.$$ **Equation 216**

For the b location

$$m_b=(\rho A((2g_c/\alpha)(H^*-H)^{1/2})_b.$$ **Equation 217**

Closure is provided when $m_a=m_b$, for the same flow rates as calculated above. A similar approach is made for the isothermal G^*-G condition.

Additionally, from

$$H^* - H = \alpha V^2 / 2g_c = (\alpha / 2g_c)(m^2 / A^2)(dH / dP)_S^2$$ **Equation 218**

and by taking the square roots,

$$(H^* - H)^{1/2} = (\alpha / 2g_c)^{1/2}(m / A)(dH / dP)_S \, .$$ **Equation 219**

Then,

$$\int (H^* - H)^{1/2} dP = (\alpha / 2g_c)^{1/2}(m / A)\int (\partial H / \partial P) dP = (\alpha / 2g_c)^{1/2}(m / A)(H^* - H)\, .$$ **Equation 220**

Solving for the mass flow rate gives,

$$m = (2g_c / \alpha)^{1/2} A \int (H^* - H)^{1/2} dP / (H^* - H)$$ **Equation 221**

where $H^* = Const$.

Referencing H^* to a zero (0) datum line gives,

$$m_a = \left((2g_c / \alpha)^{1/2} \frac{A \int_*^a H^{1/2} dP}{H} \right)_a$$ **Equation 222**

and

$$m_b = \left((2g_c / \alpha)^{1/2} \frac{A \int_*^b H^{1/2} dP}{H} \right)_b \, .$$ **Equation 223**

APPENDIX F

SUMMARY OF MACROSCOPIC BALANCES

Table 32 - Summary of Macroscopic Balances

Summary of the Macroscopic Balances for Nonisothermal Flow Systems			
Balance	Special Form	Steady State	
Mass		$\Delta\, m = 0$	
Momentum		$F = -\,\Delta\left(\frac{\langle v^2\rangle}{\langle v\rangle} m + PS\right) + m_{tot} g$	
Energy		$\Delta\left(U + P/\rho + \frac{1}{2}\frac{\langle v^3\rangle}{\langle v\rangle} + \Phi - W\right)$	
Mechanical Energy	Isothermal	$\Delta\left(\frac{1}{2}\frac{\langle v^3\rangle}{\langle v\rangle} + \Phi + G\right) + W + E_v = 0$	
	Isentropic	$\Delta\left(\frac{1}{2}\frac{\langle v^3\rangle}{\langle v\rangle} + \Phi + H\right) + W + E_v = 0$	
Macroscopic Energy Balance for Variable Potential Energy Systems			
$\frac{d}{dt}\left(U_{tot} + \phi_{tot} + K_{tot}\right) = -\Delta\left[\left(\widehat{U} + \widehat{K} + \widehat{\phi}\right)w\right] + Q - W + \int_V \rho \frac{\partial \phi}{\partial t} dV$			
Energy quantities defined as:		$U_{tot} = \int_V \rho \widehat{U}\; dVol$	Internal energy
		$K_{tot} = \int_V \frac{1}{2}\rho v^2\; dVol$	Kinetic energy
		$\phi_{tot} = \int_V \rho\phi\; dVol$	Potential energy